SESSION VI

PARTICLE COLLECTION

Tuesday, August 3, 1976
CO-CHAIRMEN: H. Gilbert, C. A. Burchsted

THE SRP SAND FILTER: MORE THAN A PILE OF SAND

D. A. Orth and G. H. Sykes
E. I. du Pont de Nemours and Co., Inc.
Savannah River Plant
Aiken, South Carolina
and
G. A. Schurr
Engineering Service Division
E. I. du Pont de Nemours and Co., Inc.
Newark, Delaware

Abstract

Sand filters at the two SRP separations plants have operated well for over twenty years, displaying steadily increasing efficiency for removal of activity. Pressure drop remained low on one filter although some sand was removed from the other to counteract rising pressure drop due to salts in the bed. Activity is not migrating through the beds and such breakthrough does not appear to be a life-limiting phenomenon. The underbed supports and air distribution systems were weakened by acid attack and erosion, with localized failure, prompting construction of new filters. Design studies and tests defined relations between sand characteristics, airflow resistance, and filtration efficiency. Appropriate sands were selected and monitored during construction to ensure that the new filters would have satisfactory efficiency, airflow, and pressure drop at startup.

I. Introduction

The two fuel processing buildings at the Savannah River Plant each have a deep bed sand filter on the exhaust air from the high level radioactive operations. Both the original plant units and a recent addition to the Savannah River Laboratory ventilation exhaust system have been described[1,2]. The general configuration and operating conditions are given in Table 1. During the first fifteen years of operation, both of the original plant units had suffered from severe acid attack and erosion of the concrete support structure, which became apparent when there was a localized loss of filter medium and resultant short release of activity from each bed (one 1969, and 1971). The holes were blocked and normal performance was restored almost immediately. The bottom support systems on both were modified to prevent further breakthrough. The failures also prompted consideration of new filters as ultimate replacements for the original units and resulted in extensive test work for both the plant filters and the Savannah River Laboratory filter[3,4]. Two new plant filters were designed and constructed; one was put into service in December, 1975, and the other is in final stages of completion.

The twenty-odd years of plant experience on the original filters, plus the continuing test work as the new filters were constructed, provide much useful performance information, which can be extended to give design and operating criteria for sand filters. The first of the sections below presents the history of the plant units and analyzes the performance data. The second section discusses the test work aimed at insuring that the replacement filters started up with

an efficiency comparable to the old filters so that there would be no increase in activity releases.

II. Plant Experience

SRP Separations Plants

The two separations plants are large, versatile facilities, in which irradiated reactor fuels and targets are processed to recover desired materials. The feed materials are dissolved, then processed primarily by solvent extraction, with some auxiliary ion exchange processes. A wide variety of materials have been irradiated or formed by irradiation, and subsequently processed in these plants, including uranium-233, -235, and -238, plutonium-238, and -239, various mixtures of higher plutonium isotopes, neptunium-237, americium and curium (various isotopes), and thorium. All of these have been associated with large amounts of fission products formed in the reactors. Some ventilation streams are treated separately and some are prefiltered with HEPA filters or packed glass fiber filters, but basically the sand filters provide the final barrier between the radioactive materials in process and the environment, and obviously are required to handle a large variety and amount of radioactive material.

Efficiency

The two plant filters originally had efficiencies of 99.7 to 99.8% as measured by input-output activity measurements, similar to other units that have been reviewed[5]. This apparent efficiency increased steadily over the years, with one filter also becoming markedly better than the other, concurrently with increasing pressure drop on that filter. The more efficient filter finally reached a limiting efficiency for activity removal approaching 99.995%, but pressure drop also became excessive and one foot of the fine sand layer was removed in 1972. Subsequent DOP tests gave an efficiency of 99.96% for this filter and 99.98% for the other, unaltered filter. Activity input-output measurements confirmed limiting efficiencies of 99.97 to 99.98% for both filters for fission product and alpha activity.

The two failures of the support structures referred to previously allowed rock and sand to run through, forming craters with a small hole in the apex. The activity releases increased for a short time until the holes were blocked and the craters filled with sand, then releases returned to normal. The supports were shored in such a way that no more complete penetrations of the beds could occur. However, some of the far reaches of the air distribution trenches could not be protected, and failures there occasionally give small depressions that thin the effective sand layer and decrease efficiency measurably without being serious. These are filled with more sand when detected, with no long-term effect on efficiency.

The term "limiting efficiency" as used above represents the efficiency that can be expected with very large inputs; it is the justifiable value to use in accident analyses and does agree with the DOP tests. The relation between apparent efficiency and input

activity is illustrated in Figure 1, where input beta-gamma activity for three different years is plotted against penetration (1-efficiency). The graph shows both the pattern of increasing efficiency with time and the increasing apparent efficiency (toward limiting values) as the input activity increased. This behavior is indicative of two mechanisms for the penetration of activity through the filter, with some re-entrainment of activity from the large inventory present as well as some fraction of input that escapes filtration in accordance with the true efficiency. The small "inventory release" gives a low background emission even when the input air is relatively clean. This background release and the proportion of long-lived activities such as ^{137}Cs and ^{90}Sr in it have not increased as the total inventory of activity on the filters has built up; indeed, it has decreased, which argues for deposited activity being at risk of re-entrainment for only some limited period.

Alpha activity has shown the same general pattern as beta-gamma activity with lower apparent efficiency at low inputs and the same limiting efficiency at high input, although the amount of alpha activity input has not been high enough to really define the limiting value. Input and output activity can be plotted as on Figure 2 to show the low level background that is independent of input and an apparent limiting efficiency of 99.98%. On such a graph, abnormal conditions in the filter, such as the small craters, are discernible above the envelope of normal conditions.

Finally, the limiting efficiencies also apply to ruthenium that initially may be evolved from the process as gaseous ruthenium tetroxide. This material can be produced in evaporators at very high nitrate concentrations and from process solutions with excess oxidizing agents such as potassium permanganate. The highest beta-gamma inputs to the filters have been associated with evolution of ruthenium in the process; hence, in these cases the high limiting efficiencies basically measured the efficiency for retention of ruthenium. The sand filter may be efficient because it offers a large surface for the ruthenium compound to decompose on, or it may be filtering particles on which the ruthenium has condensed after hydrolyzing in the generally humid off-gas streams. The mechanism is not as important as the fact that the ruthenium is collected.

Pressure Drop and Water Effects

As noted previously, the pressure drop on one filter became excessive and one foot of the fine sand was removed. The increasing pressure drop probably had several causes: a concrete dust loading from some in-building construction activity; concrete and sand fines from the severe acid erosion found later in the entrance tunnel and bed support structure; nonsilica minerals present in the sand in greater abundance in this filter than the other. Superimposed on the steady increase were a marked semiannual variation (Figure 3). This variation may result from moisture; samples of sand from deep in the bed appear damp in moist air and now contain appreciable chemicals, primarily calcium and magnesium salts. The annual changes in humidity and temperature in the humid southeastern environment, plus hygroscopic salts, provide a reasonable explanation of the cyclic effect. Additionally, there were specific episodes where external

ground water and rain reached the bed; these events were eliminated by appropriate repairs. Most noteworthy, the free water reaching the bed gave high pressure drop but did not hurt filtration efficiency. At the low air velocity, water apparently did not aspirate up through the bed and carry activity through to the outlet side.

Life of Sand Filters

The limiting useful life of a sand filter is not known and a filter without structural defects may last the life of the processing plant judging from the SRP experience. The limiting factors would be breakthrough of activity and pressure drop. SRP data show that activity is not moving through the filter and that pressure drop can remain stable if the sand is not reactive and dust loadings are not excessive. Radiation profiles through the filters have been monitored since startup with a network of bore tubes. Activity peaks are found at interfaces between the coarse sand layers below the thick bed of fine sand, which in effect acts as a polishing filter. Successive profiles over the years show the activity peaks moving lower (Figure 6). The radiation profiles basically measure recently deposited fission products and do not preclude a slow migration of old material; the lack of increase in the background release is the best evidence against migration.

Pressure drop does not have to be a life-limiting factor either, according to SRP experience. Although the pressure drop on one filter increased markedly, pressure drop on the other increased only a small amount, as noted previously. Measurements through the bed with lower pressure drop do not show any specific interfaces responsible for the bulk of the pressure drop (Figure 4). The data dispelled fears that some specific zone might be gradually plugging and offer potential for a large increase in pressure drop with the addition of only a small amount of additional dust. In essence, pressure drop on this filter could be projected to be tolerable for the foreseeable future.

The filter with high pressure drop and from which sand was removed, also had no sharp pressure drops at interfaces, with the flow resistance basically spread through the entire fine sand layer (Figure 5). As noted previously, nonsilica minerals and calcium and magnesium salts are in this bed. Again, the data imply that pressure drop would not be a problem if foreign materials were excluded during construction and operation. Finally, the success in removing a foot of sand from this filter, though at some sacrifice in efficiency, shows that maintenance is possible and that sand probably could be removed and replaced whenever necessary to maintain both satisfactory pressure drop and efficiency.

New Filters, Initial Operation

The deterioration of the structures prompted work on new filters and resulted in the extensive test work discussed previously. Sands were selected on the basis of the experimental work and ordered for the new filters. Continuing test work, covered in Section III of this report, showed the sand as supplied had lower efficiency than the test batches and a thin layer of different sand was added to

attain better performance. The first new unit, 30.5 by 110 meters, was put into operation in December 1975, in parallel with the original filter. Initial flow velocity through the new unit, 1.2 cm/sec, is lower than ultimate design basis of 3 cm/sec. The old filter that is being operated in parallel has a resultant flow velocity of .75 cm/sec versus the former 2.5 cm/sec on that unit. DOP tests on the combined, parallel system gave an efficiency of 99.99+%, as would be expected at the low velocity, according to the design tests. The old unit will be operated in parallel for as long as it can be maintained, because of the benefits of low flow. The average releases of radioactivity from the combined filter units did decrease by a factor of about two for the first four months of combined operation as compared to the last four months with just the old filter.

III. Design Work for New Filters

Design Bases

The original sand filter installation at Hanford provided the filter model for those designed for the Savannah River Plant[6]. In this design, a relatively deep prefilter section of graded coarse aggregate, characterized by a large void volume, high air permeability (low pressure drop for a given flow), and modest filtration efficiency, is followed by layers of finer sands which provide high efficiency filtration with an attendant lowering of air permeability. Reports on the characteristics of this design for specific sand types show the prefilter acts as a storehouse for all but the finest dust and aerosols, protecting the finer layers and prolonging useful filter life[3]. In these filters, sands falling in the size range from 20 to 50 mesh have been critical in controlling both overall efficiency and permeability. Data have also been presented in performance, dependent upon sand grain shape characteristic of the deposit from which it was taken[4]. The variability in naturally occurring sands makes the design of a filter more complex than simply creating a pile of sand. Design criteria used for the construction of new filters at the Savannah River Plant are presented to illustrate the importance of testing and quality control in meeting performance criteria.

Long life, high efficiency, and high air permeability are the goals in sand filter design. The optimization of these is limited by physical and economic restraints which make compromise essential. A superficial flow velocity in the range of 2.5 to 3.0 cm/sec has been found to provide a suitable compromise for efficiency and permeability and still provide a manageable size filter. Prefilter sections built to specifications given in Table 2 have been demonstrated effective in over twenty years of service in existing filters at Savannah River. A 30.5 cm (12 in.) layer of sand in the size range from 8 to 20 mesh (F grade) provides a transition between coarse gravels and the finer sands. It is the sand finer than 20 mesh which becomes limiting for both filter efficiency and air permeability. Its selection and placement control the ultimate performance of the filter. Work reported here is concentrated on this area of filter design.

Sand Selection

Ten sources of sand with size distributions falling within the 20 to 50 mesh range were evaluated as filter media[4]. Characteristics varied widely according to size distribution and surface texture. Some good sands were eliminated due to inadequate source or vendor capability. One of the best sources available from a vendor with adequate facilities at a competitive price was selected. A test program was initiated to verify the properties and uniformity of the sands taken from this deposit and provide ongoing design assistance throughout the construction phase of the project.

Sands with two different size specifications, subsequently called types G and H, taken from the single deposit, were carefully evaluated for suitability as sand filter media. The Photoscan technique for measuring surface texture was used to check shape uniformity throughout the sample. All samples had a surface texture of 17.5 ± 0.5 units. This is considered sand of good surface uniformity. An acid leachability test using a 10% boiling HNO_3 acid solution was devised. Sands from this deposit were found not to lose weight after 48 hours of exposure.

Test Work

The type G sand was used in the previously constructed Savannah River Plant filters for the high efficiency section, and as noted previously, efficiency was only moderate at startup. For the new filters, the sand had to provide a higher efficiency, comparable to the final efficiency reached by the old filter, and a test program was initiated to assure adequate performance. Samples of the type G sand were taken from each car loaded at the mine, and size and permeability were measured to determine uniformity. Composite samples of sand were taken at the filter site and tested for size distribution, permeability, and relative filtration efficiency as determined by DOP aerosol test criteria.

Laboratory test work was performed in a 20-cm square filter column, 150 cm deep. The relative effect of the fine sands measured alone was found to correlate well with results obtained in the 61-cm square filter column used for earlier test work in which the coarser prefilter sand and gravel were included. Permeability and efficiency of the sand were determined. Variations were found among the composite samples. Typical results are shown in Table 3 where the size distributions, pressure drops, and filtration efficiency using a 0.8 micron average polydisperse DOP aerosol are reported. It is noted that the size distribution of sand varies among the samples. The finer distributions tend to have lower permeability (higher pressure drop) and better efficiency.

The effect of depth of "G" sand on collection efficiency is illustrated in Figure 7. Here, "G" sand depths ranging from 90 to 140 cm were tested at superficial velocities between 2.5 and 3.5 cm/sec. The pressure drops at respective test points are shown. Here it is seen that substantial improvements in efficiency can be obtained by increasing the depth of the fine sand at a subsequent

penalty in terms of higher pressure drop.

As "G" sand was shipped, a running composite was obtained that projected the average sand size distribution for the "G" sand. It was determined that it was best approximated by sample C given in Table 3. The performance of this sand was evaluated and results are shown in Figure 8.

An alternate to a greater depth of "G" sand was also evaluated. A type H sand with the size specification shown in Table 4 was tested as an "add-on" to type G. Its effectiveness is shown by the efficiencies and pressure drops illustrated in Figure 9. A bed with 91 cm of "G" plus 20 cm of "H" is seen to give a measured efficiency of 99.98% at a flow of 2.5 cm/sec with a pressure drop of 150 mm WG.

Conclusions

Data presented here show the importance of sand selection in filter design. Furthermore, careful monitoring of the fine sands at delivery is needed to assess the effect of variations throughout the natural deposit. These can make the final composite different than would be anticipated from only surface samples taken at the mine. In the case discussed, it was found that a shift in the size distribution between rather narrow limits was sufficient to affect filter performance while shape and texture remained constant. The test program showed performance fluctuations could be handled by varying bed depth in a single grade, "G", or adding another grade, "H", to a "G" sublayer. The newest filter at the Savannah River Plant has 91 cm of "G" sand topped by 20 cm of "H" grade. This filter was started up with an old filter in parallel so that its performance with regard to the specifications has not been determined independently. However, past experience indicates its performance will closely match that predicted from small scale model testing.

Table I. Original sand filters.

Dimensions, meters	
Length	73.15
Width	30.48
Depth	2.44
Superficial velocity, cm/min	152.40
Initial ΔP, cm WG	19.30
Total air flow, m^3/min	3000-3500

Table II. Sand prefilter materials.

Gravel Type	Depth	Specification
A	12 in.	0% retained in 3" screen; less than 2% passing 1-1/4" screen.
B	12 in.	0% retained on 1-1/2" screen; less than 2% passing 5/8" screen.
C	12 in.	0% retained on 5/8" screen; less than 5% passing 1/4" screen.
E	6 in.	Less than 1% retained on 1/4" screen; less than 5% passing 8 mesh screen.

Table III. Type G sand characteristics.

Size Analysis

Mesh	Sample A, %	Sample B, %	Sample C, %
+20	0.3	0.2	0.1
+30 -20	47.6	40.7	48.3
+40 -30	41.2	42.6	46.2
+50 -40	9.1	12.8	4.8
-50	1.8	3.7	0.6

Performance in 20-cm Square Filter Column (91-cm Sand Depth)

Sample →	A	B	C
Velocity, cm/sec	2.6	2.6	2.6
ΔP, mm WG	153	157	127
Efficiency, % DOP	99.96	99.94	99.88

Table IV. Size specification for type H sand.

Mesh	Percent
+30	1.0
-30 +40	65.0
-40 +50	30.0
-50 +70	3.5
-70	0.5

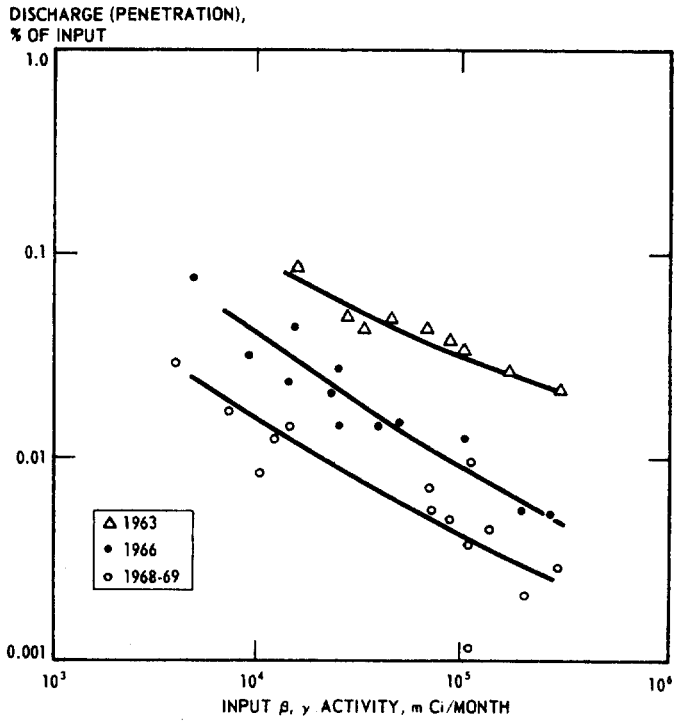

FIGURE 1. FILTER PERFORMANCE

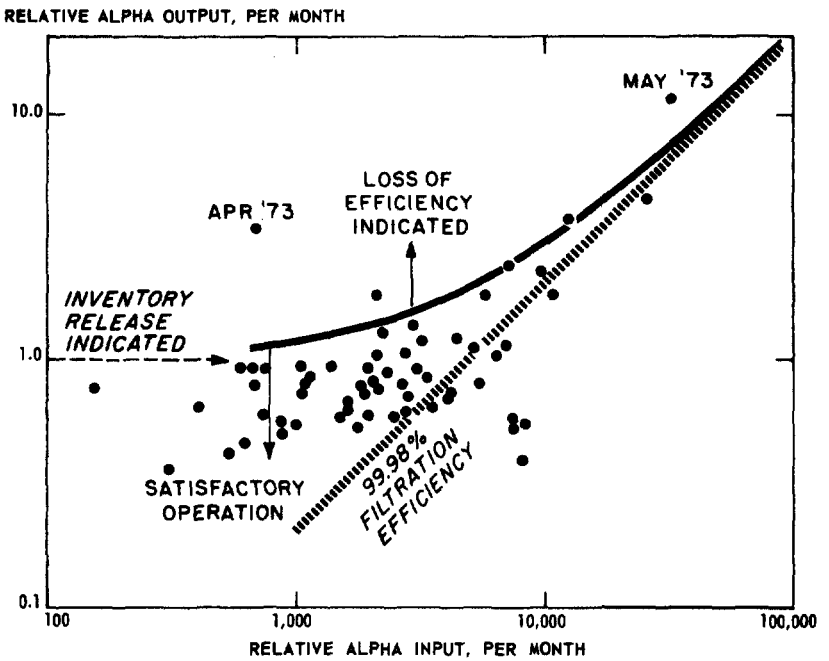

FIGURE 2. H-AREA SAND FILTER PERFORMANCE

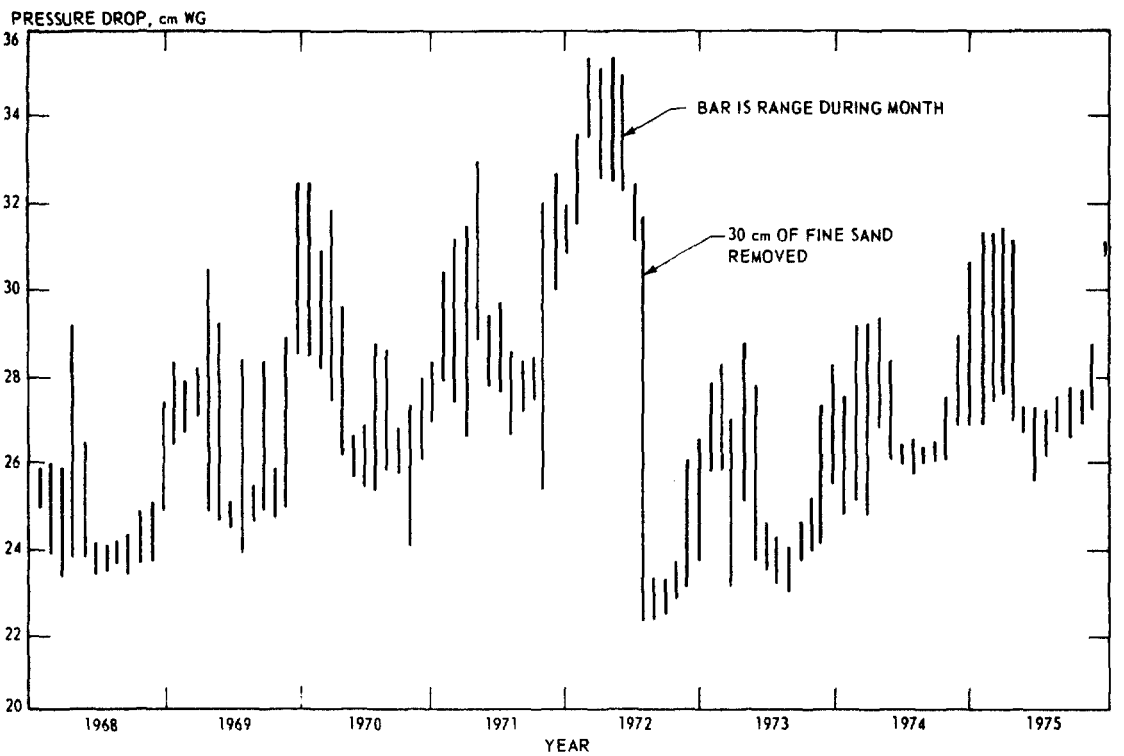

FIGURE 3. PRESSURE DROP HISTORY

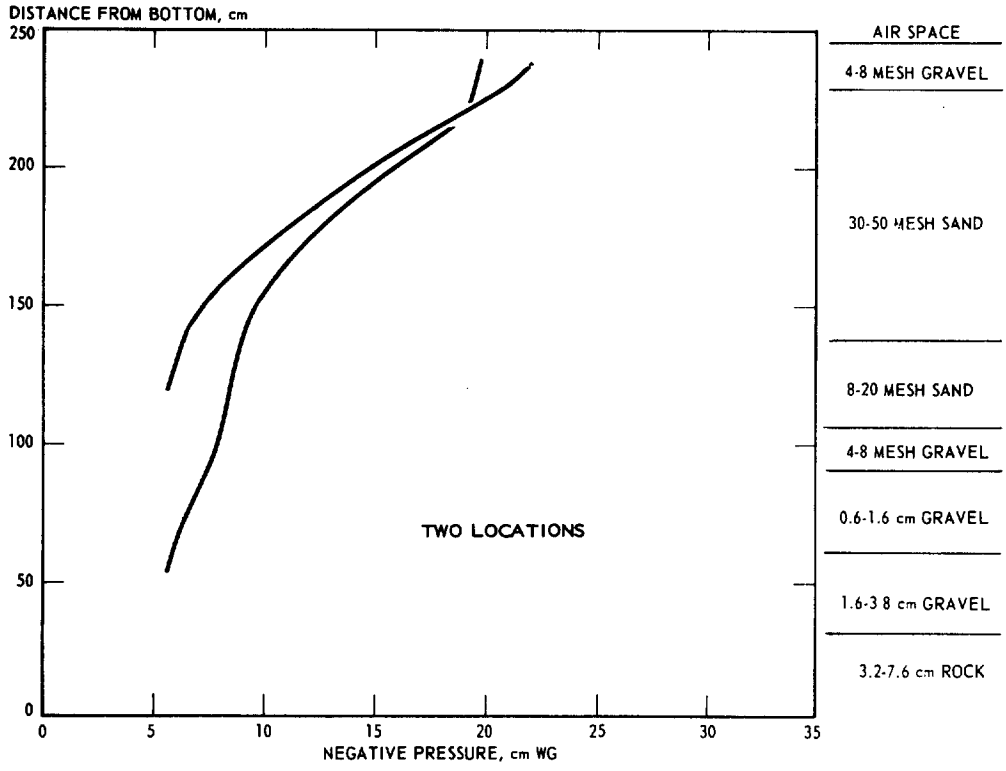

FIGURE 4. DISTANCE FROM BOTTOM VERSUS NEGATIVE PRESSURE

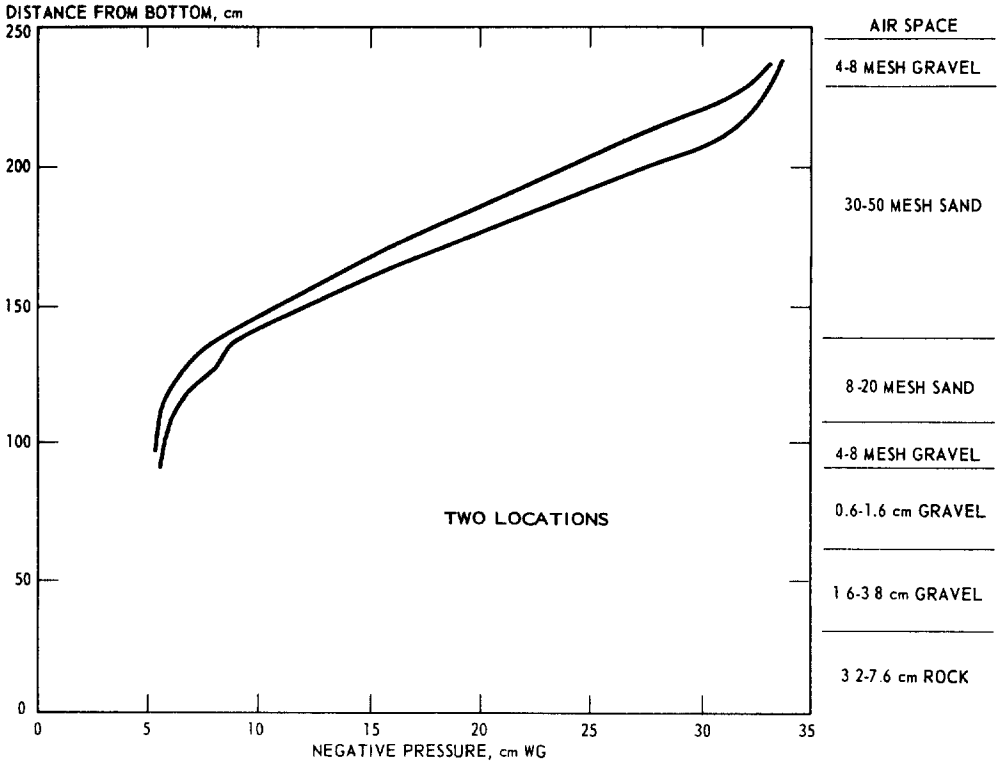

FIGURE 5. DISTANCE FROM BOTTOM VERSUS NEGATIVE PRESSURE

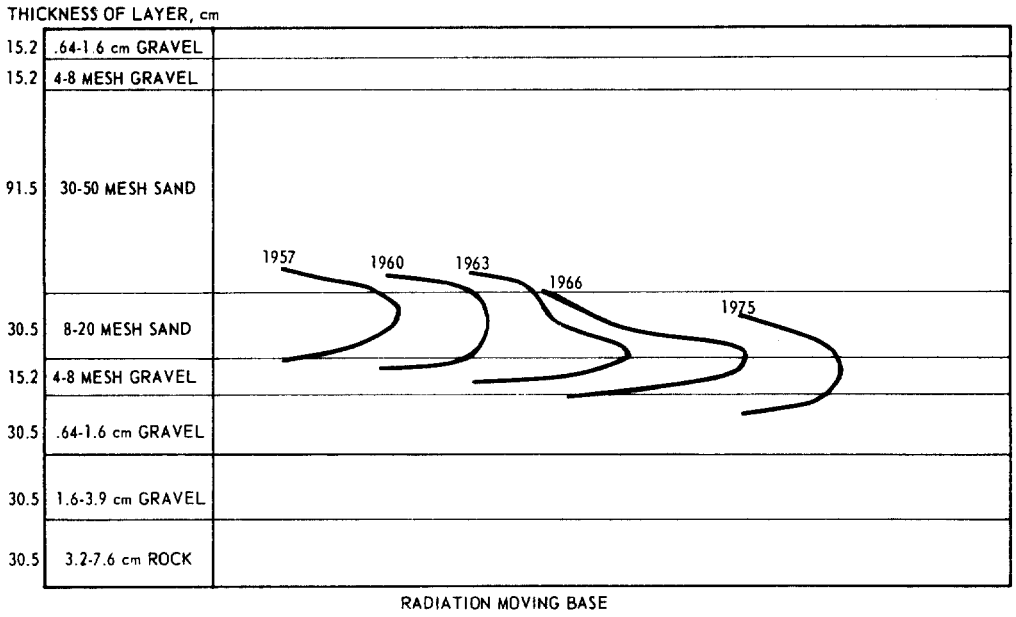

FIGURE 6. RELATIVE DEPTHS OF RADIATION PEAKS

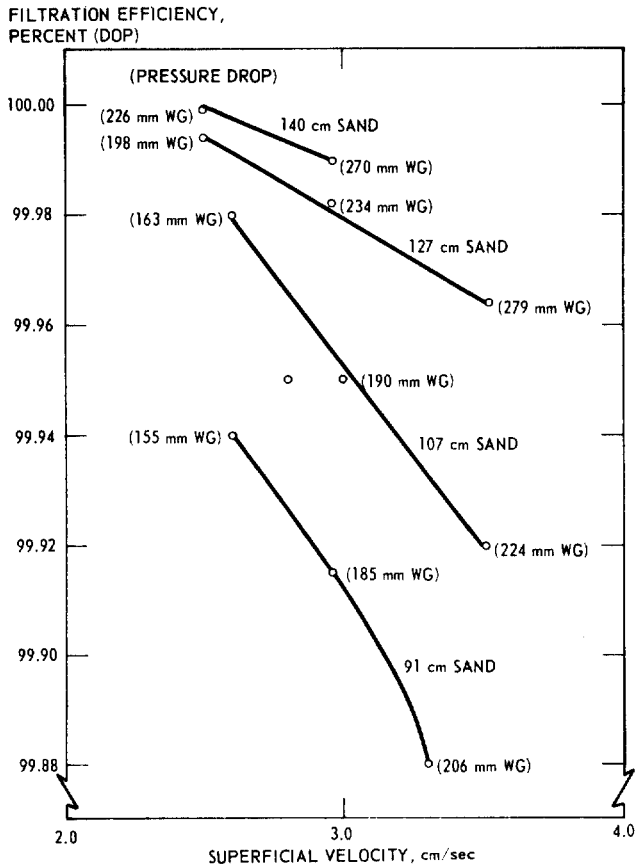

FIGURE 7. FILTRATION EFFICIENCY VERSUS VELOCITY SAMPLE B "G" SAND

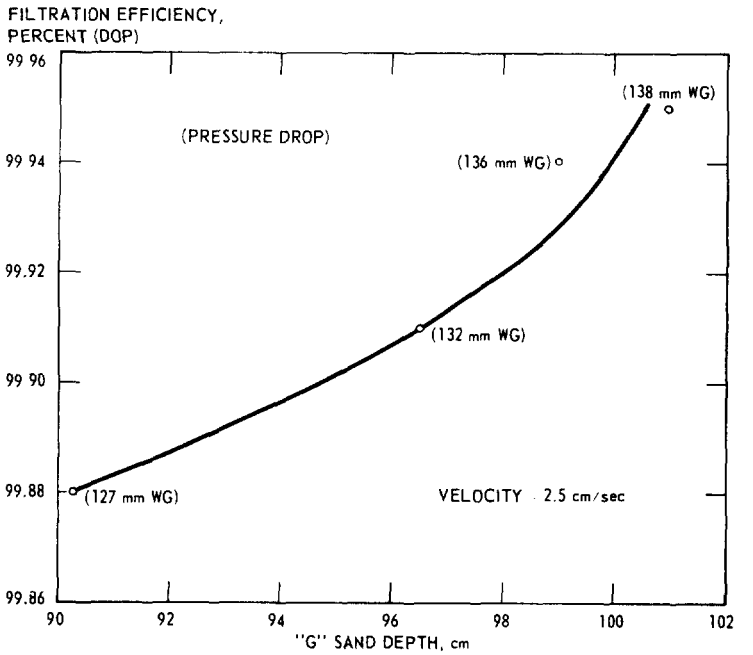

FIGURE 8. FILTRATION EFFICIENCY VERSUS DEPTH SAMPLE C "G" SAND

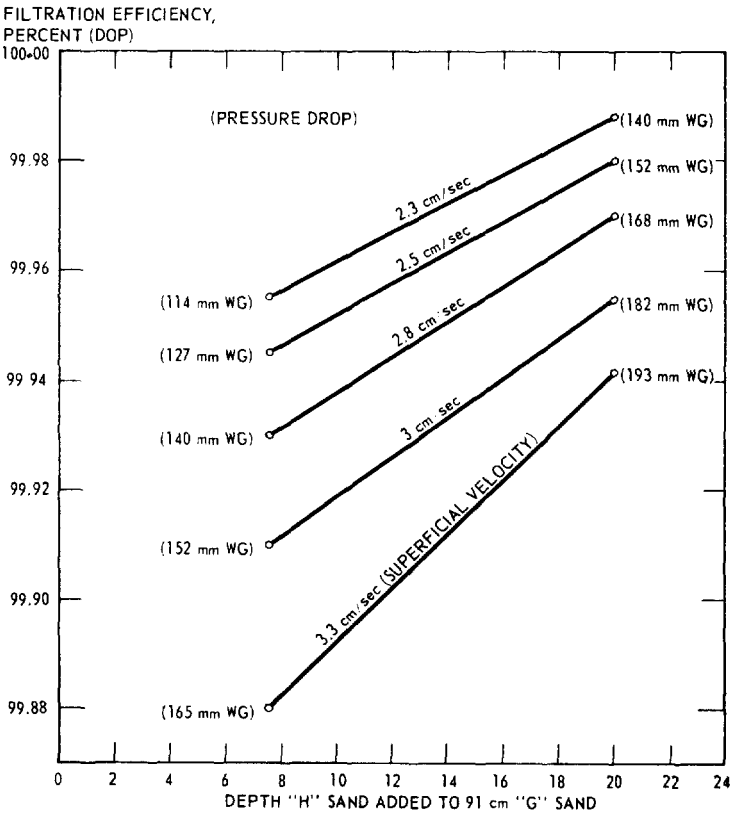

FIGURE 9. EFFECT OF "H" SAND ADDITION ON EFFICIENCY

References

1. Sykes, G. H., and J. A. Harper, "Design and operation of a large sand bed for air filtration," Treatment of Air Borne Radioactive Wastes (IAEA Symposium), CONF 680811-13 (1968).

2. Moyer, R. A., J. H. Crawford, and R. E. Tatum, "Deep-bed sand filter at Savannah River Laboratory," 13th USAEC Air Cleaning Conference (1974).

3. Schurr, G. A., D. B. Zippler, and D. C. Guyton, "Deep-bed filter performance tests," 12th AEC Air Cleaning Conference (1972).

4. Schurr, G. A., and J. E. Johnston, "Characterizing sand grains to optimize filter performance," 13th USAEC Air Cleaning Conference (1974).

5. Juvinall, R. A., R. W. Kessie, and M. J. Steindler, "Sand-bed filtration of aerosols: a review of published information of their use in industrial and atomic energy facilities," ANL-7683 (1970).

6. Lapple, C. E., "Deep-bed sand and glass-fiber filters," Second Air Cleaning Seminar, WASH-149 (1954).

DISCUSSION

SCHIKARSKI One disadvantage of sand filters is the large amount of contaminated sand. As we reported at the San Francisco Air Cleaning Conference you can optimize the mass without losing efficiency by special arrangement of layers of different mesh size sand. Have you optimized your filter in that respect and thus avoided the large amount of sand used in earlier installations?

ORTH: I'm not sure I completely understand the question. If you're talking about optimizing to obtain the minimum depth of sand, just to minimize the amount of final waste, I think the answer is yes, we could do that, but at higher pressure drop. Our system is a compromise within our engineering constraints.

SCHIKARSKI: Usually, the sand filter designs have too much sand in them. We optimize for just sufficient mass to give the result we want.

ORTH: What you say is correct. We could optimize and just arrive at a certain efficiency. We're trying to do the best we can within the limits of the pressure drop we can tolerate. Minimizing waste was not a consideration.

SCHURR: I might also answer that question. We did optimize the designed sand depth on the criteria of life expectancy, efficiency, and pressure drop. The problems of commercial availability and quality control make us have more sand than would be required, ideally.

DUST FILTRATION ON A PANEL BED OF SAND

W.R.A. Goossens, A. Francesconi, G. Dumont, R. Harnie

S.C.K./C.E.N.
Mol (Belgium)

Abstract

The development of a panel bed of sand as dust filter is described. The results obtained in a technical set-up with a filtering area of 1 m^2 are given. The data of a 2^4 factorial design experimental campaign are presented in the form of the resulting statistical equation.

I. Introduction

Dust filtration with the help of granular materials has been applied since many years [1]. For example at the Hanford site, deep beds of graded sand and gravel are in use to remove dust and aerosols from nuclear off-gases [2].

Recently, attention has been drawn again on the possible use of a tall and narrow vertical layer of granular solids in order to filter a gas stream passing this layer in cross-flow [3]. Such a set-up, called panel bed, has been investigated at S.C.K/C.E.N. too. The main objective was to gather information on performance of such a panel bed for the filtration of hot outlet gases released by a radioactive waste incinerator.

This paper describes the results obtained in a technical set-up in which the trapping of fly ash by a panel bed of sand was investigated in order to allow proper design of the panel bed for the waste incinerator. Preliminary, the panel bed concept was tested in a laboratory unit.

II. Preliminary experiments in a laboratory unit

The filtration possibilities of a vertical layer of granular solids were investigated in a laboratory unit made of perspex. The 5 cm thick layer of 350 μm sand grains was kept in place by a louvered wall at the gas inlet side and a special low resistant perforated plate "Conidur" at the gas outlet side as shown schematically in Fig. 1. The gas crossing this vertical layer in the

horizontal direction was artificially loaded with fly ash at a concentration of 300 mg per m^3. The effective filtration area was 90 cm^2.

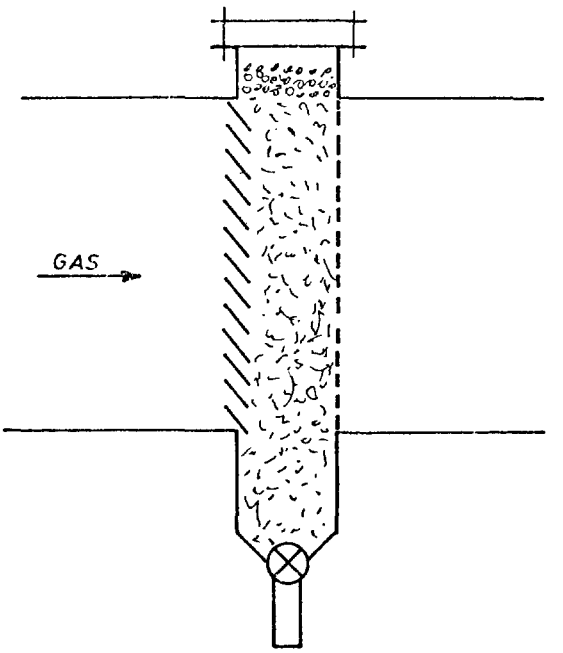

FIG. 1 CROSS-SECTION OF THE BENCH SCALE PANEL-BED FILTER

The dust trapping efficiency reached 99.5 % at a face velocity of 40 cm s^{-1}. The dust appeared to get trapped in the front layer of the filter. The resulting pressure drop increase is shown on Fig. 2. The pressure drop increase offered only a limited operation time to this batch type operation of the granular layer, so that a layer renewal system had to be developed for long operation times.

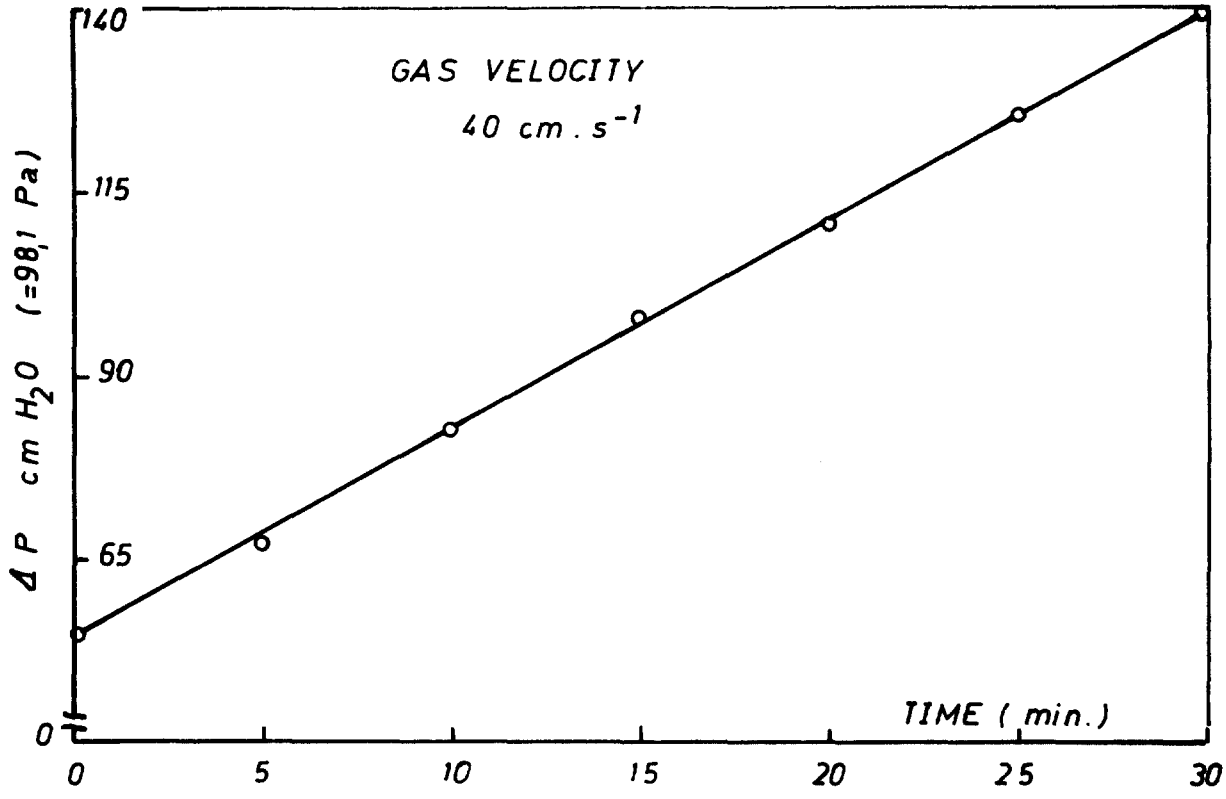

FIG. 2 PRESSURE DROP AS A FUNCTION OF FILTRATION TIME

III. Experimental procedure in the technical set-up

In the technical set-up with an effective flow area of 1 m^2 the solids recycling was performed with an air lift and a vibrating screen was applied for the necessary dust sand separation. As schematically indicated on Fig. 3, two louvered walls were now applied to keep the vertical sand layer in place. The distance between both walls was variable so that a sand layer tickness between 3.9 cm and 18.9 cm was obtainable. A standard sieve ASTM No. 35 (sieve opening 0.5 mm) was used to separate the sand and the dust in a vibrating device. The dust collected was reloaded to the inlet gas with the help of a home-made dust feeder. A view of the

installation is given in Fig. 4.

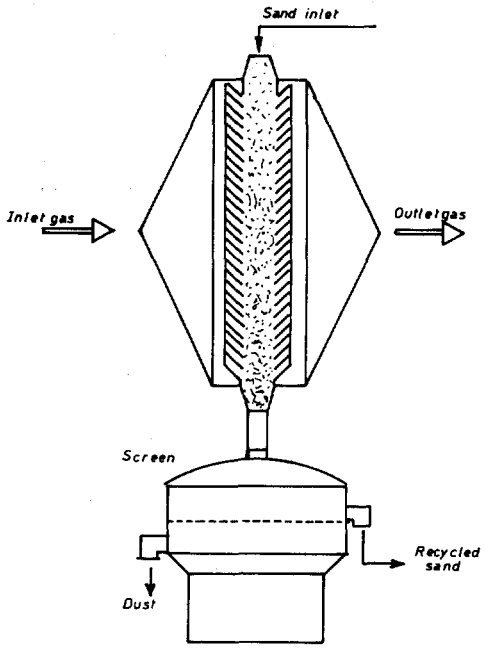

FIG. 3 SCHEME OF A PANEL BED FILTER

FIG. 4 VIEW ON THE INSTALLATION

The carrier gas was compressed air at a maximum flow rate of 450 $m^3.h^{-1}$. The dust used was fly ash from a coal power station with a maximum size of 110 µm. The carrier gas was artificially loaded with this fly ash at a mass flow rate between 176 and 1580 $g.h^{-1}$.

Dust samples were taken isokinetically in the 9.5 cm diameter inlet or outlet tube. The inner diameter of the sampling line was 5 mm. The dust present in the sampled gas was quantitatively trapped on a millipore membrane filter with a diameter of 47 mm and an average pore size of 0.6 µm. The quantity of dust collected during a definite time was determined by differential weighing.

IV Results

In a first experimental campaign, 1.5 mm sand particles were kept at rest in the 4.5 cm thick panel bed. A filtration efficiency higher than 99 % was thus obtained at an air flow rate of 400 m^3h^{-1} and a dust load rate of 430 $g.h^{-1}$. When the sand circulation was

installed at a mass flow rate of 1700 $kg.h^{-1}$, the filtration efficiency became slightly smaller. However, gas leaks from the air lift to the panel bed were observed so that various adaptations on the circulating line were necessary. To increase the linear gas velocity the filtering area was decreased by obstructing part of the panel bed. In this way, it was shown that a maximum linear gas velocity of 90 $cm.s^{-1}$ could be allowed in the panel bed without any sand entrainment while the dust trapping efficiency remained above 99 %.

To complete the technical data, a 2^4 factorial design experimental campaign was performed with the sand at rest during the runs, each three hours long. This way of operation was possible since the average pressure drop increase during the filtration was only 25 Pa ($\simeq$ 2.5 mm H_2O) per hour. Further, the dust trapped during a run was removed by screening the panel bed load during 1 h and 1 1/2 h with a distance between the louvered walls of 3.9 and 8.9 cm respectively.

The following parameter levels were used : 150 and 200 $m^3\ h^{-1}$ for the gas flow rate ; 0.32 and 0.48 $g\ m^{-3}$ for the inlet dust concentration ; 0.9 and 1.5 mm for the average size of the sand ; 3.9 and 8.9 cm for the tickness of the vertical sand layer. The conditions of the various runs are enumerated in Table I on the basis of the factorial design principle.

TABLE I
Symbols for the set of combinations

Symbol of the combination	Level of parameters G	c	Dp	d
(1)	-	-	-	-
a	+	-	-	-
b	-	+	-	-
a b	+	+	-	-
c	-	-	+	-
a c	+	-	+	-
b c	-	+	+	-
a b c	+	+	+	-
d	-	-	-	+
a d	+	-	-	+
b d	-	+	-	+
a b d	+	+	-	+
c d	-	-	+	+
a c d	+	-	+	+
b c d	-	+	+	+
a b c d	+	+	+	+

The statistical analysis of the experiments gave the best independent results when the outlet dust concentration was taken as the dependent variable. This leads to the following regression equation for this outlet dust concentration, c_o, in mg m^{-3} :

$$c_o = 3.124 + 3.422\ D_p - 0{,}660\ L \pm 1.11$$

where : D_p is the average diameter of the sand in cm and L is the bed tickness in cm. The confidence level of both effects was higher than 99 %

The flow rate and the inlet dust concentration dit not show a significant effect under these operating conditions, while also the interactions between the various parameters were negligable.

The value of the standard deviation was estimated on the basis of the mean square value of all interactions observed during these non-repetitive runs.

A similar statistical analysis of the data obtained for the pressure drop increase per hour resulted in the following expression:

$$\Delta P = 0.8537 + 0.0176\ G - 2.233\ D_p \pm 0.63$$

where : ΔP is the hourly pressure drop increase in mm H_2O (=9.8 Pa) per hour and G is the gas flow rate in $m^3 h^{-1}$.

Hence, the gas flow rate and the grain size of the sand have an important effect on the pressure drop.

V. Conclusions

The practical results obtained in the technical set-up gave sufficient information for an engineered design of a panel bed of sand as a dust filter for incinerator gases. This pilot unit working at 2.800 $m^3 h^{-1}$ (STP) and at 600°C will have a guaranteed outlet dust concentration of less thant 50 mg m^{-3}. Its mechanical reception is in progress.

Notations

d	: tickness of sand layer	L
d_p	: sand particle average diameter	L
G	: carrier gas flow rate	$L^3\ T^{-1}$
c	: inlet dust concentration	$M\ L^{-3}$
c_o	: outlet dust concentration	$M\ L^{-3}$
ΔP	: pressure drop in filter bed	$F\ L^{-2}$
μ	: filtration efficiency	%

REFERENCES

(1) R.H. PERRY, C.H. CHILTON, Chemical Engineers Handbook 5th ed., Mc. Graw-Hill, N.Y., 1973, p. 20/87 - 89

(2) H.A. LEO, Guide to Fire Protection in Caves Canyons and Hot Cells, ARH-3020 (1974)

(3) A.M. SQUIRES, R. PFEFFER, Panel bed filters for simultaneous removal of fly ash and sulfur dioxide, APCA Journal, 20, 534-538 (1970)

DISCUSSION

MICHELS: Would you please comment on the ability of the panel filter to withstand pressure surges? Also, does the sand remain free-flowing and does it discharge readily from the panel after service?

GOOSSENS: The ability of the panel filter to withstand pressure surges depends on the geometrical characteristics of the panel filter assembly. The filter described in our paper shows only a limited resistance against pressure surges since the grains can get entrained fairly easily. During our experimental investigation we have never had discharge difficulties after service. The sand remained free-flowing, as you call it. Nevertheless, the angle of repose and the flow properties of the sand plus dust mixture differ slightly from the flow properties shown by new sand. Furthermore, it must be stressed that our investigation was performed at ambient temperature.

INHOMOGENEOUS ELECTRIC FIELD AIR CLEANER*

B.G. Schuster
Los Alamos Scientific Laboratory
University of California
Los Alamos, New Mexico 87545

Abstract

For applications requiring the filtration of air contaminated with enriched uranium, plutonium or other transuranium compounds, it appears desirable to collect the material in a fashion more amenable to recovery than is now practical when material is collected on HEPA filters. In some instances, it may also be desirable to use an air cleaner of this type to substantially reduce the loading to which HEPA filters are subjected.

A theoretical evaluation of such an air cleaner considers the interaction between an electrically neutral particle, dielectric or conducting, with an inhomogeneous electric field. An expression is derived for the force exerted on a particle in an electrode configuration of two concentric cylinders. Equations of motion are obtained for a particle suspended in a laminar flow of air passing through this geometry. An electrical quadrupole geometry is also examined and shown to be inferior to the cylindrical one. The results of two separate configurations of the single cell prototypes of the proposed air cleaner are described. These tests were designed to evaluate collection efficiencies using mono-disperse polystyrene latex and poly-disperse NaCl aerosols. The advantages and problems of such systems in terms of a large scale air cleaning facility will be discussed.

I. Introduction

In many cases, particularly for recovery and/or simplified solid waste disposal purposes, it is desirable to have an air cleaning system in which the particulate material collection may be concentrated. This goal may possibly be attained by flowing the aerosol laden air through a matrix of coaxial cylinders with a high electric field across each coaxial pair. The electric field will induce a dipole moment on the aerosol particles which will then be subject to a force in the direction of the central cylinder due to the field gradient produced by the coaxial configuration. Calculations based on such a system indicate the possibility of 100% collection for 1.0 μm particles in slow laminar flow, providing the particles stick to the collector surface. Power requirements are not expected to be high since the only work to be done is that required to overcome viscous drag forces acting to resist the particle motion, permitting operation of this air cleaner during emergency conditions with use of a capacitor bank. The interaction of the carrier gas (air) with the electric field is considered negligible.

*Work supported by the U.S. Energy Research and Development Administration, Contract No. W-7405 - Eng-36.

II. Trajectory Analysis, Coaxial Cylinder System Radial Motion

We consider a flow of particulates in air, with the particulates assumed to be electrically neutral. The principle to be invoked for the transport of the uncharged particles to a collection surface is that of an induced dipole interaction between the particle and an applied inhomogeneous electric field.

The induced dipole moment of a spherical particle in a locally uniform field approximation is given by

$$\vec{p} = 4\pi R^3 \epsilon_o \frac{k-1}{k+2} \vec{E} \tag{1}$$

where $\vec{p}$ = induced dipole moment
$\vec{E}$ = electric field strength
R = particle radius
ϵ_o = permittivity of vacuum
k = dielectric constant

A typical value of k is 10. For conductors, (k-1)/(k+2) approaches unity.

The field at a radial distance r produced by a potential, V, applied between two coaxial cylinders is given by

$$\vec{E} = \frac{-\hat{r}}{r} \frac{V}{\ln b/a} \tag{2}$$

where b = radius of outer cylinder
a = radius of inner cylinder
$\hat{r}$ = unit radius vector.

The force on the particle is given by

$$\vec{F} = (\vec{p} \cdot \nabla)\vec{E} = -4\pi R^3 \epsilon_o \frac{k-1}{k+2} \frac{V^2}{\ln^2 b/a} \frac{\hat{r}}{r^3} = \frac{-\alpha \hat{r}}{r^3} \tag{3}$$

Besides the electrical driving force on the particle, a viscous velocity-dependent force will exist. This is given, for small particles, by the product of the Stokes force and the slip correction factor, i.e.,

$$\vec{F}_d = \frac{6\pi \eta R}{1+A\,\lambda/R} \vec{v} = \beta \vec{v} \tag{4}$$

where η is the viscosity [which must be transformed to the mks units used in Eq. (3)], v is the velocity, λ the molecular mean free path, and A is a constant.

Combining Eq. 3 and 4 with the particle inertial term yields radial and tangential equations of motion. The tangential motion immediately damps out because of the lack of a driving force, leaving the radial equation of motion in the form.

$$m\ddot{r} + \frac{6\pi\eta R}{1+A\lambda/R}\dot{r} + 4\pi R^3\epsilon_0\left(\frac{K-1}{K+2}\right)\frac{V^2}{\ln^2 b/a}\frac{1}{r^3} = 0 \quad , \tag{5}$$

where m is the particle mass and r the radial distance.

This equation is not amenable to analytic solution, however, the inertial term is negligible, i.e., the relaxation time is very small, and so $\ddot{r}$ can be set equal to zero. The resulting equation may now be integrated from the outer cylinder at radius b, to some other position at radius r to yield

$$r^4 = b^4 - \frac{8R^2\epsilon_0 V^2}{3\eta \ln^2 b/a}\left(\frac{K-1}{K+2}\right)t \quad , \tag{6}$$

where t = time. Defining

$$\frac{8R^2\epsilon_0 V^2}{3\eta \ln^2 b/a}\left(\frac{K-1}{K+2}\right) \equiv \alpha \quad , \tag{7}$$

Eq. 6 may be written as

$$r^4 = b^4 - \alpha t \tag{8}$$

Axial Motion

The longitudinal equation of motion is obtained from the laminar flow profile of air moving in the annular region under consideration. Following Joos', the differential equation for the velocity profile may be written as

$$\frac{d}{dr}\left(r\frac{dv}{dr}\right) = -\frac{(P_1-P_2)}{\eta l}r \quad , \tag{9}$$

where P_1-P_2 is the pressure drop along a length, l, of the system. Performing two integrations results in

$$v = -\frac{(P_1-P_2)}{4\eta l}r^2 + c_1 \ln r + c_2 \quad . \tag{10}$$

The integration constants C_1 and C_2 may be evaluated from the boundary condition at the walls, which are

$$v = o \text{ when } r = a,\ r = b.$$

Substituting the values of C_1 and C_2 thus obtained into Eq. 1 yields the final form of the velocity profile for laminar flow in an annular region.

$$v(r) = \frac{P_1-P_2}{4\eta l}\left[a^2-r^2 + (b^2-a^2)\frac{\ln r/a}{\ln b/a}\right], \tag{11}$$

This velocity profile is plotted in Fig. 1.

The flow rate, Q, for this system may be obtained by integrating the velocity profile over the cross section to yield, for b>>a,

$$Q = \frac{\pi}{2}b^2\left(\frac{P_1-P_2}{4\eta l}\right)\left(1-\frac{1}{\ln b/a}\right) \tag{12}$$

The average velocity, $\bar{v}$, is given by the flow rate divided by the cross sectional area:

$$\bar{v} = \tfrac{1}{2}b^2\left(\frac{P_1-P_2}{4\eta l}\right)\left(1-\frac{1}{\ln b/a}\right) \tag{13}$$

The maximum velocity can be obtained by differentiating Eq. 11 and setting the result to zero. Letting $\gamma = \frac{P_1 - P_2}{4\ \eta l}$,

$$\frac{dv}{d} = \gamma\left[\frac{b^2-a^2}{\ln b/a} \times 1/r - 2r\right] = 0 \tag{14}$$

Solving for r results in

$$r_{max} = \sqrt{\frac{b^2-a^2}{2\ln b/a}} \doteq \frac{b}{\sqrt{2\ln b/a}} \tag{15}$$

Substituting this value of r_{max} into Eq. 11 yields

$$v_{max} \doteq \gamma\left[\frac{b^2}{\ln b/a}\left\{\ln\left(\frac{b}{a\sqrt{2\ln b/a}}\right) - 1/2\right\} + a^2\right] \tag{16}$$

The trajectory of a particle introduced into the airflow at radius b may now be computed from Eqs. 8 and 11. Letting dz/dt = v(r) where z defines the axial coordinate and substituting Eq. 8 into Eq. 11 wherever r occurs results in

$$\frac{dz}{dt} = \gamma\left[a^2-(b^4-\alpha t)^{1/2} + \left(\frac{b^2-a^2}{\ln b/a}\right)\left(\tfrac{1}{4}\ln\left[b^4-\alpha t\right] - \ln a\right)\right] , \tag{17}$$

Integrating this expression between the limits z_o to z and o to t results in

$$z-z_0 = \gamma\left\{a^2t + 2/3\,\frac{(b^4-\alpha t)^{3/2}}{\alpha} - \left(\frac{b^2-a^2}{\ln b/a}\right)\left(\frac{b^4-\alpha t}{4\alpha}\,[\ln(b^4-\alpha t)-1] + t\ln a\right) - 2/3\,\frac{b^6}{\alpha} + \left(\frac{b^2-a^2}{\ln b/a}\right)\left(\frac{b^4}{4\alpha}\,[\ln b^4-1]\right)\right\} \qquad (18)$$

Substituting for t from Eq. 8, Eq. 18 becomes

$$z-z_0 = \frac{\gamma}{\alpha}\left\{a^2(b^4-r^4) + \frac{2r^6}{3} - \left(\frac{b^2-a^2}{\ln b/a}\right)\left(r^4[\ln r-\tfrac{1}{4}] + [b^4-r^4]\ln a\right) - 2/3\,b^6 + \left(\frac{b^2-a^2}{\ln b/a}\right)\left(b^4[\ln b-\tfrac{1}{4}]\right)\right\} \qquad (19)$$

The maximum downstream displacement of the particle occurs when it hits the inner cylinder, i.e., when r = a. For this condition, and b >>a such that $b^n - a^n = b^n$, Eq. 19 can be evaluated as

$$(z-z_0)_{max} \doteq \frac{\gamma}{\alpha}\left\{a^2b^4 - b^6\,\frac{\ln a}{\ln b/a} - 2/3\,b^6 + \frac{b^6}{\ln b/a}\,(\ln b-\tfrac{1}{4})\right\} \qquad (20)$$

As an example of the values to be expected from such a system, consider the design parameters of b = .0102 m, a. = .0016 m, v = 10^4 volts, average flow velocity of .05 m/s and a 5.0 μm particle. Using Eq. 13 with v equal .05 m/s, a value of $\gamma = 1.98\text{x}10^3$ is obtained. Using this figure in evaluating Eq. 20, a value of 2.0 m is obtained as a minimum collector length for 5.0 μm conducting particles entering the system at the outer perimeter. Smaller particles which enter the system closer to the collector electrode will also be captured.

III. Trajectory Analysis, Quadrupole System

The translation and subsequent collection of uncharged particles in an electric field requires that the field be inhomogeneous, i.e., that there exist a strong field gradient in the direction of the field. The coaxial cylinder geometry is one configuration that will perform this task, and is amenable to analysis. A simpler configuration, from the viewpoint of engineering and construction, would be more desirable. One such system might consist of an array of oppositely charged rods or wires aligned with the airflow.

In order to analyze such a system, a sub-set of this array, consisting of four elements was chosen. A system such as this is often referred to as a quadrupole (Fig. 2). The calculations of field and field gradient for this system are readily accomplished in rectangular coordinates. Unfortunately, the resulting differential equations of motion for this system are very complex and coupled, even with the omission of the acceleration (inertial) term.

From the symmetry of the system and the lines of zero potential, one quadrant of this configuration can be isolated for analysis in a circular cylinder coordinate system. However, the resultant equations of motion are expressed in terms of an infinite series in two variables, which are again coupled and would require a numerical rather than an analytical solution.

In order to obtain an analytical solution, the equipotentials in each quadrant are approximated as cylindrical hyperbolas (Fig. 3). The electrostatic potential of such a system may be represented by

$$\Phi_1 = \frac{\Omega}{2}(x^2-y^2) \tag{21}$$

where Ω represents the strength of the potential, ϕ_1. This equation represents a family of hyperbolas, e.g., for $\Phi = 0$, Eq. 30 may be solved to yield $y = \pm x$, which are the equations of the planes intersecting at the origin. The electric field, E_1, is given by

$$\vec{E}_1 = -\nabla\Phi_1 = -\Omega(\hat{i}x-\hat{j}y) \tag{22}$$

where $\hat{i}$ and $\hat{j}$ are unit vectors. The dipole moment of a spherical particle is given by

$$\vec{P} = 4\pi\epsilon_0\left(\frac{K-1}{K+2}\right)R^3\vec{E} \doteq 4\pi\epsilon_0 R^3\vec{E} \tag{23}$$

The approximate expression above is valid for large values of K and for conductors. The force term is now given by

$$\vec{F} = (\vec{P}\cdot\nabla)\vec{E}_1 = 4\pi\epsilon_0 R^3\Omega^2(\hat{i}x+\hat{j}y) \tag{24}$$

which may be summed with the acceleration term and the viscous (Stokes) term to yield

$$4\pi\epsilon_0 R^3\Omega^2(\hat{i}x+\hat{j}y) = 4/3\,\pi\rho R^3(\hat{i}\ddot{x}+\hat{j}\ddot{y}) + \frac{6\pi\eta R}{F}(\hat{i}\dot{x}+\hat{j}\dot{y}) \tag{25}$$

where ρ is the density of the particle, η is the viscosity of the medium (air) and F is the slip correction factor. The single and double dotted variables may be recognized as velocity and acceleration components, respectively. For convenience, let $4\pi\epsilon_0 R^3\Omega^2 = C$, $4/3\,\pi\rho R^3 = A$, and $6\pi R\,\eta/F = B$. If it is assumed, as for the coaxial cylinder case, that the inertial term is negligible, then

$$C(\hat{i}x+\hat{j}y) = B(\hat{i}\dot{x}+\hat{j}\dot{y}) \tag{26}$$

Solving this differential equation for the appropriate components yield the solutions

$$x = x_0 e^{C/B\ t}, y = y_0 e^{C/B\ t} \tag{27}$$

where x_0 and y_0 are the initial coordinates of a particle in the system. Elimination of the time parameter in Eq. (27) results in

$$y = \frac{y_0}{x_0} x \tag{28}$$

where, because of the systems geometry, $0 \leq y_0/x_0 \leq 1$. For a particle initially at the origin i.e., $x_0 = 0$, $y_0 = 0$, no motion will exist, according to Eq. 27. Physically this is because the electric field is zero at this position. Referring back to Eq. 26. the vector $\hat{i}x + \hat{j}y$ and its time derivatives are equal, respectively, to the vector r and its time derivatives. Hence, the general solution to Eq. 26, analogous to Eq. 27, is

$$\vec{r} = \vec{r}_0 e^{C/B\ t} \tag{29}$$

Now, return to the complete equation of radial motion, Eq. 25 which may be written as

$$\ddot{\vec{r}} + B/A\,\dot{\vec{r}} - C/A\,\vec{r} = 0 \tag{30}$$

This may be solved exactly to yield

$$\vec{r} = \vec{r}_{01} \exp\left[-\tfrac{1}{2}\left(B/A - \sqrt{\frac{B^2}{A^2} + \frac{4C}{A}}\right)t\right] + \vec{r}_{02} \exp\left[-\tfrac{1}{2}\left(B/A + \sqrt{\frac{B^2}{A^2} + \frac{4C}{A}}\right)t\right] \tag{31}$$

It will now be shcwn that for typical values of particle size and density, and a realistic value of potential, that the solution, Eq. 29 is an extremely good approximation, i.e. the contribution of the inertial term is negligible. Letting the potential Φ, be 5 x 10^3 V and the distance from the origin to the vertex of the hyperbolic surface be .01 m, the value of Ω becomes 10^8. For a 1.0 μm particle, the slip correction factor is 1.16. The values of A, B, and C are A = .52x 10^{-15}, B = 14.71 x 10^{-11}, C = 13.90 x 10^{-14}. Referring to the exponentials in Eq. 31, it can be seen that $B^2/A^2 >> 4\ C/A$, hence, the expansion to first order,

$$\sqrt{\frac{B^2}{A^2} + \frac{4C}{A}} = B/A\sqrt{1 + \frac{4CA}{B^2}} \doteq B/A\left(1 + \frac{2CA}{B}\right) \tag{32}$$

is essentially exact. Substituting this last expression into Eq. 31 results in

$$\vec{r} = \vec{r}_{01}\, e^{+C/B\, t} + \vec{r}_{02}\, e^{-(C/B + B/A)\, t} =$$

$$\vec{r}_{01}\, e^{.00095\, t} + \vec{r}_{02}\, e^{-(.00095 + 2.8 \times 10^{5})\, t} \qquad (33)$$

The second term in the above damps out almost instantaneously. The factor 2.8×10^5 is the reciprocal of the relaxation time for a 1.0 μm particle. The first term of Eq. 33 is identical to Eq. 29, hence, steady state motion may be described by an abridged differential equation of motion such as Eq. 26.

The trajectory calculation is now continued from the hyperbolic surface to a physical rod of radius a which is the actual element of the quadrupole field. In order to locate the position of this rod, the radius of curvature of the hyperbola, at its vertex, must be calculated. The radius of curvature, G, is defined by[2]

$$G = \frac{[1 + (dy/dx)^2]^{3/2}}{|d^2y/dx^2|} \qquad (34)$$

Solving Eq. 21 for y^2 yields

$$y^2 = x^2 - \frac{2\Phi_1}{\Omega} \qquad (35)$$

The required derivatives are

$$\left(\frac{dy}{dx}\right)^2 = \frac{x^2}{x^2 - \frac{2\Phi_1}{\Omega}} \quad \text{and} \quad \frac{d^2y}{dx^2} = \left(x^2 - \frac{2\Phi_1}{\Omega}\right)^{-1/2} - x^2 \left(x^2 - \frac{2\Phi_1}{\Omega}\right)^{-3/2} \qquad (36)$$

Substitution of tnese expressions in Eq. 34 result in

$$G = \frac{[y^2 + x^2]^{3/2}}{|y^2 - x^2|} \qquad (37)$$

which evaluated at x = b, y = 0, yields

$$G(b,o) = b \qquad (38$$

hence locating the cylindrical electrode at a distance 2b from the origin.

For the remainder of the trajectory calculation it is assumed that the electrostatic field between the rod at 2b and the hyperbolic

potential surface at b can be described by a field produced by coaxial cylinders. If Φ_1 is the potential of the outer cylinder (hyperbolic surface) of radius b, and Φ_2 is the potential of the rod of radius a, then the electric field, E_c between them is given by

$$\vec{E}_c = \frac{-(\Phi_2-\Phi_1)}{\ln b/a}\,\frac{\hat{r}_c}{r_c} \tag{39}$$

where r_c is the radial distance between the two cylinders and $\hat{r}_c$ is the corresponding unit radius vector. Invoking continuity of the normal components of the displacement vector, $\varepsilon_o E$, between the two regions separated by the hyperbolic surface requires that

$$|\vec{E}|_{x=b,y=0} = |E_c|_{r_c=b} \tag{40}$$

Evaluating Eqs. 22 and 39 in this fashion leads to

$$-\Omega b = \frac{-(\Phi_2-\Phi_1)}{b \ln b/a} \tag{41}$$

or

$$\Phi_2 = \Phi_1 + \Omega b^2 \ln b/a \tag{42}$$

which determines the potential at the rod. The calculation for the radial component of this part of the trajectory is essentially that given in Eq. 6 with $r^4 = 0$, i.e.,

$$\tau_2 = \frac{3\eta \ln^2 b/a}{8fR\epsilon_0(\Phi_2-\Phi_1)^2}\, b^4 \tag{43}$$

where τ_2 is the time required for the particle to go from the hyperbolic surface to the collector rod. Using Eq. 42 to substitute for $\Phi_2-\Phi_1$ yields

$$\tau_2 = \frac{3\eta}{8fR^2\epsilon_0\Omega^2} \tag{44}$$

The time required to traverse the first portion of the trajectory is, from Eq. 29 or 33 ,

$$\tau_1 = B/C \ln r/r_c \tag{45}$$

For a hypothetical case of the quadrupoles arranged on a 2-cm radius bolt circle, opposite poles charged to plus and minus 10KV, the sum of T_1 and T_2 yields a radial transit time, for an initial position 1mm from the center of the bolt circle, which is comparable to the concentric cylinder configuration of radii 2 cm and .1 cm. The deciding factors which favor the cylindrical configuration are the absence of a null interaction region and a voltage difference only half that of the quadrupole case. The airflow profile is also much less favorable for the quadrupole case in that the highest velocity occurs in the weakest interaction region, hence requiring a longer flow distance, i.e., a longer collecting configuration.

Consideration of the relative merits of the two types of electrode configurations leads to the conclusion that the coaxial cylinder geometry is more efficient.

IV. Preliminary Experimental Results

Figure 4 schematically displays the very low velocity laboratory scale coaxial inhomogeneous electric field apparatus initially designed to confirm the theoretical development of part II. Monodisperse PSL aerosol dispersed by a Lovelace generator is sent through a Kr^{85} aerosol charge neutralizer. A charged particle precollector composed of two parallel plates .30 m x .06 m with .015 m spacing was constructed to filter out charged particles not neutralized by the Kr^{85} neutralizer. A coating of silicon oil was used on these plates to enhance their retentivity. After leaving the precollector, the aerosol is introduced into a second, smaller precollector (.19 x .13 x .015 m) housed in a box which has as one of its sides a HEPA filter to allow pressure within the box to stay at the ambient value. The aerosol within the box is drawn in through the outer annular region of the inhomogeneous field collector. This outer annulus serves to define the initial conditions so that a monodisperse aerosol will be localized on the .63m collector rod. Detection of particles was with a single particle laser spectrometer.

The design airflow turned out to be too low to introduce a significant amount of aerosol into the system, so the average flow velocity was increased to .05 m/s. This, coupled with the fact that the spectrometer was limited to an upper size of 2.9 μm restricted particle size to standard 2.01 μm PSL particles. Although very little loss in transmission was anticipated, 100% collection was obtained at 8KV, as shown in Fig. 5. In order to determine if a large population of charged particles still existed, the precollectors were deactivated. This resulted in only a 25% increase in total population but resulted in an almost identical penetration curve as illustrated in Fig. 5.

If a Boltzman distribution for the charge is assumed, 10% of the particles have zero charge, and 9% have one charge of + 1 and -1. Singly charged particles should still be capable of getting through the collector. The results of an approximate calculation of the collection efficiency, pre-supposing this distribution, is shown by the solid line in Fig. 5.

A calculation was performed assuming that the particles drawn into the drift tube immediately migrated to a position midway between

the tube and collector. These results also indicated that the uncharged particles would not be collected. The possibility of corona charging from the collector was discarded by using a radio to detect corona discharge. The current flow was also monitored with a microammeter.

Various coatings were applied to the collector to enhance the sticking of particles. Substances used were silicon oil, silicon grease, apiezon grease, glycol, and water. All but the latter two had no effect on the transmission curve. Water and glycol produced zero penetration at 6 to 7 KV not only for 2 μm particles but all the way down the spectrum to .1 μm particles (penetration <1%). The collection was accompanied by corona. Visual examination of the apparatus disclosed aerosol on the interior of the drift tube. In the case of glycol, the glycol was also found in the drift tube. The mechanism appears to be that of electrostatic spraying of the medium coating the collector electrode. The droplets thus formed would be expected to be highly charged and thus attracted to the drift tube. During their traverse, they inter-act with the aerosol particle so that the system of particle and droplet are deposited on the surface of the drift tube.

A typical transmission plot for a mixture of 2.0, 1.0 and .53 μm particles, collector coated with glycol, is shown in Fig. 6.

V. Future Work

A two meter precollector and 3 meter drift tube have been constructed for further investigation of both neutral particle collection and the electrostatic spraying phenomenon. At present, the latter method appears to be a much more efficient air cleaner but suffers from collection taking place on the drift tube rather than being localized on a small center electrode which can be more readily cleaned.

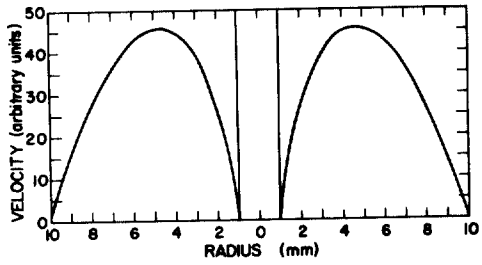

Fig. 1.
Coaxial Cylinder Flow Profile.

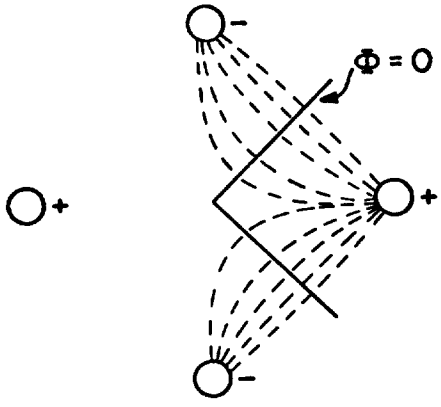

Fig. 2.
Electric Quadrupole Showing Equipotentials and Field Lines.

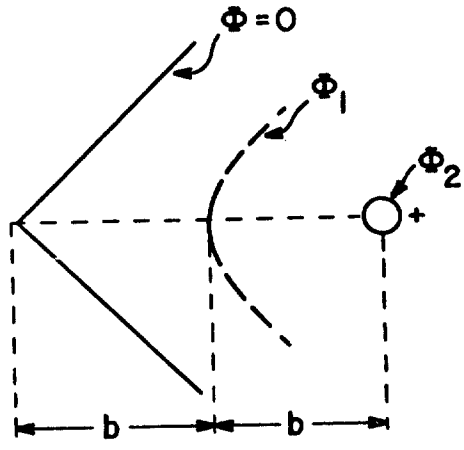

Fig. 3.
Approximate Quadrupole.

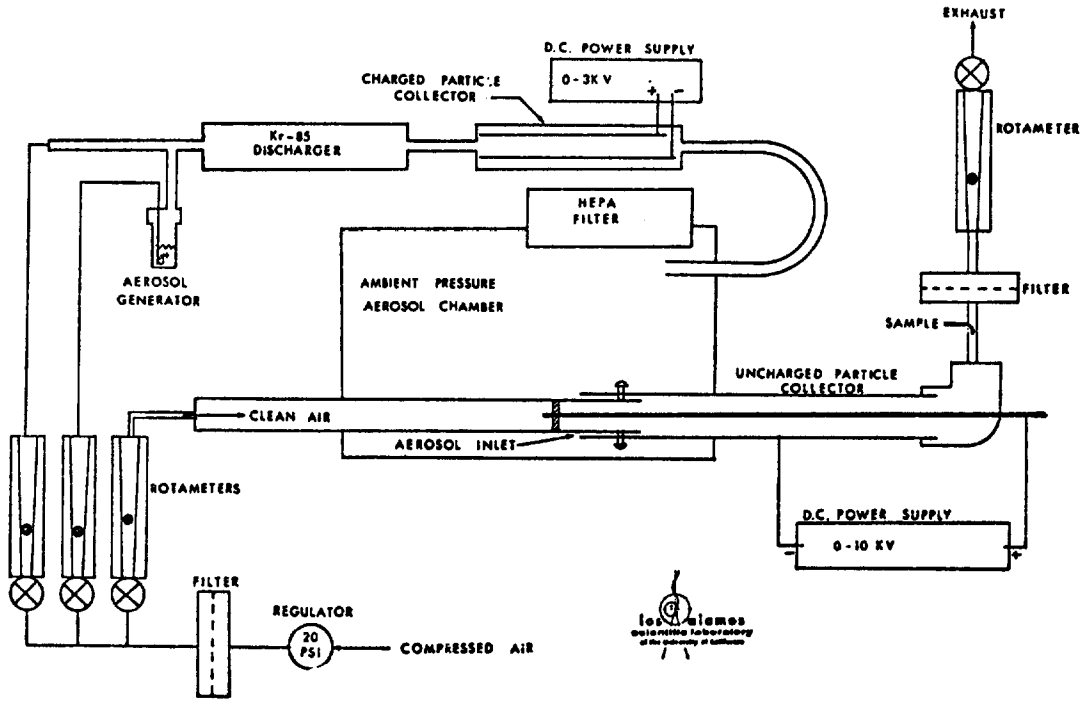

Fig. 4.
Inhomogeneous Field Apparatus.

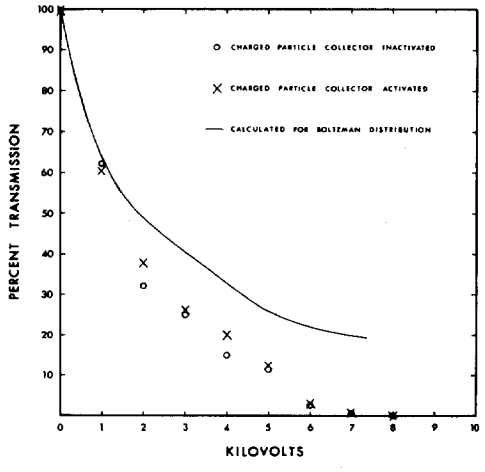

Fig. 5.
Aerosol Transmission as a Function of Applied Voltage.

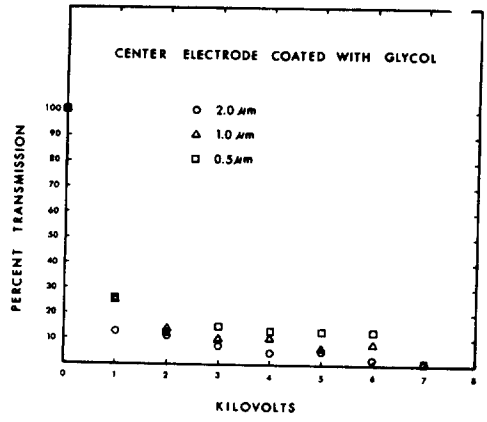

Fig. 6.
Aerosol Transmission as a Function of Applied Voltage.

References - Inhomogeneous Field

1. Georg Joos, Theoretical Physics, 2nd edition, Hafner Publishing Co., New York, 1950, P.P. 212-213.

2. R.R. Middlemiss, Differential and Integral Calculus, McGraw-Hill Book Company, Inc., New York and London, 1946, P.129.

DISCUSSION

HINDS: Would you comment on how this system would perform with dielectric particles and conductive particles?

SCHUSTER: The dielectric particles will need a longer path length. The force is maximized when we have a conducting particle. The force on the particle decreases by the ratio of K-1/K+2. Typically, very small particles have some reasonable conductivity and I think that the ratio of K-1/K+2 will always be greater than one half.

RIVERS: I can't discover in your paper what your efficiency determination method is.

SCHUSTER: The velocity for that particular device is 300 centimeters per minute. It's not particularly fast. The particle sizes used were two μm polystyrene latex. Although my calculation isn't really an efficiency calculation, it can easily be transformed into one. I have taken the worst case, where the particle enters at the very outer boundary. The closer the particles enter to the central collector, the more efficiently they will be collected. If you get very close to the central collector, you can collect a tenth of a micron particle in the same length of system.

RIVERS: What was your experimental method of measuring efficiencies?

SCHUSTER: We measured efficiency by transmission, as we use the single particle detector that I described earlier to look at the particles going through, initially, without any potential, and then we vary the potential difference or velocity, as the case might be, and look at the transmission. We have all of the particles going through the single particle counter, which provides the flow for the system.

RIVERS: I would be interested in some sort of weight measurement, such as using membrane filters, to determine the overall efficiency of this unit by an alternate technique. Our experience would indicate the efficiencies you obtained are very high for operating conditions given.

SCHUSTER: Have you tried the configuration in your laboratory?

RIVERS: Very similar things.

THE ELECTROSTATIC CAPTURE OF SUBMICRON PARTICLES IN FIBER BEDS*

D. L. Reid and L. M. Browne
Battelle
Pacific Northwest Laboratories
Richland, Washington

Abstract

The emission of submicron sized particles is the most difficult to effectively control with current state-of-the-art technology. Experiments at Battelle-Northwest led to the discovery that charged particles could be efficiently captured by a thick fiber bed having a high bed-volume to fiber-volume ratio and a very low pressure drop. Interim results are presented for the removal efficiency as a function of particle resistivity, superficial gas velocity, bed depth and aerosol concentration. In general, for bed pressure drops less than 0.5 in H_2O efficiencies greater than 90 percent were obtained at 300 ft/min (~152 cms/sec) face velocity over the particle size range of 0.06-0.7 μm AMD and a particle resistivity range of 10^8 - 10^{12} ohm-cm. The most important variable was the bed face velocity with the collection efficiency varying inversely with velocity. The bed depth and volume void fraction were other significant variables bearing on the efficiency of the system.

Emperical equations indicate a 100 percent collection efficiency might be attainable near or somewhat below a bed face velocity of 50 ft/min (~25 cms/sec). However, a more sensitive measurement method would be required for experimental confirmation.

Introduction

The cost/benefit ratio for the control of particulate emissions has increased significantly with the decreasing control limits and for the more resistant submicron particulates there is a large imbalance which will probably increase as attention becomes focused on the submicron species once the "boulders" are under control. Consequently, there is a great need for control technology that will meet the atmospheric disposal limits and yet have a marked influence on lowering both the capital investment and operating expense. It is recognized by all that as the particle resistivity increases and the size decreases, the efficiency of the electrostatic precipitator (ESP) is significantly degraded. The trend to burn Western low sulfur coal to reduce the sulfur emission has initiated a large effort in gas-particle conditioning in an effort to offset the ESP loss of

---

* Work performed under EPA Grant #R-801581

efficiency due to the higher particle resistivity. Present-day mechanical devices control the "rocks" reasonably well but are found wanting for the smaller submicron particulates. Bag filters are the most effective present technology for filtration of submicron particulates, but have a very significant drawback in the limited face velocity and high pressure drop. Consequently, for high volume discharge gases the filter area required is extremely large producing high capital and operating costs. The problem initiated a myriad of research programs aimed at improving or developing a system or device to meet the emission standards and somewhat secondarily for more economically controlling emissions. A significant portion of the work was oriented toward the use of electrical charges or electrical properties for enhancement of filtration efficiencies. The novel concept described utilizes the electrostatic properties of particles and fibers of high dielectric strength to effectively remove submicron and other particulates from waste or process gas streams.

Background

During the course of experiments based on charged water spray-droplet scrubbing, it was discovered that a dry demister pad of a non-conducting fiber was acting as an effective filter for submicron particulates of unipolar charge and produced significantly greater efficiencies than observed for the charged particle-charged spray drop tests. This observation, by A. K. Postma and W. K. Winegardner,* initiated a few confirmatory tests that reduced the phenomenon to practice and led to an Environmental Protection Agency (EPA)** grant to explore the boundary conditions of the variables thought to be of importance. Funding was later obtained from the Battelle Energy Program office (BEP) for a phase of the work specifically directed toward fly ash and for continued mathematical modeling of the observed phenomenon.

Availability and cost of a new system dictated the use of the spray-drop system for the initial parametric tests. The variability of the data and unexplained observations highlighted the inadequacies of the system for the more refined tests addressing parametric boundary conditions. However, the data were sufficiently encouraging to warrant a new wind tunnel that would provide a unidirectional, constant velocity flow between the principal sampling points. This discussion of interim information relates, principally, to the experimental data obtained with the new wind tunnel and addresses only the interim experimental tests assigned to the EPA grant program.

The mathematical modeling of the phenomenon by D. L. Lessor (BNW) is too extensive for this discussion and will be issued in detail at a later date. At this point in time, a logical equation-of-state has been developed but an equation providing apriori predictions is not yet completed.

---

* Patent pending.

** Work performed under EPA Grant No. R-801581-02-2.

Methods of Approach

The collection mechanism involves the deposition of charged particles by self-induced electric fields within a bed of electrically non-conducting fibers. Since the electrical field in the bed is induced by molecular ion or charged particle deposition, efficient operation of the system depends on the development of electrical fields of the same polarity sufficient to overcome the coulombic repulsion of the fiber within times smaller than the residence time of the particle within the bed. From this criteria, the following variables might be expected to play an important role:

Particle Size -	influences mobility
Air Velocity -	residence time of particles in the vicinity of a fiber
Pad Resistivity -	charge leakage rate and field strengths and distribution
Pad Thickness -	target area residence time
Dust Surface Coverage -	flow geometry, charge leakage rate
Particle Resistivity -	charge leakage for continuous coating and particle charge level
Charge Level of Particles -	mobility of particles in field
Total Charge Interception Rate -	maximum field in bed due to particle deposition
Fiber Density -	mean free path between particle and fiber -- localized residence time
Humidity -	influence on bed conductivity for hygroscopic particles

A complete block experimental plan involving the ten parameters listed would require more than a practical number of tests for proof of the concept. Therefore the program was designed to explore ranges of most of the variables listed. The boundary conditions of the parameters to be explored included the following:

Particle Size - not to be considered a prime variable. All tests will involve submicron particles near the 0.1 to 0.3 μm size range, which corresponds to minimum mobility and maximum challenge to the system. The removal efficiency would be expected to be higher for particles above 1 μm.

Air Velocity - to be varied from 50 to 400 ft/min (∿25 to 200 cms/sec) superficial bed velocity.

Pad Resistivity - Available demisters of stainless steel, polypropylene and teflon will be used. The stainless steel will show the effect of pad conductivity. Teflon fibers would allow operation at temperatures near 300°F and should be examined for application.

Pad Thickness - Thickness of 3, 6 and 12 in. beds will be tested for comparative efficiencies.

Particle Resistivity - Highly important, generation of particles having resistivities of 10^7, 10^9, 10^{11} ohm-cm will be sought -- the highest resistivity reflecting a severe challenge to electrostatic precipitators.

Particle Charge Level - not considered as a primary parameter for study at this time. Saturation or near saturation charge appears advantageous and the charger will be operated at a voltage to produce same.

Dust Loading - Particle concentrations will be varied from 10 to 100 milligrams per cubic meter.

The data for each experiment included the removal efficiency, pressure drop, relative humidity, air flow rate, and dust loading. The particle size and particle resistivity was determined for each generating condition thought to alter these characteristic properties of the particle. The electrical properties of the bed, e.g. field charge level, would be dependent primarily on charge deposition and leakage rate through some finite resistance for the ungrounded bed. Consequently, some indication of the relative field charge level and distribution within the bed was obtained during "steady state" conditions by inference from current measurements. These measurements were considered as important input for support of a mathematical model and possibly desirable for scaleup with a design engineering model.

Experimental Equipment

The initial investigation of the observed phenomenon was conducted in the available charged spray-drop test apparatus which experimentally left much to be desired for the more definitive parametric study attempting to define the influencing variables and the related boundary conditions. A new wind tunnel system was designed to provide a unidirectional uniform velocity from particle generation point to the last downstream sampling point.

Test System

Figure 1 is a schematic drawing of the system which consists of a 7 foot long 24 in. diameter pipe, a short corona charging section with an effective cross-sectional charging area equal to that of the duct, a 3 foot long section between the charger and fiber bed to preclude any direct field charge effects from the charge section, and a bed frame for the knitted fiber mats. The inlets and outlets to the bed were 24 in. diameter. The bed dimension was made 28 in. x 28 in. to extend the experimental run time before edge leakage became the predominant source of downstream particles. The frame was made with lucite and was electrically isolated from the rest of the system as was the charging section. The system was built in sections for future alteration of configurations and distances between principal components and was held together with electrically

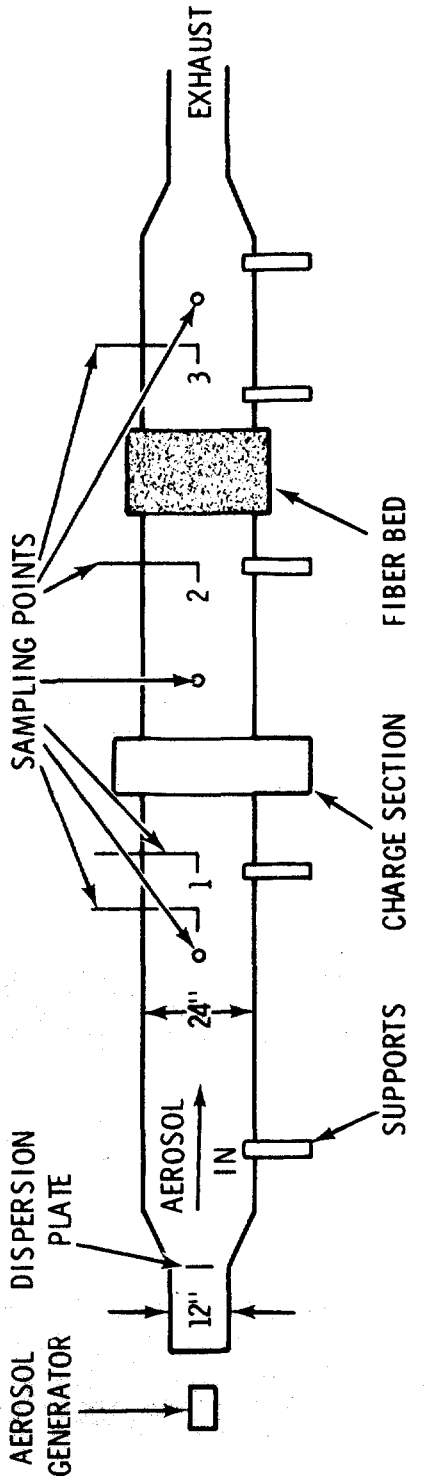

FIGURE 1 Wind Tunnel Schematic

insulated external straps. A dispersion plate was placed in the 12 in. diameter inlet at the transition point to produce the required uniform velocity profile at the three principal sampling points at positions 1, 2 and 3.

Corona Charging Section

The charging section was designed for rather easy alteration of the electrode-to-ground spacing to vary the particle deposition on the ground rods. Half-inch diameter rods rather than plates were used for the ground in an effort to reduce deposition, to minimize the sparkover rate late in the runs and to extend run time without particle charging degradation. The effective field depth of about 15 cms gave a particle residence time of about 100 milliseconds at 300 ft/min (∿150 cms/sec) face velocity - more than adequate to reach near saturation charge.

Fiber Bed Section

The frame holding the fiber bed was made of 1/2 in. thick lucite for visibility and for its high dielectric properties. The bed surface area extended 2 in. beyond the duct diameter to eliminate early edge leakage along the framing where the fiber density is at a minimum as was observed in experiments using the spray-drop test system. This apparently delayed leakage until a significant load had accumulated on the front face and the increase in the pressure drop diverted some particles to the region of a lower pressure drop. From visual observation this edge leakage, which was accentuated by the support wires, appeared to lower the efficiencies for some of the last tests in a run series just prior to bed cleaning. The observed "frame" leakage is strictly a function of the experimental bed construction and could be designed out of a bed made specifically for electrostatic filtration. Also, under industrial applications the bed would normally be cleaned before the pressure drop increased sufficiently to alter the flow pattern and increase the velocity through a much smaller bed fraction.

The bed was supported within the frame by a teflon coated wire grid with about a 4 in. wire spacing. The used demister pads were disassembled and the individual knitted mats layered into the supporting frame. Since the maximum width of the mats was about 14 in., alternate layers were juxtapositioned at 90° angles to each other to preclude gaps or any major lower density regions that might "short circuit" the bed. This method of forming the bed also provided a means for varying the void volume fraction -- that space unoccupied by fibers.

Experimental Conditions

Fiber Bed Void Fraction

The void fraction of the fiber bed was defined as that volume of the bed not occupied by the fiber volume and was determined from the bulk weight of the fiber mats, density of the fiber per unit length and the fiber diameter. For this series of tests the 6 in.

bed was packed to a void fraction (VF) of ∿0.96. For the 12 in. bed, the flow direction of the frame was reversed and the first 6 in. then packed to a VF of ∿0.975. The lower fiber density was used in the first 6 in. to increase particle penetration depth and increase the load to bed-pressure-drop ratio. The lower density in the first 6 in. accomplished both goals, but appeared to be detrimental with respect to efficiencies in the later stages of a continuous run series and to the length of operating time before breakthrough. This was true particularly for MgO which normally showed a greater penetration depth than NH_4Cl or Na_2O. Breakthrough of the bed is defined as the appearance of agglomerates on the sample downstream from the fiber bed which were not observed in the previous samples. A conducting copper wire surrounded the fiber bed and small screens were placed on the front and back faces to intermittently measure the current to ground as an indication of the bed electrical conditions during operation.

Particle Generation and Characteristics

Three particles were used in this series of experiments to highlight any change in efficiency with particle resistivity -- namely ammonium chloride, magnesium oxide and sodium oxide. The NH_4Cl particle was generated by air sparging of HCl and NH_4OH solutions with interception of the gas streams at the inlet to the system. The particle generation rate was controlled by varying both the concentration of the solutions and the sparge air flowrate. The MgO and Na_2O particles were generated by metal vaporization and oxidation. The metal was heated inductively in an enclosed boat. An inert gas forced the metal vapors out the end of the tube where ignition to the oxide occurred. The generation rate was controlled principally by the temperature but also to a small degree by the inert gas flow. It was found that the aerodynamic mean diameter (AMD) was rather simply altered by varying the flow rate of the inert carrier gas. No special attempts were made to obtain a specific particle size or develop a technique for generating a monodisperse aerosol since this was not a specific part of the program. Since the technique was available for varying the particle size, some tests were made with MgO particles having an AMD of less than 0.1 μm.

An eight-stage Anderson sampler was inserted upstream of the charge section to obtain the aerodynamic mean diameter for each generation in which the conditions were altered. It should be recognized that the last stage of the available sampler had an effective cutoff diameter of about 0.4 μm for the isokinetic flow conditions. Since about 90 percent of the particle mass was collected on the filter, extrapolation of a log normal plot to obtain the AMD was a questionable practice although it was the only approach available at the time. Consequently, the stated AMD's are thought to be high. The apparent particle sizes and particle properties, shown in Table I, are the predominant observations for all generations. The mass median diameter (MMD) was calculated assuming a unit particle density and is related to the AMD by $MMD = \frac{AMD}{\sqrt{\rho}}$ where ρ is the particle density.

TABLE I
PARTICLE PROPERTIES OF GENERATED AEROSOLS

Particle	AMD in Microns	MMD in Microns	Resistivity in Ohm-Cm
NH_4Cl	0.25, 0.38	0.16-0.24	$\sim 10^8$
Na_2O	0.25, 0.3, 0.4, 0.6, 0.7	0.17-0.56	$\sim 10^{10}$
MgO	0.06, 0.1, 0.15, 0.25	0.03-0.13	$\sim 10^{12}$

Sampling

Mass samples were collected upstream of the corona charger and upstream and downstream of the fiber bed with the time increased as the rate of generation decreased. Millipore filters (0.65 μ pore size) were satisfactory for NH_4Cl and lower mass/unit-of-time generations for Na_2O and MgO. Fiber glass filters were required for the higher particle concentration tests of Na_2O and MgO to avoid changing the pressure drop across the calibrated flowmeters and to prevent sampling flow reduction or premature plugging of the filter.

The weight increase of the filter without particle generation, balance sensitivity (±0.02 mg) and high filtration efficiency of the fiber bed prevented efficiency measurements at 50 ft/min face velocity and limited the maximum efficiency that could be determined at 100 ft/min to ∿99.9 and ∿99.6 percent for 100 mg/M³ and 25 mg/M³ concentrations without extensively increasing each test period. The weight gain of the filter was determined by sampling the tunnel air with charger on using double millipore filters. The top filter was tossed and the bottom filter weighed before and after desiccation at room temperature for up to four hours. The average weight gain was 0.02 mg and was not altered by drying in the desiccator. This suggested that bound moisture was creating the weight bias. The fiber glass filters created an opposite problem since some sloughing off or loss of fibers generally resulted when removing the paper from the holder. This weight loss was reduced from about 0.15 mg to 0.04 mg by carefully brushing off the edges of the paper before weighing and inserting into the sampler. However, since these were used only for the higher flow rates at high air loadings, the fractional influence on the efficiency was around .002.

Test Procedure

The aerosol generator was started along with the elapsed generation timer and brought up to the desired generation rate as quickly as possible, the conditions for which had been previously, roughly established. Samples were collected at three points; namely, (1) upstream of the charger, (2) between the charger and bed and (3) downstream of the bed. The average volume flow rates and superficial bed velocities for any setting were based on pitot tube profiles of the duct at the flow rates of interest. Velocity profiles

at the three sampling points were not significantly different. Consequently, the same sampling flow rate was used for the three mass sampling points. The high particle and field charges at the second sampling point produced some odd results that defied interpretation and precluded the use of the data for determining the bed efficiency. For example, indicated bed efficiencies were 10 and 92 percent for two successive runs under identical conditions with both showing about 98 percent total efficiency. Consequently, the results reported are for the total efficiency of the system. More recent tests have shown a marked improvement in the comparative bed and system efficiencies -- within 1 to 2 percent with some being identical. The only change made to the system for these tests was an increase in the distance between the electrodes and ground rods of the charger which reduced the current to one-half of that observed with the original configuration. This further indicated the problem was associated with sampling in a high electrical field since a major reduction in the field downstream of the charger ameliorated the discrepancies markedly.

Generally, sampling was continuous until the end of the day or until apparent breakthrough (whichever came first) except during adjustment of generation rate and flow. Low aerosol concentration runs generally required two days of operation. When this occurred, the system was shut down over night. Prior to particle generation the second day, the charger was turned on to impose a field charge on the bed and a reentrainment test made at 300 ft/min flow (∿150 cms/sec). There were no apparent degrading effects even though the bed charge was at zero over night. For a series of measurements, the flow rate was varied from low to high and back to low or in the reverse order. Generally, two consecutive measurements were made before changing the flow and/or concentration.

It should be recognized that the collection efficiencies noted were based on mass measurements for submicron particles and comparative efficiencies would be expected to be higher for aerosols having a mass median diameter greater than 1 μm.

Results and Discussion

Six Inch Thick Polypropylene Bed- NH_4Cl and Na_2O

The void fraction for this bed was approximately 0.96. Figure 2 shows the average efficiency as a function of velocity as well as the sample 2σ limits. For both, the efficiency up to 200 ft/min (∿100 cms/sec) filter face velocity is approximately linear and then appears to change to some other function or to a linear function with a different slope. Sufficient data are not available to describe the point of change and relationship between 200-300 ft/min (∿100-150 cms/sec). The single NH_4Cl measurement at 250 ft/min (125 cms/sec) was the last measurement taken before bed cleaning and is thought to be low due to observed breakthrough which, from visual observation, was assigned to migration of the particles along the lucite frame. This short circuiting was observed only after the pressure drop increase in the original flow regime of the bed diverted some of the flow to the outer edges. The supporting wire grid

work appeared to accentuate the diversion of particles to the bed fringes as evidenced by the predominant earlier particle migration along the wires. This leakage along the bed frame would be eliminated with a fiber bed designed for this specific application. The equations developed from a linear regression fit of the data, 200 ft/min (∿100 cms/sec) velocity and below, are shown in Table II and represented by the solid line in Figure 2. These equations also indicate an efficiency of 100 percent might be expected at a face velocity below 50 ft/min (∿25 cms/sec).

The total efficiency measured for Na_2O was significantly lower than that for NH_4Cl which has a lower resistivity than Na_2O. Since this was contradictory to the developed theory which predicts a decreasing efficiency with decreasing particle resistivity due to a lower space charge, an investigation was initiated to shed some light on the observation. During examination of all operating data it was noted that the current flow in the charger during this series of measurements increased with time and was uncharacteristically very high during the last few measurements at 200 and 300 ft/min (∿100 and 150 cms/sec). Examination of the charging section showed that a buildup of Na_2O on the terminal weights of the electrodes, which were nearly touching the ground rods, created a more conductive path to ground through absorption of moisture and subsequent formation of the more conducting NaOH. Thus this effectively reduced the corona field and apparently the particle charging efficiency resulting in an anomalous low system efficiency at least near the end of the series. Another indicator of this problem was the necessity to reduce the power supply voltage gradually with time to prevent automatic cutoff by the power supply current limit switch. The moral of this sequel is to never use Na_2O particles at high air humidity (>40 percent) when the electrode weights are in close proximity to an electrical ground that produces a direct short -- principally a geometric design problem.

Twelve-Inch Thick Polypropylene Filters

The first 6 in. of this bed were packed to a void fraction of 0.975 with the last 6 in. at ∿0.96 principally to extend the run time for NH_4Cl aerosols of the higher concentrations. Since there was no discernable effect of particle concentration on system efficiency over the range of 6-148 mg/M^3, only higher concentrations were used in this series of tests in an effort to reduce the run time and maintain reasonable reproducibility. This was accomplished to some degree but again sensitivity of the measurements produced a higher variability than desired. However, the frequency of unexplained "fliers" was significantly lower.

The efficiency for NH_4Cl, MgO and Na_2O is plotted against flow rate in Figure 3. As shown by the least squares fit curves, the efficiency decreased linearly with increasing velocity at least up to 300 ft/min (∿150 cms/sec) rate -- the maximum flow attainable with the present system. The Na_2O data points are the average of all measurements at a single velocity. The 95 percent confidence limits are also shown. The MgO and NH_4Cl data are duplicate measurements. Consequently, all data are plotted and no limits shown.

FIGURE 2

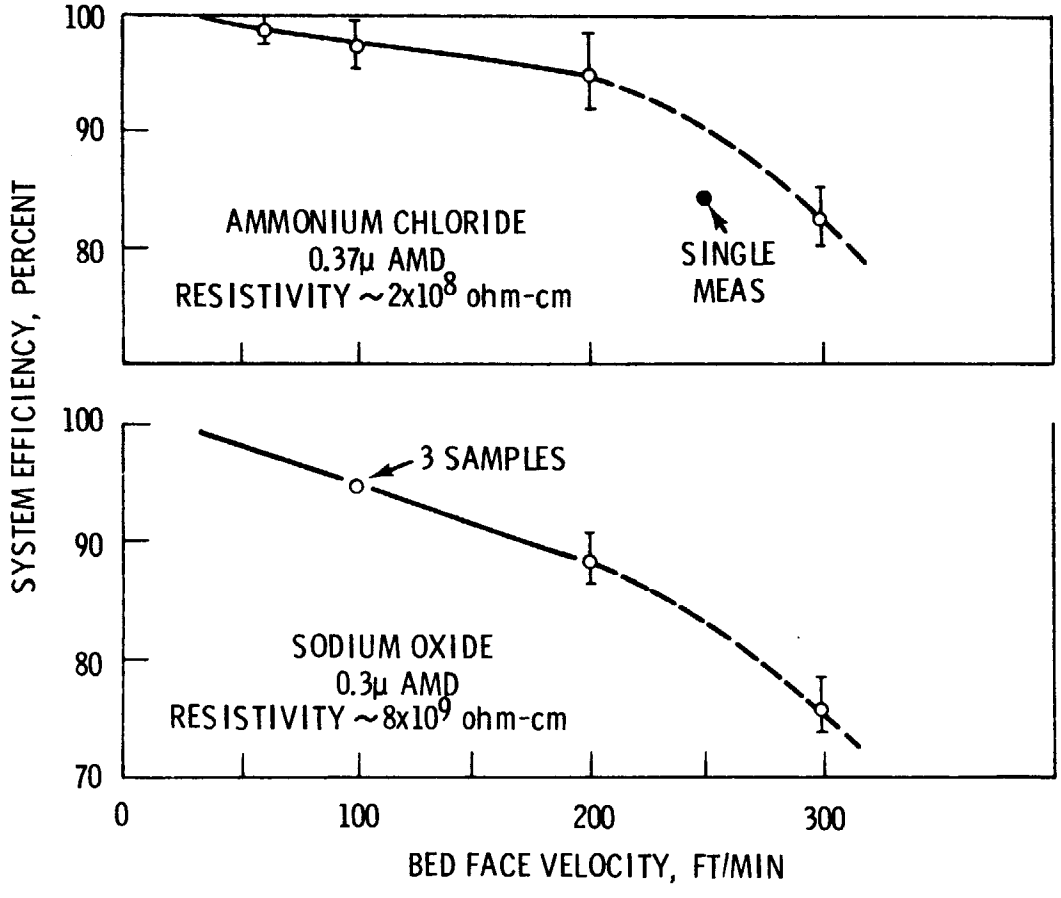

SYSTEM EFFICIENCY VS FLOWRATE
6" POLYPROPYLENE BED
0.96 VOID FRACTION

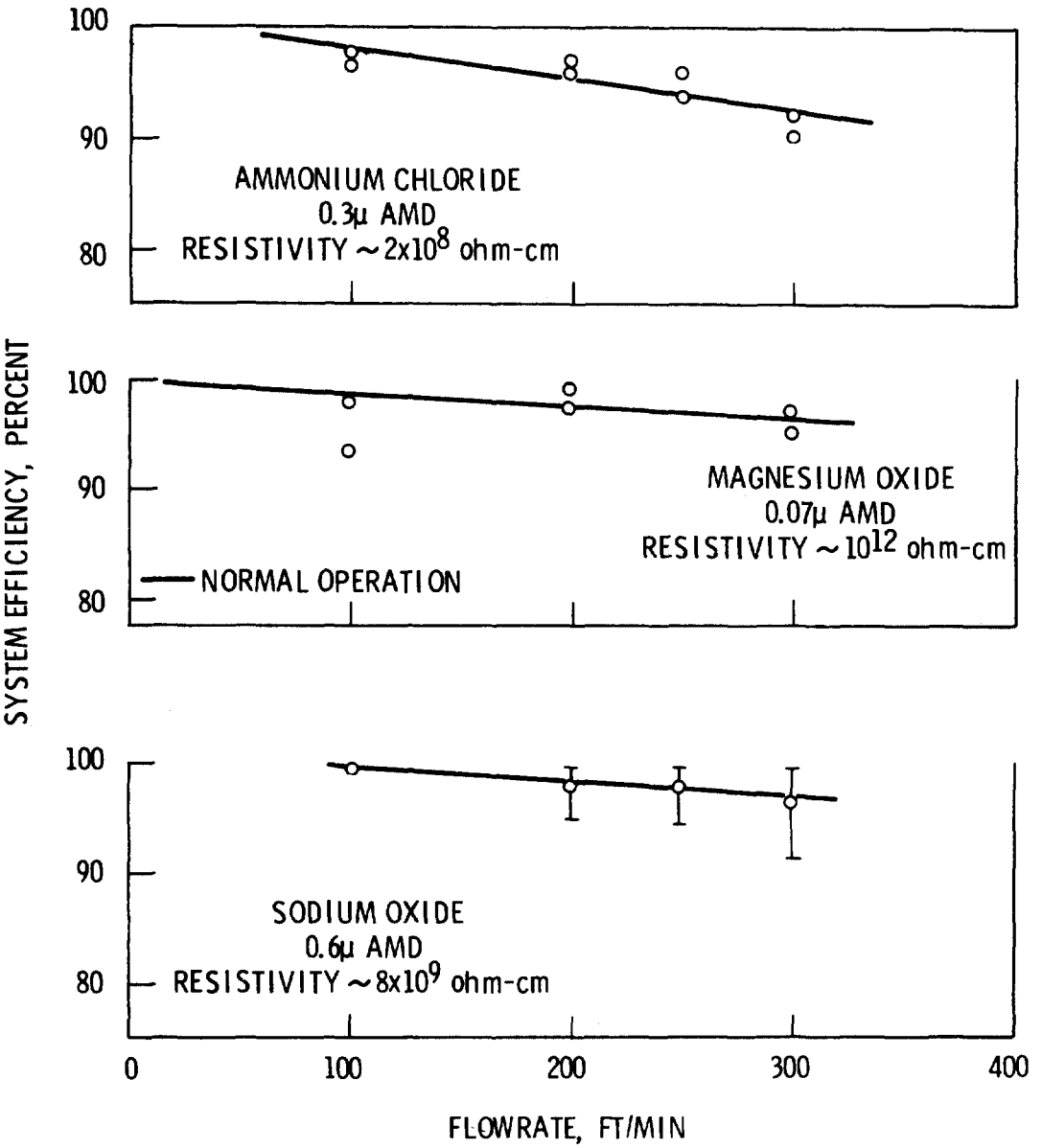

SYSTEM EFFICIENCY VS FLOWRATE
12" THICK POLYPROPYLENE
GRADED BED VOID FRACTION

FIGURE 3

The low point at 100 ft/min (∿50 cms/sec) for MgO appears to be one of those "fliers" that occur now and then without any apparent explainable reason. However, with a statistically significant number of tests, these generally fall out as "outliers". Consequently, it was not used in the linear regression analysis. Although this value was not used, the data indicate an efficiency less than 100 percent at zero flow -- not very probable. This suggested that these last two measurements in the run series at 100 ft/min (∿50 cms/sec) flow were probably on the low side.

The average efficiency for NH_4Cl was lower than that of MgO or Na_2O by about 2 to 5 percent over the range of 100-300 ft/min (∿50-150 cms/sec) face velocity. This is the first data that might confirm the model's prediction that efficiency should decrease with decreasing resistivity. Since the bulk of the data does not indicate a like trend, final judgment is reserved until a statistically significant number of measurements are completed. Also bearing on the reservation is the lack of any discernable difference in the bed field charge, inferred from current measurements, between the three aerosols used. Thus, it is not unlikely that significantly lower efficiencies would be observed only for a much more conducting particle and the threshold for this effect would occur at a lower resistivity than the 10^8 ohm-cm of NH_4Cl. The linear equations for the lines, Figure 3, are shown in Table II. All equations, except that for MgO, indicate 100 percent efficiency will be attained at some velocity lower than 50 ft/min (∿25 cms/sec).

TABLE II

EMPERICAL EQUATIONS OF EFFICIENCY

Particle	6" Bed - <200 ft/min	12" Bed - <300 ft/min
Na_2O	E = 101.5 - 0.065V	E = 100.91 - 0.0116V
MgO		E = 99.8 - 0.0116V
NH_4Cl	E = 100.513 - 0.028V	E = 101.286 - 0.0283V

Where E = Efficiency in Percent and,

V = Superficial Bed Velocity - ft/min.

Aerosol Decontamination Factor

The calculated decontamination factors for both the 6 in. and 12 in. beds are plotted as a function of velocity in Figure 4. The data approximate the expected relationship with the log of the decontamination factor varying linearly with the power of the velocity. For the 6 in. bed, all data were considered to be from the same population for the least squares fit which is represented by the solid line. This appears to be a reasonable assumption since the coefficient of determination was 0.9 and all data fell within the 2σ limits of sampling and measurement errors. Consequently, the fitted equation probably represents a reasonable average for the experimental conditions.

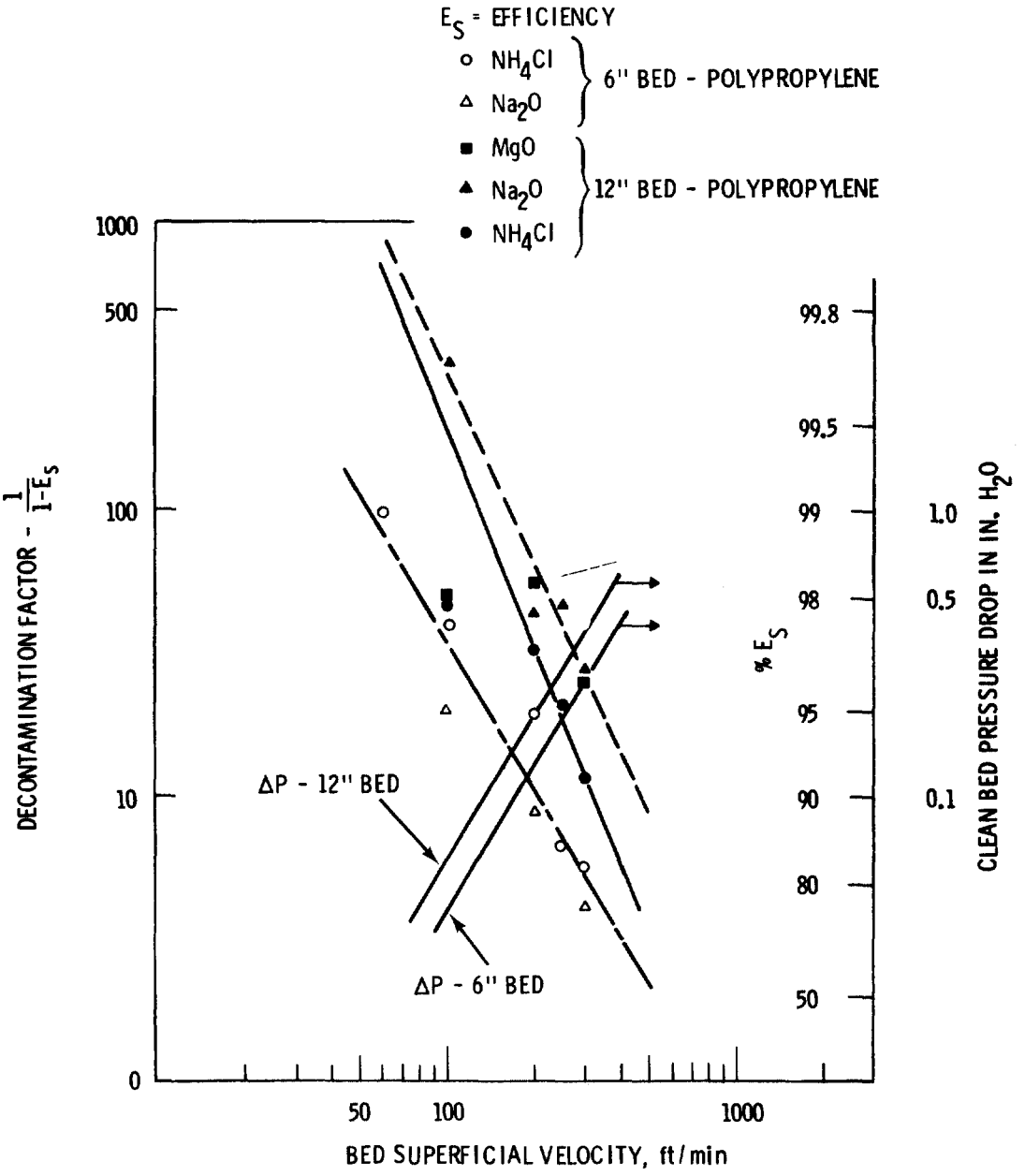

FIBER BED DECONTAMINATION FACTORS

FIGURE 4

For the 12 in. bed, the log-log plot of the data suggests a real, although small, difference in the bed efficiency for NH_4Cl particles compared to that for Na_2O and MgO and were segregated for calculation of the linear regression fit of the data while the Na_2O and MgO data were lumped together. The apparently anomalously low values for NH_4Cl and MgO (100 ft/min - 50 cms/sec) were the last samples taken in each series when the operating log noted leakage along the bed edges. Since it is unrealistic, based on the preponderance of data, that the efficiency should decrease with decreasing velocity, the bed leakage was assigned as the major cause for the low values which were not included in the curve fitting process. The pressure drop curves shown in Figure 4 are for the previously described void fractions in a clean state. The equations for the fitted curves are contained in Table III.

TABLE III

DECONTAMINATION FACTOR EMPIRICAL EQUATIONS
(New Wind Tunnel)

Fiber Bed	Partical Type	Partical Size	
6 in. V.F. - 0.956	NH_4Cl	∿0.3	$D_f \cong (9.5\times10^4)V^{-1.72}$, $r^2 = 0.9$
	Na_2O	∿0.25	
12 in. V.F. - 6 in. at 0.975	NH_4Cl	∿0.25	$D_f \cong (2.12\times10^7)V^{-2.52}$, $r^2 = 0.99$
and 6 in. at 0.956	MgO	∿0.06	$D_f \cong (7.8\times10^6)V^{-2.21}$, $r^2 = 0.97$
	Na_2O	∿0.25	

Three Inch Thick Fiber Bed

Since the efficiency appeared to be dependent upon fiber density as well as the demonstrated dependence on thickness, a run series was made with the NH_4Cl aerosol using a 3 in. thick bed packed to a void fraction of 0.946 -- the maximum packing density that could be restrained by the grid wires to a 3 in. dimension. Also, a folded fiber mat was placed along each bed edge in an effort to reduce the leakage along the frame and extend run time to edge breakthrough. In this test series a minimum of four successive measurements were taken at one system flow rate before altering the conditions and at 100 ft/min (∿50 cms/sec) face velocity and about 75 mg/M^3 aerosol particle load, twenty, thirty-minute samples were taken over a thirteen hour period.

The equation developed from the least squares fit of the efficiency versus velocity was

$$E_S = 102.8 - 0.0514\ V$$

where E_S = system efficiency in percent and,
V = bed face velocity in ft/min and,
$r^2 = 0.986$.

The plot of the decontamination factor vs. velocity (Figure 5) again shows the expected relationship with relatively good agreement as indicated by the 0.94 coefficient for the lease squares fit. The average values for each velocity are plotted along with the 95 percent confidence levels. The equation developed from the least squares fit was

$$D_f \cong (3.87 \times 10^7) V^{-2.74}$$

where $D_f = \frac{1}{1-E_S}$, dimensionless and

V = bed face velocity in ft/min.

Comparatively, this thinner bed with a lower void fraction exhibited an efficiency about equal to the 6 and 12 in. beds at 100 ft/min (∿50 cms/sec) flow rate and was about 5 percent higher and lower than the 6 and 12 in. beds at 300 ft/min (∿152 cms/sec) flow rate. The initial pressure drop across this bed was slightly higher and lower than the 6 and 12 in. beds.

This test illustrates that for low flow rates and low aerosol load the thinner bed would have a practical application. The dependency of efficiency on both the fiber bed thickness and density was demonstrated but not in sufficient detail to develop a mathematical relationship.

Six Inch Thick Stainless Steel Bed

The series of experiments leading to the discovery of this concept suggested that an electrically non-conducting fiber bed was required to obtain the observed high collection efficiencies. To support this idea, a conducting bed of stainless steel was tested under equivalent conditions. As suspected, the efficiencies obtained were very low, between 35 and 43 percent at 350 and 50 ft/min (∿175 and 25 cms/sec), and approximated that calculated for collection due to image forces under the test conditions.

Bed Loading Runs

Data collected during two NH_4Cl loading runs at 100 ft/min (∿50 cms/sec) face velocity are shown in Figure 6A for a clean bed at the start of the run and Figure 6B which started with a partially loaded bed from the previous day's tests. Obviously, the scatter in the data was greater at 50 mg/M^3 aerosol concentration than at twice that concentration. As discussed previously, this scatter in the data was ascribed to the sensitivity of the mass measurement for the downstream sampling position which was hovering around the

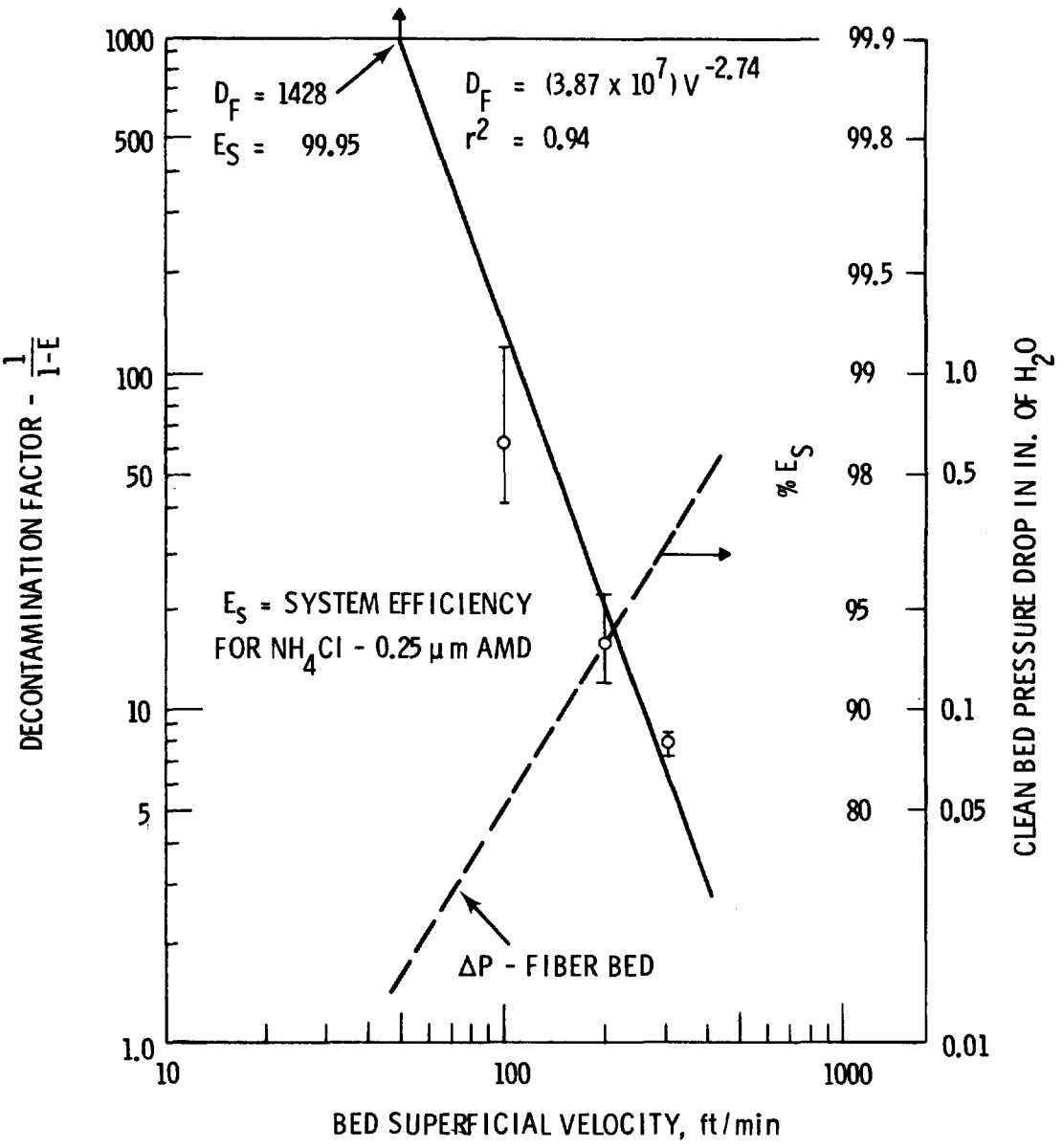

DECONTAMINATION FACTOR FOR FIBER BED
3 INCH POLYPROPYLENE - 0.946 VOID FRACTION

FIGURE 5

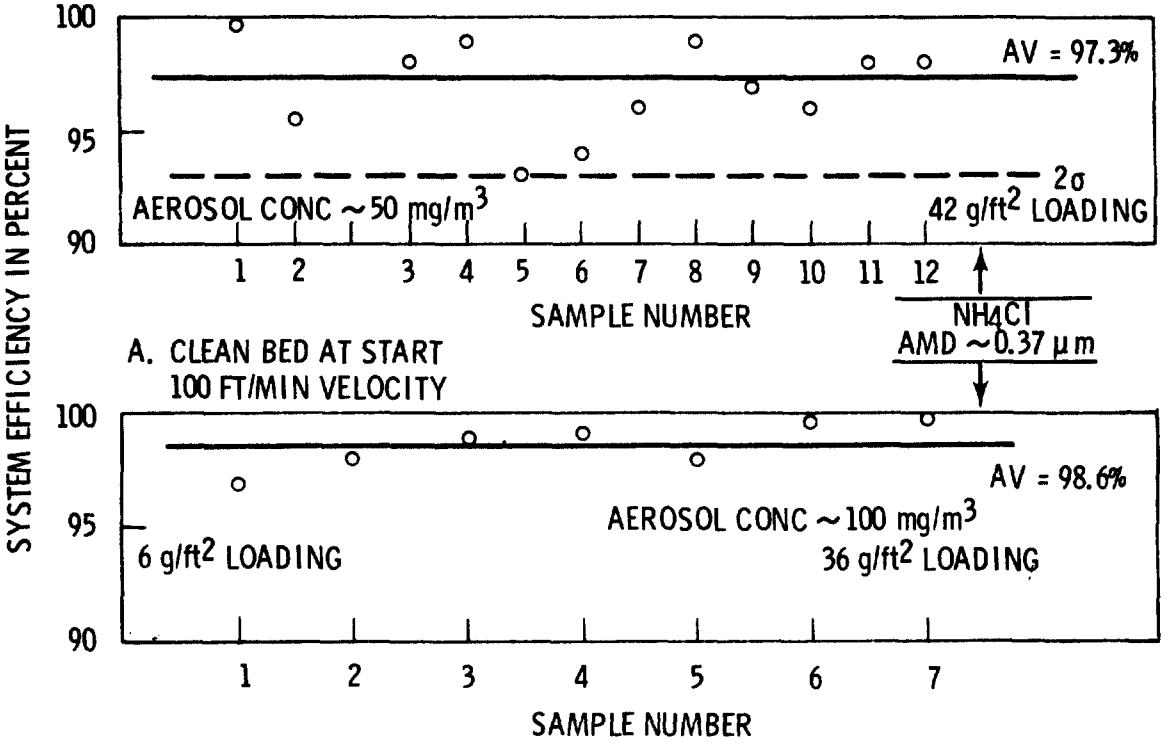

EFFICIENCY VS LOADING - 6" BED
0.96 VOID FRACTION

FIGURE 6

balance sensitivity at these high efficiencies and aerosol concentrations. Although the averages appear to be different, it is thought to be principally an artifact of the sensitivity rather than a real difference since differences in the efficiency due to aerosol concentration over the range tested were not discernable. There appears to be a slight trend for the efficiency to increase with bed loading, Figure 6B, which was also observed with other loading runs made at a constant velocity.

Pressure Drop Increase

The increase in pressure drop with bed loading appears to be predominantly a function of both the bed void fraction and particle characteristics which apparently influence the predominant plane of deposition perpendicular to the flow, at least for the submicron size range. The aerosols of 2 μm AMD size and above may also influence depth of penetration into the bed. The velocity of air flow might also be a factor in directing the depth of penetration but cursory visual observations indicate that it would be of a second order magnitude. This later impression was obtained from the NH_4Cl aerosols over a flow range of 50-300 ft/min (∿25-152 cms/sec). For these tests, visual inspection did not reveal any dramatic change in the plane of principal deposition which would have been required to be discernable. This is also supported to a degree by the much faster pressure drop increase for the higher flow rates under equal aerosol concentrations. Specific tests to define the effect of velocity on the pressure drop-bed load relationship have not been made. Relative comparisons, for a bed void fraction of 0.96, 100 ft/min (∿50 cms/sec) face velocity and an approximately equal pressure drop increase from 0.08 to 0.3 in. of H_2O, gave bed loadings of about 540, 650 and 970 g/M^2 for approximately 10^8, 10^{10} and 10^{12} ohm-cm particle resistivities having nearly equal AMD's.

For non-characteristic aerosols, like the ones used, any tests defining the load - ΔP - VF relationship would be of academic interest only. The information obtained to date suggests that for industrial applications, particle characteristics, principally resistivity and concentration and secondarily size, as well as the control system operating conditions are necessary to optimize the efficiency, cleaning frequency and area of the fiber bed.

Pictures of a loaded bed, Figure 7, show the upstream and downstream faces of a fiber bed loaded with NH_4Cl particles. The pictures are somewhat deceiving since the front face gives the appearance of being plugged. However, the pressure drop across this 12 in. thick bed under this particle load of ∿80 g/ft^2 (860 g/M^2) was about 0.6 in. of water at 300 ft/min (∿150 cms/sec) face velocity. Although not readily visible, there was a very slight deposit on the rear face fibers and support wires which demonstrates the effectiveness of this filtration concept.

Electrical Properties of Bed

The electrical properties of the bed could only be inferred from the leakage current of the bed and from the screens positioned on the upstream and downstream bed faces. The bed leakage current

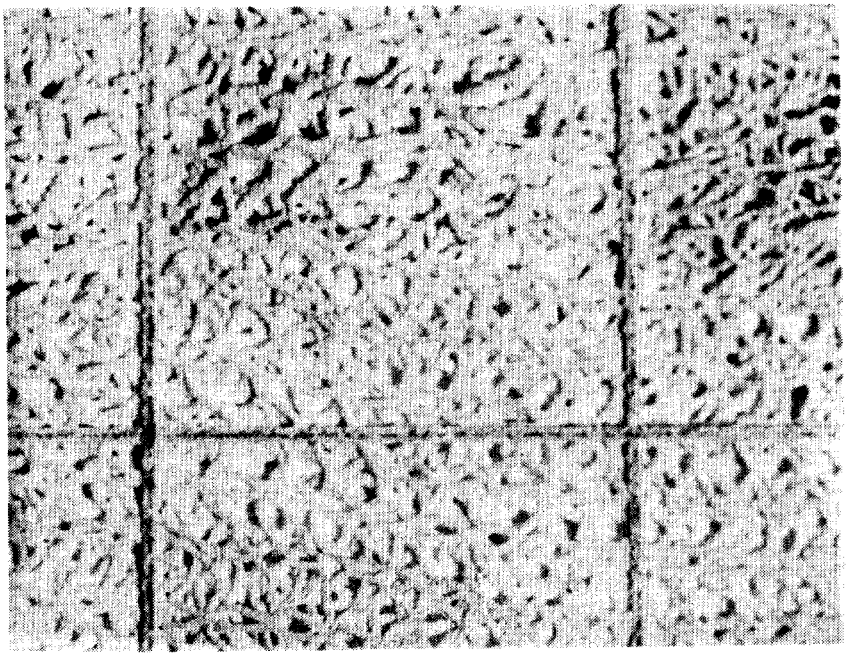

UPSTREAM FACE

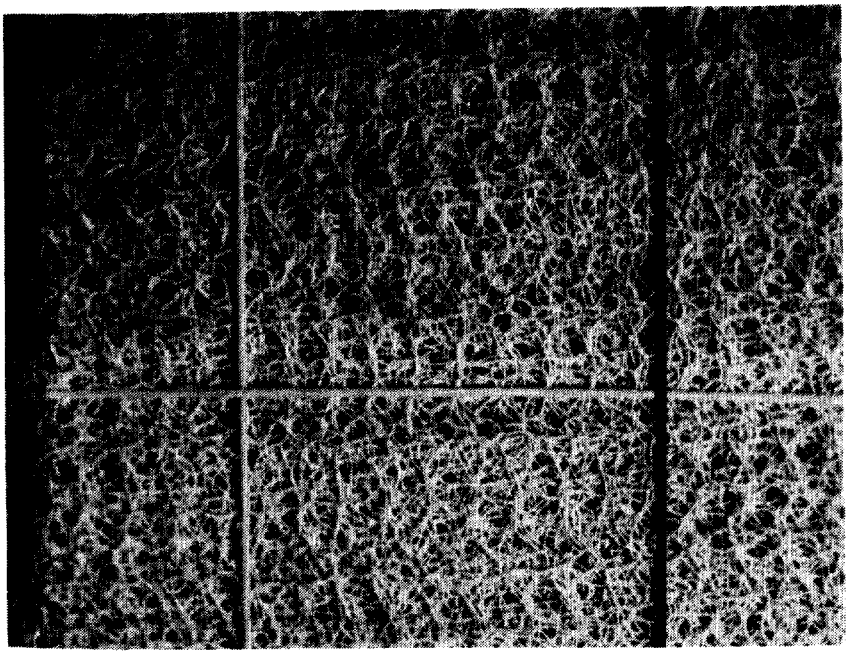

DOWNSTREAM FACE

FIGURE 7 12" Polypropylene Fiber Bed - NH_4Cl Load ∿80 g/ft^2

was obtained from a bare wire encompassing the bed at the frame-bed interface. A single wire was found to produce the same leakage current as a full width aluminum foil. From the measured leakage current of the bed and the four screens, the space charge of the bed built instantaneously upon activation of the charger to about a factor of ten less than that observed during particle generation and deposition and increased proportionally with flow rate. This suggests that molecular ion or charged Aitken nuclei deposition produces a significant contribution to the bed field charge and impaction of charged particles is not required to initiate the action. The charge varied with mass per unit time depositing on the filter but only by about a factor of five over the range tested (10-150 mg/M^3). At any one particle deposition rate the space charge increased immediately by an order of magnitude and then remained constant indicating that charge leakage from the bed was equal to that being deposited with the particles.

By assuming that the charge distribution in the bed is directly proportional to current measurement, some inferences relative to its shape can be made from the current measurements of the planted screens. For the 6 in. bed, there is an order of magnitude decrease between the front and rear face which prevailed throughout the run and was present with or without particle deposition. This suggests essentially an instantaneous equalization of the charge deposited by the particles. The field charge distribution transverse to the flow appeared to be uniform within the rather approximate measurements resulting from the fluctuating meter. The above observations prevailed also for the 12 in. thick bed except the average reduction in the inferred field charge front to rear was about 20 and was more variable than for the 6 in. bed.

It was observed from the runs where electrode shunting occurred and the charger current increased continuously throughout the test from 18 to 21 ma that the inferred field charge decreased to about one fourth of the initial charge in addition to that expected from particle concentration variations. Although not a sensitive indicator, it confirmed the suspected reduced particle charging efficiency from electrical shunting in the charger and the related lower system efficiencies discussed previously.

Summary and Conclusions

The efficient removal of charged submicron particles from flowing gas streams with a bed consisting of fibers having a high dielectric constant was demonstrated experimentally. Although not all of the facets of operation for optimization of the concept have been explored in detail, the tests conducted to date suggest many practical applications for relatively economical particle control not attainable with presently available concepts. Based on mass measurements, the emperical equations developed from the data collected to date indicate a 100 percent collection efficiency at some face velocity below 50 ft/min ($\sim$25 cms/sec). Other observations from the information accumulated to date were as follows:

1. Velocity was the prime variable with respect to efficiency. For the 6 in. thick bed, the efficiency decreased linearly with increasing velocity up to about 200 ft/min (∿100 cms/sec) bed face velocity. The minimal data beyond this velocity are suspect and need redefinition. For the 12 in. thick bed the linear relationship existed up to the highest flow rate tested of 320 ft/min (∿160 cms/sec). Both produced efficiencies above 90 percent at the above-stated flow rates for the submicron particles used.

2. Bed thickness apparently had a pronounced effect on collection efficiency. However, bed thickness and fiber volume density are dependent variables as evidenced by the compressed 3 in. bed which showed a higher efficiency than the 6 in. bed having a slightly higher void fraction. Although not directly comparable due to void fraction differences the 12 in. filter showed about a 10 and 2 percent higher efficiency than the 6 in. bed at 300 and 100 ft/min (∿150 and 50 cms/sec) face velocity. This difference in the slope of the curves suggests a deeper penetration with increasing velocity which appears reasonable providing all other conditions are equal. Thus the ratio of the efficiencies (12 in./6 in.) should increase with velocity for equivalent particle characteristics.

3. Particle Size. Although not a prime variable, there was no detectable influence on efficiency over the range tested -- ∿0.06 to 0.83 μm AMD. The stated AMD's are thought to be high due to the uncertainty of extrapolation from about 90 to 50 percent of the log normal plot.

4. Pad Resistivity. There was no discernable difference between polypropylene or teflon fibers with respect to efficiency and apparent field charge strength and shape. The principal criteria for a fiber are that it be electrically non-conducting and have a significantly larger diameter than the submicron particles. A 6 in. thick stainless steel demister pad produced very low collection efficiencies -- about equal to that expected for image force collection.

5. Particle Resistivity. The majority of the data indicated there was no significant trend in collection efficiency over the range of approximately 10^8 - 10^{12} ohm-cm particle resistivity. Since one test series showed a slightly lower efficiency for the 10^8 ohm-cm NH_4Cl and the model suggests that efficiency should decrease with decreasing particle resistivity, particles with a much lower resistivity should be studied to better describe any differences and establish the lower boundary limit, if one exists. The depth of particle penetration into the bed was directly related to particle resistivity.

6. Dust Concentrations. Particle concentrations ranging from 10 to 250 mg/M^3 were used without any significant differences except for the apparent higher field charge for the higher concentrations. Since measurement reproducibility increased and length of test time varied inversely with concentration, most of the new wind tunnel tests were made at 50-100 mg/M^3 dust loading.

7. Particle Charge Level. The fraction of uncharged particles challenging the filter is apparently more pertinent to the success of the concept than the charge level of the particles at least if near saturation charge is obtained. As would be expected, the bed had no affinity for uncharged particles at the higher velocities and showed about 8 percent retention at 50 ft/min (∿25 cms/sec). The instrumentation used was not sensitive enough to provide the refinement required to accurately define the fraction of uncharged particles downstream of the charge section. Consequently, valid information is not available on the ratio of charged to uncharged particles reaching the filters. However, the efficiencies obtained indicate that the uncharged particles must have been a very small fraction of the total particle load. Faraday cage measurements indicated both near and supersaturation charge of the particles. The variability of the data is believed to be a function of the measurement of small currents in the presence of relatively high electrical fields and very little credence is given to the data.

8. Humidity. No attempts were made to study humidity of the aerosol as a variable. The maximum relative humidity observed during the experiments was 50 percent and generally hovered between 30-40 percent. Consequently, no generally applicable effects of humidity were discernable. For the special case with Na_2O particles, humidity in excess of about 45 percent produced a degraded operation. The principal cause for the loss of efficiency, particle charging or bed collection or a combination of both, was indeterminant.

Acknowledgments

The authors wish to acknowledge the assistance of co-workers D. A. Nelson for his experimental work and D. L. Lessor for discussions on the mathematical modeling of the phenomenon.

DISCUSSION

ETTINGER: Did you perform, or do you plan to perform any tests to indicate what the effect of high humidity air will be on the collection efficiency?

REID: We feel that this should be done. We have not been able to do it up to this point. We had one test in which we were using sodium oxide and the humidity in the room increased to about 47 per cent. We created sodium hydroxide from this and quite a mess internally. The efficiency under that condition decreased from about 85 per cent down to 72 per cent over a period of about seven hours. We feel humidity needs to be investigated. However, if the humidity is not sufficient to give us a conducting fiber, we do not feel it will have any significant effect. Another important part of this system is that it can be cleaned easily. You don't have to remove it to clean it.

UNDERHILL: The previous question almost answered the question I had. How much moisture pickup was there during the course of your experiments and was the aerosol basically oxide or was it sodium hydroxide? Thermodynamic equations lead me to believe that it was NaOH or Na_2CO_3.

REID: It's pretty dry at Hanford. Most of the time, humidity was running about 35 to 40 per cent during the test. We're not certain whether we had sodium oxide or sodium carbonate. We did not have sodium hydroxide until we reached a humidity above 45 per cent, then we developed sodium hydroxide. This we were certain of from resistivity measurements.

UNDERHILL: Phase diagrams of sodium hydroxide and sodium carbonate as a function of relative humidity might be of interest to you.

FIRST: We've been doing experiments with sodium aerosols, also, and we find particle sizes almost on order of magnitude larger than you are reporting for the concentrations that we are dealing with. Our relative humidity for these experiments was 20 per cent. This certainly corresponds with yours. Could you tell us how you determined the size?

REID: It was with an Anderson Cascade impactor sampler. Possibly, the way we generated the particle would account for the different sized particles. We don't believe that particle size is normally distributed by the method in which we generated the particles because we were getting about 90 per cent of the particles on the filter paper downstream in the last stage. So, the particle sizes stated in the paper are probably larger than what we actually had. We saw no relationship between efficiency and particle size over the particle size range from .06 to about .7 μm AMD. We need a better method of measuring particle size when you get down into this range.

RIVERS: An earlier question suggested that the conductivity of the fiber bed might be a significant factor in the performance of the filter. It may be, but I would guess that a conductive fiber bed would be better than a dielectric fiber bed. The reason is that if particles captured in the bed retain their charge, they would tend to repel similarly charged particles later. Fields within the fiber bed voids can be produced by the space charge of uncaptured particles - and dielectrophoretic forces exist between a charged particle and a grounded fiber. A conductive fiber bed could be considerably less flammable than a plastic fiber.

AIR FILTRATION ENHANCEMENT USING ELECTRONIC TECHNIQUES*

G. O. Nelson, C. P. Richards, A. H. Biermann,
R. D. Taylor, and H. H. Miller
University of California, Lawrence Livermore Laboratory
Livermore, California 94550

Abstract

Dielectrophoretic filtration experiments were conducted on glass, polyester, dacron, Teflon, wool, acrylic and polypropylene filter media. A polydispersed (σg = 2.0, ammd = 0.95 μm) sodium chloride particle was used as a test aerosol. All materials exhibited significant increases in efficiency with increasing field strengths. Efficiencies of >99% could be obtained from glass fiber mats using a 13 kV/cm electric field at 16.3 cm/s face velocity.

I. Introduction

High-efficiency particulate air (HEPA) filters are commonly used at radioactive handling facilities to remove airborne contaminants. A survey by Cooley indicated that approximately 16 000 HEPA filters were used in the United States in 1973[1]. Although the original cost averages $150/filter, the total expense to buy, install, test, remove, decontaminate and dispose of the filter has been estimated to be three to ten times the initial filter cost[2],[3]. Hence, a significant savings could be realized if filter service life could be extended.

A number of approaches were considered. Most of these were focused on the design of an adequate prefilter rather than some modification of the HEPA filter. Inertial devices such as cyclones or impaction plates would probably be inappropriate because of the small particle size usually encountered (typically 0.05-5 μm)[4],[5]. Wet- and foam-type scrubbers, although efficient for submicron particles, generate too excessive liquid wastes to be practical.

The direction which appears to show the most promise is the dielectrophoretic or non-ionizing electrostatic air filter[6],[7],[8]. This involves placing a non-conducting filter media between two perforated metal plates maintained at a potential difference of 5-10 kV/cm. The media distorts the electric field and creates higher field intensities near the individual fibers. When a particle enters the electric field, it is polarized and attracted more effectively toward the locations of highest field intensities. Power requirements are generally quite low (typically less than 1 μA) when compared to conventional electrostatic precipitation techniques since particle charging is not required. However, any net charge present on the particle or filter media which occurs naturally or is induced from small current leakages only serves to enhance an already powerful particle-fiber interaction.

*This work was performed under the auspices of the U.S. Energy Research & Development Administration, under contract No. W-7405-Eng-48.

The purpose of this investigation is to present the results from our dielectrophoretic filtration experiments using glass, carbon and polymeric filters tested with a polydisperse sodium chloride aerosol. This report is intended to be interim in nature since several crucial experiments involving filter configuration and particle charging as well as theoretical modeling calculations have yet to be completed.

II. Experimental

Aerosol Generator

Filters were tested using the apparatus shown in Fig. 1. The system consists of an air mover, a sodium chloride aerosol generation system, prefilter test section, and experimental diagnostic equipment.

Filtered air is drawn into the system by a high-volume air sampler, and the flow is measured using a mass flowmeter. A variable transformer between the sampler and the power source maintains the flow between 5 and 25 litres/s.

The aerosol is produced by using four air-driven modified Wright-type nebulizers, shown in Fig. 2. The nebulizer screws into a 500-ml polyethylene bottle containing a solution of dissolved salt. Air pressure supplied to the nebulizer aspirates the solution from the reservoir to the nebulizer where it is atomized into small droplets.

The droplets mix with air in the aging chamber, evaporate, and subsequently form a test mixture of cubical salt particles in a moving air stream. The resultant aerosol characteristics are a function of the airflow, nebulizer air pressure, solution concentration, and the number of nebulizers used.

Particle size characteristics using a 1% sodium chloride solution at a nebulizer pressure of 340 kPa show the aerodynamic mass

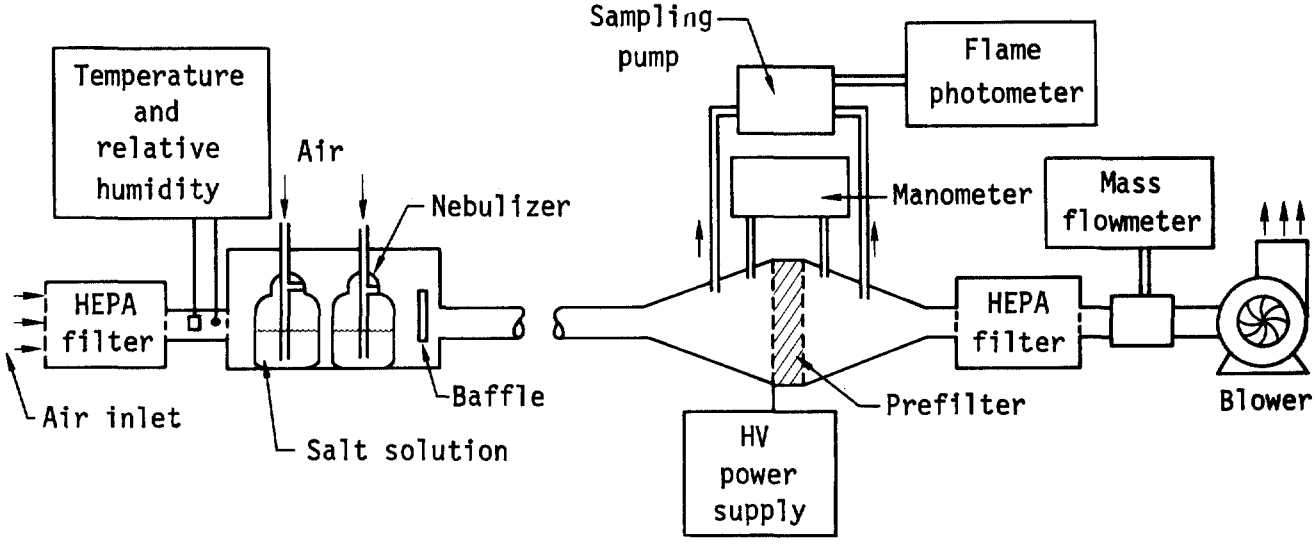

Fig. 1. Schematic Diagram of Aerosol generation system.

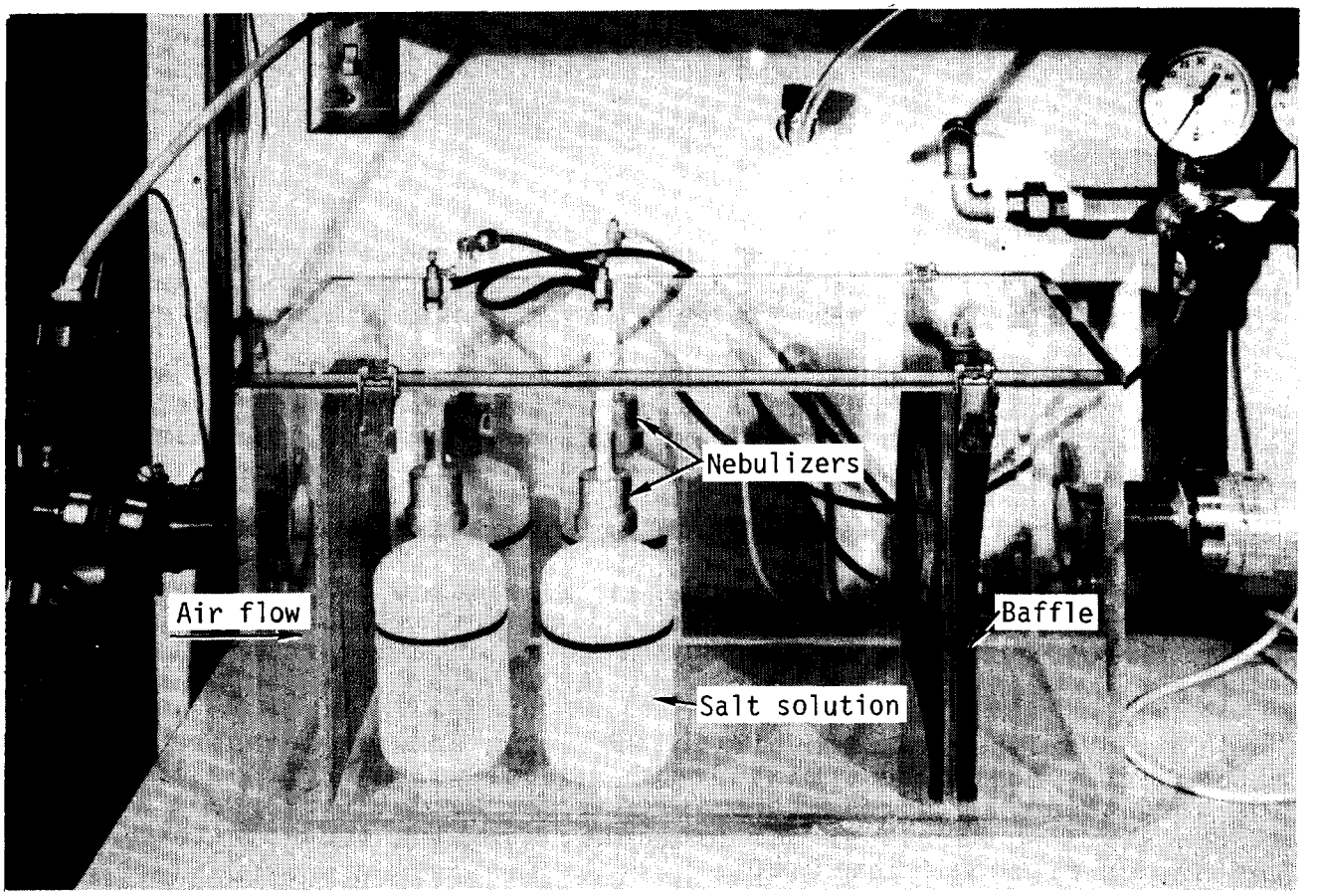

Fig. 2. Sodium chloride aerosol generation system. Four Wright-type nebulizers situated inside the aging chamber.

median diameter to be 0.95 μm with a geometric standard deviation of 2.0. The mass concentration using all four nebulizers at 23.6 litres/s is 4.5 mg/m^3.

System diagnostic equipment includes a flame photometer to determine filter efficiency and an electronic manometer to record pressure differential as a function of time. Relative humidity, temperature and air flowrate are monitored throughout the experiment.

Filter Testing Assembly

The dielectrophoretic filtration experiments were conducted in the test section located just in front of the HEPA filter. The disassembled test assembly is shown in Fig. 3. The 5-cm-diam duct expands to accommodate a 19.1- × 19.1-cm-square filter. The filter is held between two 0.5-mm-thick perforated stainless steel plates (29% open) spaced 13 mm apart by two polyethylene spacers. A negative d.c. high-voltage lead is connected to the front screen, and the rear screen is grounded.

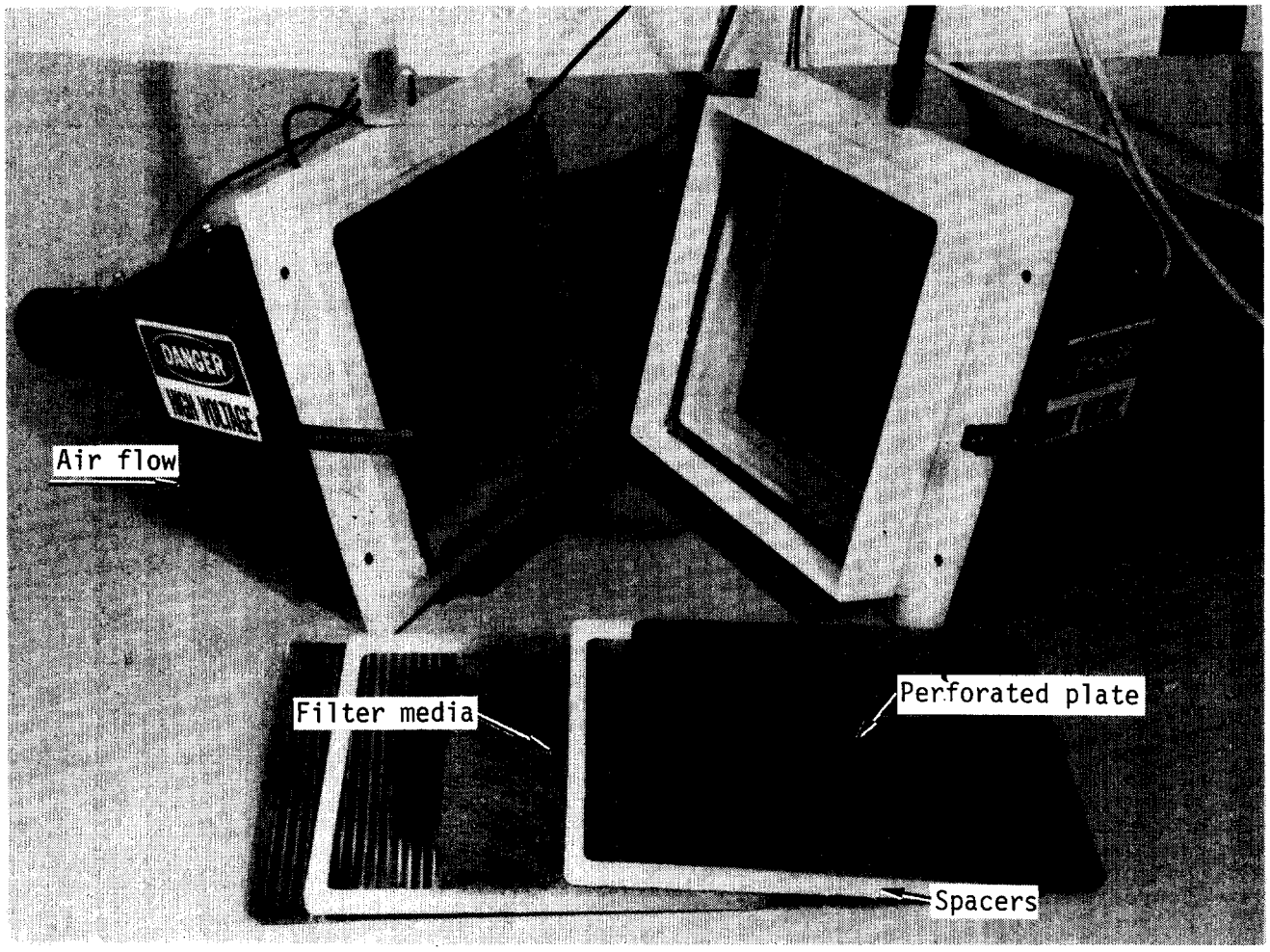

Fig. 3. Disassembled filter test section.

The 33 filtering media shown in Table 1 were tested between the electrified perforated plates. Testing was normally conducted at face velocities of 65 cm/s. However, a glass and a polyester filter were tested at face velocities of 16.3, 32.5, 48.8 and 65 cm/s.

The efficiency was measured at voltages ranging from 0-15 kV, and the pressure differential was monitored throughout the testing period. The enhancement coefficient (the ratio of the dielectrophoretic-to-initial efficiency) was then calculated.

Table I. Characteristics of filter media.

Run No.	Fiber Material	Designation	Source	Uncompressed Thickness (mm)
5A	Glass Mat	Aeroglass	Alfco Products[b]	16
9	Glass Mat	High density	Dow Corning	7
13	Glass Mat	FM 004	Owens Corning	7
14	Glass Mat	Type C	Owens Corning	18
15	Wood-Polypropylene Mat	50%/50%	Globe Albany	4
17	Wool-Acrylic Mat	50%/50%	GAF	4.8
18	Glass Mat	AU-300	Owens Corning	12.5
20	Teflon Mat	Armalon XT 2663	Dupont	2
21	Polyester Mat	#5/8-in.	Filpaco	16
22	Glass Mat	Packing material	Owens Corning	12
23	Glass Batting	Basic filtration fiber	Owens Corning	70-90
24	Glass Mat	High density	Dow Corning	6-8
25	Glass Mat	Commercial filter media	Owens Corning	20
26	Glass Mat	Dust stop filter media	Owens Corning	16
27	Glass Mat	Microlite Insulation	Johns Manville	28
28	Glass Mat	Microlite Insulation	Johns Manville	14
29	Glass Mat	Type A	Owens Corning	20
30	Glass Mat	FM 060	Owens Corning	1-2
31	Teflon Mat	XT 2363	Dupont	2
32	Glass Mat	U-trim-it	Owens Corning	4-5
33	Carbon[a]Mat	1/8-in	Fiber Materials Inc.	4
34	Polyester Batting	—	Fabco	4-4
35	Dacron Batting	DA CH-101	Filpaco	4
36	Teflon Mat	XT 7600	Dupont	2-3
37	Glass Mat	Prefilter mat	Owens Corning	1
38	Polypropylene Fabric	222-013-17	National Filter Media	0.5-1
39	Glass Mat	B-100	Hitco	3
40	Glass Mat	Duct insulation	Owens Corning	14
41	Polyester Fabric	192-014-03	National Filter Media	1
42	Wool/Acrylic	50%/50%	J. C. Penny	1-2
43	Polypropylene Fabric	222-018-03	National Filter Media	1.5
44	Polyester Batting	—	J. C. Penny	15
45	Polyester Fabric	190-010-06	National Filter Media	0.3

[a]Glass fiber filter (Lennox, #30024, 40-mm uncompressed thickness) added to prevent shorting of carbon filter.

[b]Reference to a company or product name does not imply approval or recommendation of the product by the University of California or the U.S. Energy Research & Development Administration to the exclusion of others that may be suitable.

III. Results and Discussions

Effect of Filter Media

The ideal filter should have a relatively high initial efficiency and enhancement coefficient, but a low initial pressure and pressure drop growth. The results shown in Table 2 indicate that no filter media is outstanding in all four categories. However, glass (runs 14, 22, 23, 25, 26, 27, 28, 30, and 40), polyester (run 21) and dacron fibers (run 35) are all strong candidates. Woven fibers and teflon mats have high initial efficiencies, but their pressure drop growth is so rapid that they are unsuitable in this type of application. The polypropylene and polyester weaves used in runs 43 and 45 experienced such a rapid pressure drop growth that there was no time to ascertain its efficiency enhancement using the electric field.

Table II. Results of filter efficiency tests.

Run No.	Fiber Material	Initial ΔP (in. H_2O)	Rate of ΔP change (in. H_2O/hr)	Filter Efficiency - 1% (E_t)							Enhancement Coefficient $[(E_t-E_0)/E_0]$					
				0(E_0)	2 kV	4 kV	6 kV	8 kV	10 kV	12 kV	2 kV	4 kV	6 kV	8 kV	10 kV	12 kV
5A	Glass	0.45	–	1.9	3.8	5.7	9.5	11.3	15.1	17.0	1.0	2.0	4.0	5.0	7.0	7.9
9	Glass	3.76	2.07	25.0	27.5	35.0	38.0	40.0	–	–	0.91	1.40	1.52	1.60	–	–
13	Glass	1.35	1.51	94.4	94.6	94.6	94.7	94.9	95.0	–	0.002	0.003	0.003	0.005	0.008	–
14	Glass	0.055	0.01	14.4	17.6	19.7	22.0	26.5	27.2	30.5	0.22	0.37	0.53	0.84	0.89	1.16
15	Wool/ Polypropylene	0.98	0.66	68.7	72.7	76.6	78.7	80.8	80.8	80.3	0.06	0.12	0.16	0.18	0.18	0.17
17	Wool/ Acrylic	0.80	0.78	85.0	86.3	86.9	87.5	87.8	88.1	89.1	0.015	0.022	0.029	0.033	0.036	0.048
18	Glass	0.40	0.15	28.7	34.7	–	–	–[a]	–	–	0.21	–	–	–	–	–
20	Teflon	2.85	4.6	80.4	81.9	–	83.0[a]	83.5	–	–	0.019	–	0.031[a]	0.039	–	–
21	Polyester	0.092	0.012	12.3	17.2	21.4	25.6	29.0	33.1	36.8	0.40	0.74	1.08	1.36	1.69	1.99
22	Glass	0.502	0.144	37.1	42.5	51.5	59.4	64.8	68.7	70.8	0.15	0.39	0.60	0.75	0.85	0.91
23	Glass	0.165	0.0084	19.0	23.5	26.8	29.5	34.8	41.5	45.7	0.24	0.41	0.55	0.90	1.18	1.41
24	Glass	2.25	1.86	91.4	92.5	93.5	94.0	94.2	94.4	94.0	0.013	0.023	0.029	0.030	0.033	0.028
25	Glass	0.065	0.0045	13.9	14.5	15.9	17.9	19.7	21.1	22.6	0.10	0.20	0.36	0.49	0.60	0.71
26	Glass	0.069	0.005	9.6	11.5	15.2	17.2	19.4	22.5	24.7	0.20	0.55	0.79	1.02	1.3	1.6
27	Glass	0.49	0.13	45.6	51.9	62.1	70.2	75.6	78.8	81.3	0.14	0.36	0.54	0.66	0.73	0.78
28	Glass	0.23	0.070	27.6	30.7	39.5	44.9	51.5	58.1	62.2	0.11	0.43	0.63	0.87	1.1	1.39
29	Glass	0.070	0.010	9.6	10.6	12.4	13.7	15.3	15.7	17.3	0.10	0.29	0.43	0.59	0.64	0.80
30	Glass	0.10	0.046	14.8	14.8	17.4	18.7	21.0	21.1	–	0	0.18	0.26	0.42	0.43	–
31	Teflon	4.0	24	90.2	–	91	–	91	–	–	–	0.008	–	0.008	–	–
32	Glass	0.075	0.003	5.5	7.8	8.8	11.9	12.7	14.5	15.4	0.42	0.60	1.20	1.31	1.64	1.80
33	Glass/ carbon	1.32	1.1	46.1	47.2	48.4	–	–	–	–	0.024	0.049	–	–	–	–
34	Polyester	0.075	0.004	14.1	14.6	15.4	16.8	16.8	19.1	–	0.006	0.015	0.031	0.031	0.058	–
35	Dacron	0.42	0.05	27.5	29.3	28.8	31.3	31.6	34.4	–	0.07	0.05	0.14	0.15	0.25	–
36	Teflon	9.55	12.3	89.6	–	–	–	–	–	–	–	–	–	–	–	–
37	Glass	0.11	0.02	7.4	8.7	10.2	10.7	11.1	–	–	0.18	0.38	0.47	0.50	–	–
38	Polypropylene	1.35	2.6	62.0	62.7	62.9	64.0	64.6	–	–	0.01	0.01	0.03	0.04	–	–
39	Glass	0.58	0.074	40.3	41.4	43.0	44.4	46.1	49.9	–	0.03	0.07	0.10	0.15	0.24	–
40	Glass	0.23	0.04	30.6	41.0	54.0[b]	63.7	70.9[c]	75.0	79	0.34	0.76[b]	1.08	1.32[c]	1.45	1.58
41	Polyester	2.08	7.7	71.0	–	72.3[b]	72.8	73.2[c]	–	–	–	0.018[b]	0.025	0.031[c]	–	–
42	Wool/ Acrylic	0.42	0.08	34.0	35.3	35.0	39.9	42.4	–	–	0.04	0.03	0.17	0.25	–	–
43	Polypropylene	2.46	>10	–	–	–	–	–	–	–	–	–	–	–	–	–
44	Polyester	0.08	0.01	8.1	10.1	12.1	14.1	17.1	18.3	–	0.25	0.49	0.74	1.11	1.27	–
45	Polyester	2.11	>20	–	–	–	–	–	–	–	–	–	–	–	–	–

[a] 5 kV

[b] 3 kV

[c] 9 kV

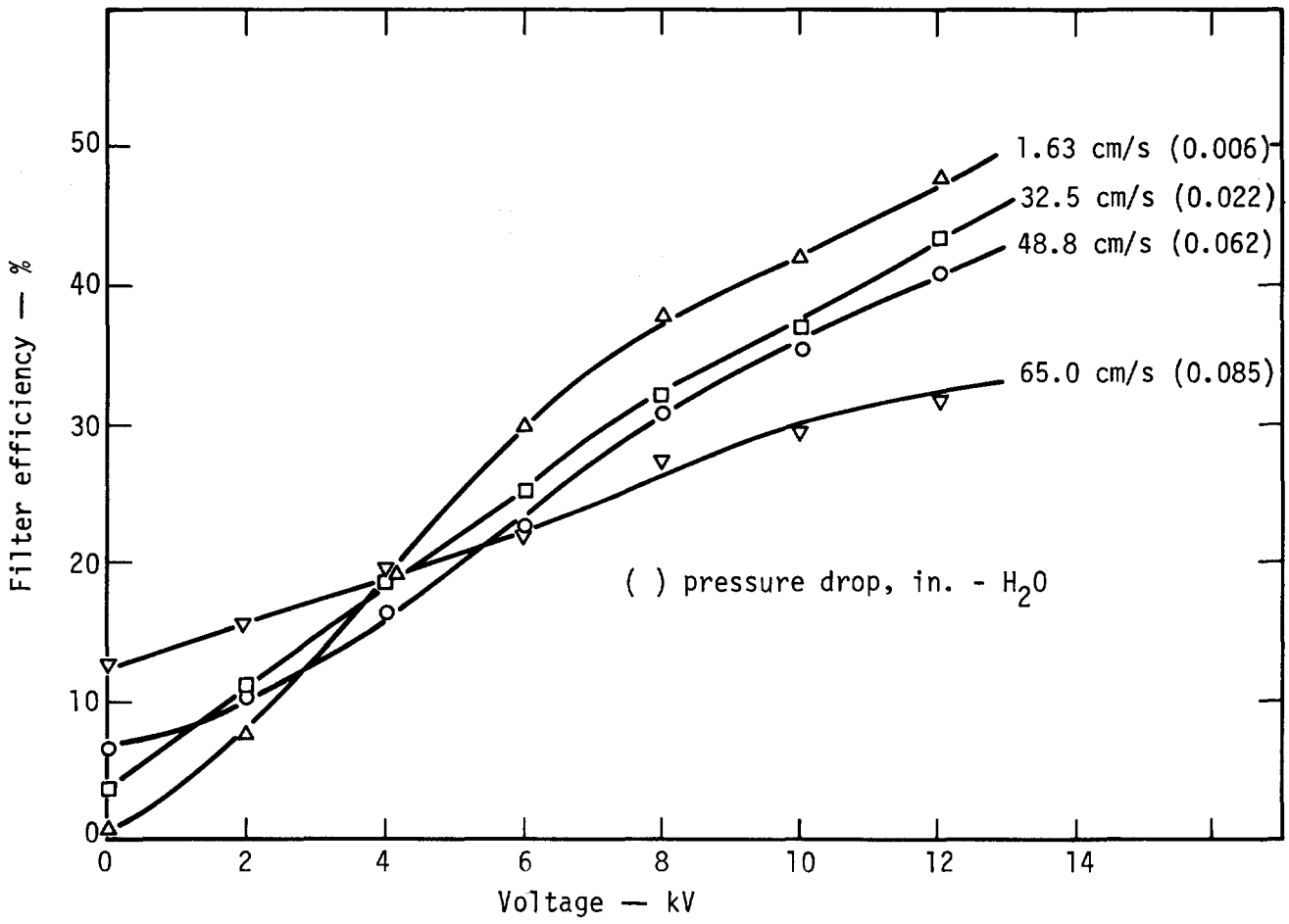

Fig. 4. Efficiency of polyester loft (Filpaco Ind #5/8-in.) as a function of voltage and face velocity.

Effect of Flowrate

Figures 4 and 5 show the efficiencies for polyester and glass fiber materials. Here the efficiency is shown as a function of applied voltage at various face velocities. With no voltage applied, the efficiency, as one might suspect, is greater with increasing face velocities. However, as the voltage between the plates is increased, the inertial component of the efficiency becomes less important and the electrical effects begin to dominate. At 16.3 cm/s, the efficiency of the polyester fiber is increased by a factor of 100 and the glass fiber increases from 29% to >99% when the voltage is increased from 0 to 12 kV. This behavior has also been observed by Fielding[6] and Borgardus[7] using a 0.3- and 1.0-μm DOP aerosol.

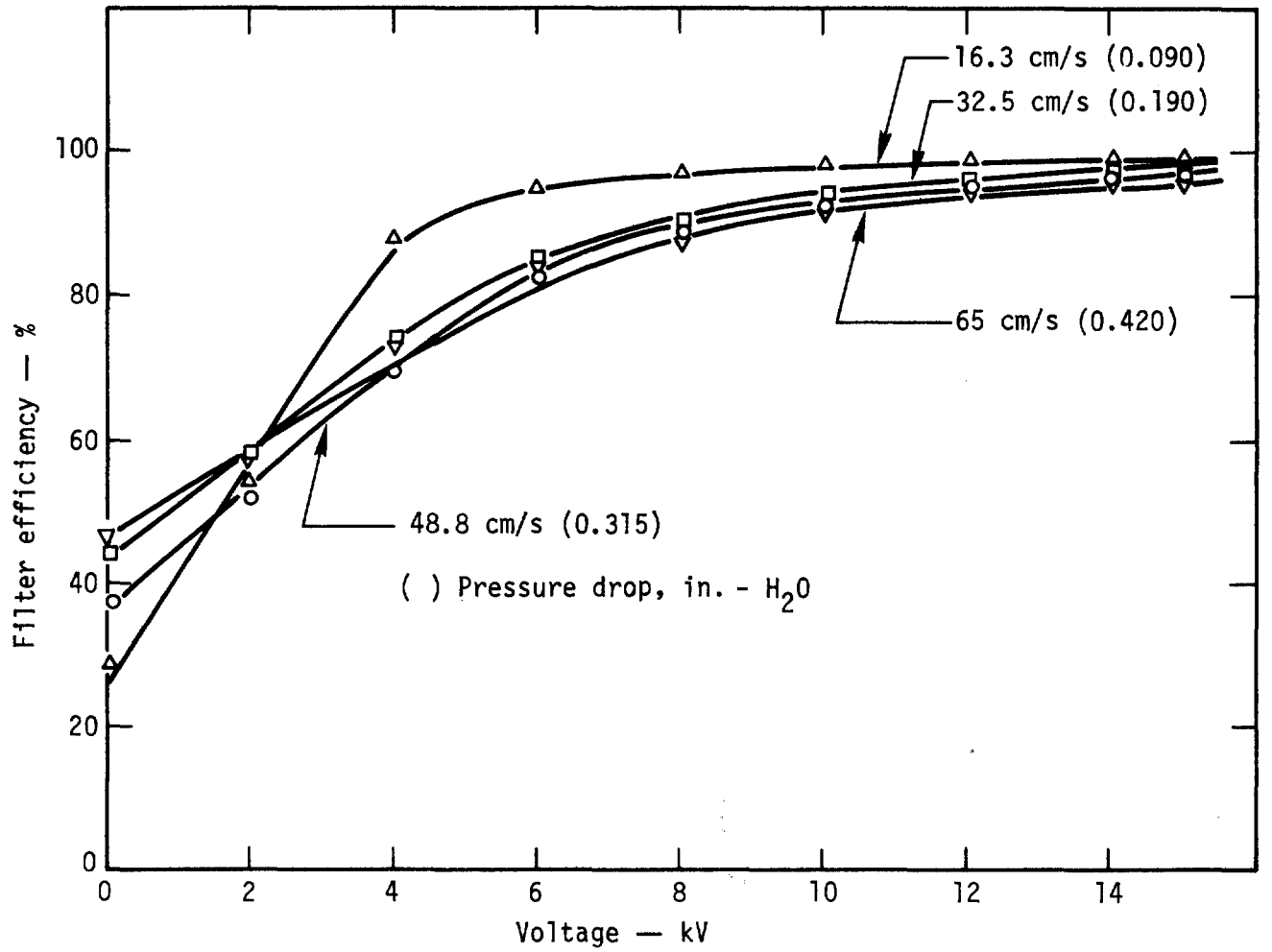

Fig. 5. Efficiency of fiberglass media (Johns Manville 1/2-in. Microlite Insulation) as a function of voltage and face velocity.

IV. Conclusions

All filter media tested with a polydispersed sodium chloride aerosol exhibited increased efficiency when placed in an electric field between two perforated plates. Glass fiber beds achieved the highest efficiency (>99% at a face velocity of 16.3 cm/s) and appear to be the best media based on initial efficiency, pressure differential, enhancement coefficient, and fire resistance. Future experimental work will include determining the effect of plate design, filter configuration and particle charge on filter media efficiency.

References

1. Cooley, C. R., "Commercial Alpha Waste Program Quarterly Progress Report," July-September 1974 HEDL TME 74-61, UC-70 (Nov 1974).

2. Lipera, J., Lawrence Livermore Laboratory, private communication.

3. Bolton, N. E., Oak Ridge National Laboratory, private communication.

4. Ettinger, H. J., Elder, J. C., Gonzales, M. "Performance of Multiple HEPA Filters Against Plutonium Aerosols," Los Alamos Scientific Laboratory, Report LA-5349-Pk, July 1973.

5. Newton, G., Lovelace Foundation, private communication.

6. Fielding, G. H., Borgardus, H. F., Clark, R. C., and Thompson, J. K., "Electrically Augmented Filtration of Aerosols," Naval Research Laboratory Rept. (1974).

7. Borgardus, H. F., Clark, R. C., Thompson, J. K., and Fielding, G. H., "Enhancement of Filter Media Performance by Corona-Face Electric Fields," Proceedings of the Thirteenth AEC Air Cleaning Conference, San Francisco, Calif., August 1974.

8. Rivers, R. D., "Operating Principles of Non-Ionizing Electrostatic Air Filters," ASHRAEJ p. 37 (Feb 1962).

DISCUSSION

GILBERT: I want to ask what the pressure drop was with a double layer of Johns-Manville's duct insulation at 99%.

NELSON: The pressure drop was about six-tenth of an inch. That includes two metal perforated plates and the filter medium itself. It was in that range. It was less than an inch. Bear in mind that we didn't do anything to maximize the surface area of the filter. It was just the flat filter right in front of the HEPA filter.

ORTH: Since the goal of your work is to reduce the volume of HEPA filter waste, 1) do you plan to work on self-cleaning electrostatic pre-filters and 2) how does the volume of waste from the pre-filters you are testing now compare with the HEPA filter waste volume that is saved?

NELSON: That question comes up. We alleviated one problem and created another. We are hoping this type of filter will have a little higher loading capacity than the HEPA. Also, being glass media, they can be removed and washed with acid and that sort of thing. There isn't an organic material to break down, such as in the HEPA filter. We hope it will be possible to leach out the contaminants and have them in a form where they can be readily recovered.

BURCHSTED: I have two points. Are the efficiencies shown in your slides count efficiency or mass efficiency? The distinction is important.

NELSON: The efficiencies are based on mass efficiencies. We use a flame photometer.

BURCHSTED: The second point is that I noted teflon, wool, and polypropylene in your slides. These are all adversely affected by heat. We would recommend the use of fire resistive media.

NELSON: Right. That is why I think eventually we will use glass fibers. None of these fibers will be suitable in a fire situation. I might mention, too, that a similar type of work was presented at the last air cleaning conference. This concept is not new. The Naval Research Laboratory has been working on it for some time. They used different media and they observed this same effect.

TESTING OF AIR FILTERS UNDER QUALITY CONTROL SAFETY PROGRAM

Charles D. Skaats
Filter Certification Laboratory
Rocky Flats Plant
Rockwell International
P.O. Box 464
Golden, Colorado 80401

Abstract:

Testing and inspection of filters used in air filtration systems are conducted at Rocky Flats Plant under the Energy Research and Development Administration and Rockwell quality control program. Some 8,000 high efficiency particulate air (HEPA) filters purchased from three principal suppliers were examined over the year by the Filter Certification group. In facilities handling radioactive materials, filters must function efficiently to provide accurate data on air contamination to safeguard personnel and the environment. Data are given on filter rejects under established criteria and on recommendations for action to the suppliers.

INTRODUCTION

Under the air-cleaning program at Rocky Flats Plant, testing and inspection of components used in air filtration systems are undertaken to certify conformance with Standards Laboratory requirements. Although programs are of interest to other plant sites under Energy Research and Development Administration contracts,* limited data are available. The function of filters in air systems must be fully effective to provide data on air contamination to assure personnel and environmental safety. Filters purchased from suppliers are inspected to assure compliance with criteria established. During the past year, filters from three principal suppliers, X, Y, and Z, were examined.

DISCUSSION

Test Procedures

Some 8,000 filters classified as Size 5 (2 by 2 by 1-foot), high efficiency particulate air (HEPA) components were tested. The tests are performed on a modified penetrometer, Q-107, manufactured by Air Techniques, Baltimore, Maryland. All HEPA filters are tested by their rated flows of 1000 cubic feet per minute (cfm) using a dioctylphthalate (DOP) aerosol. The DOP is controlled at

*Humphrey Gilbert. "The Filter Test Program, and Installation Manual, and Filter Research." Paper presented at the Seventh Atomic Energy Commission Conference, Brookhaven National Laboratory, New York. October 10-12, 1961.

a particle size of 0.3 micrometres (μm). At the same time, the resistance or pressure drop is noted. Classified as rejects are: (1) filters that exceed a penetration of 0.03 percent of the 0.3 μm particle; (2) those that exceed a one-inch pressure drop; (3) those that are damaged out of square or for other mechanical defects; and (4) those that do not meet filter media specifications. Reject filters are destroyed and replaced by the manufacturer as advised.

To indicate the various phases of testing, categories of rejects have been established. The bar graph of Figure 1 shows the percentage of filters rejected every six months, excluding carrier damage. In Figure 2, data are given on the percentage of rejects on a 6-month basis of filters supplied by Manufacturer X. Table I shows the rejects by category.

TABLE I. Number of Manufacturer X Rejects by Category.

Category	1974 Sep-Dec	1975 Jan-June	1975 June-December	1975 January-June
High Penetration	14	29	95	*7
Hole in Media	6	4	5	
Unusual Damage	2	9	6	
Handling Damage			3	

*Decline relates to manufacturer cooperation to improve filters.

Figure 3, shows the percentage of rejects on a six-month basis of filters supplied by Manufacturer Y. Table II shows the rejects by category.

TABLE II. Number of Manufacturer Y Rejects by Category.

Category	1975 July-December	1976 January-June
High Penetration	61	10
Hole in Media	5	0
Unusual Damage	1	0
Handling Damage	2	
Loose Pack	1	3
Banding Damage		6

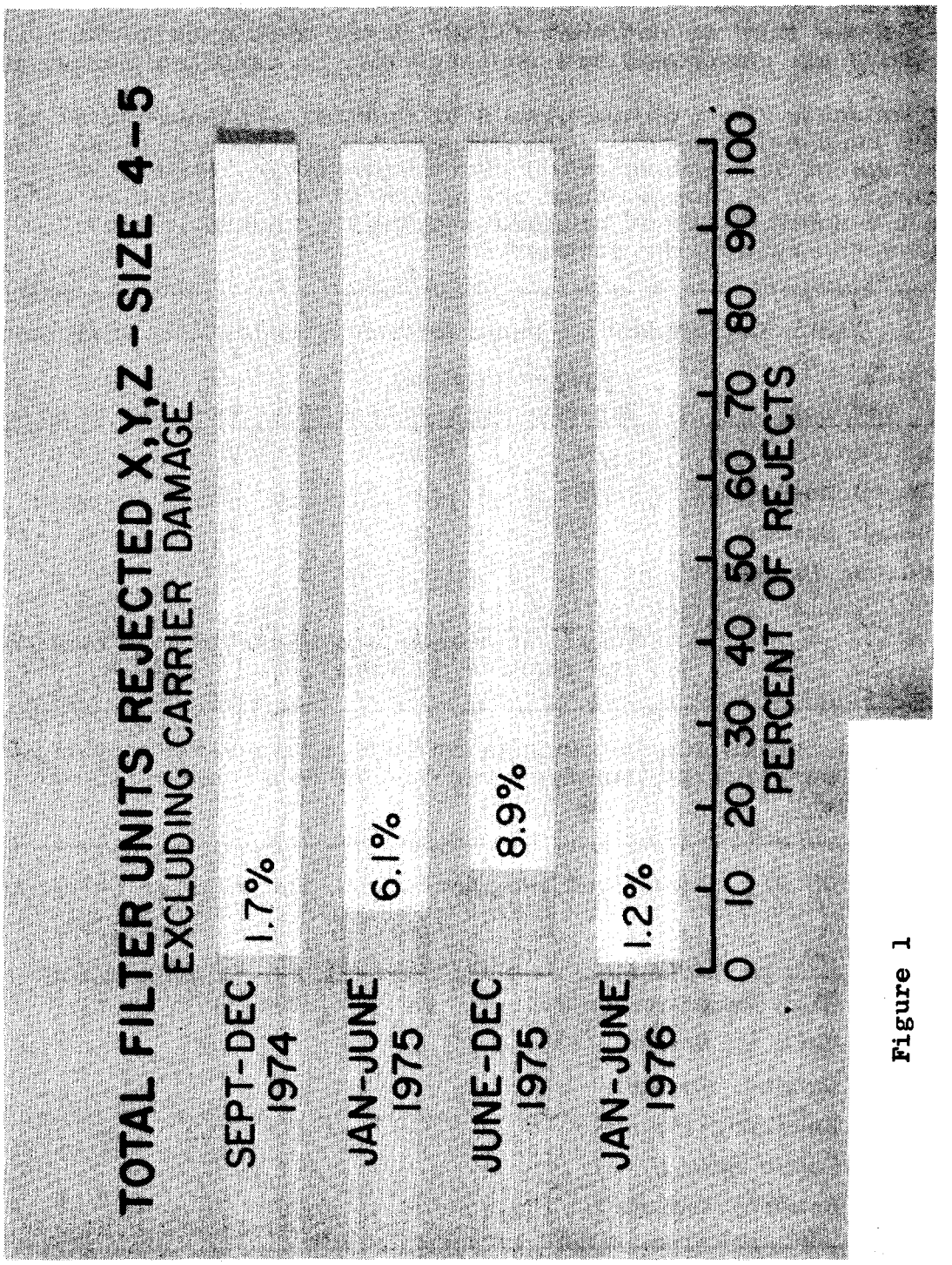
TOTAL FILTER UNITS REJECTED X,Y,Z - SIZE 4-5
EXCLUDING CARRIER DAMAGE
SEPT-DEC 1974
1.7%
JAN-JUNE 1975
6.1%
JUNE-DEC 1975
8.9%
JAN-JUNE 1976
1.2%
0 10 20 30 40 50 60 70 80 90 100
PERCENT OF REJECTS

Figure 1

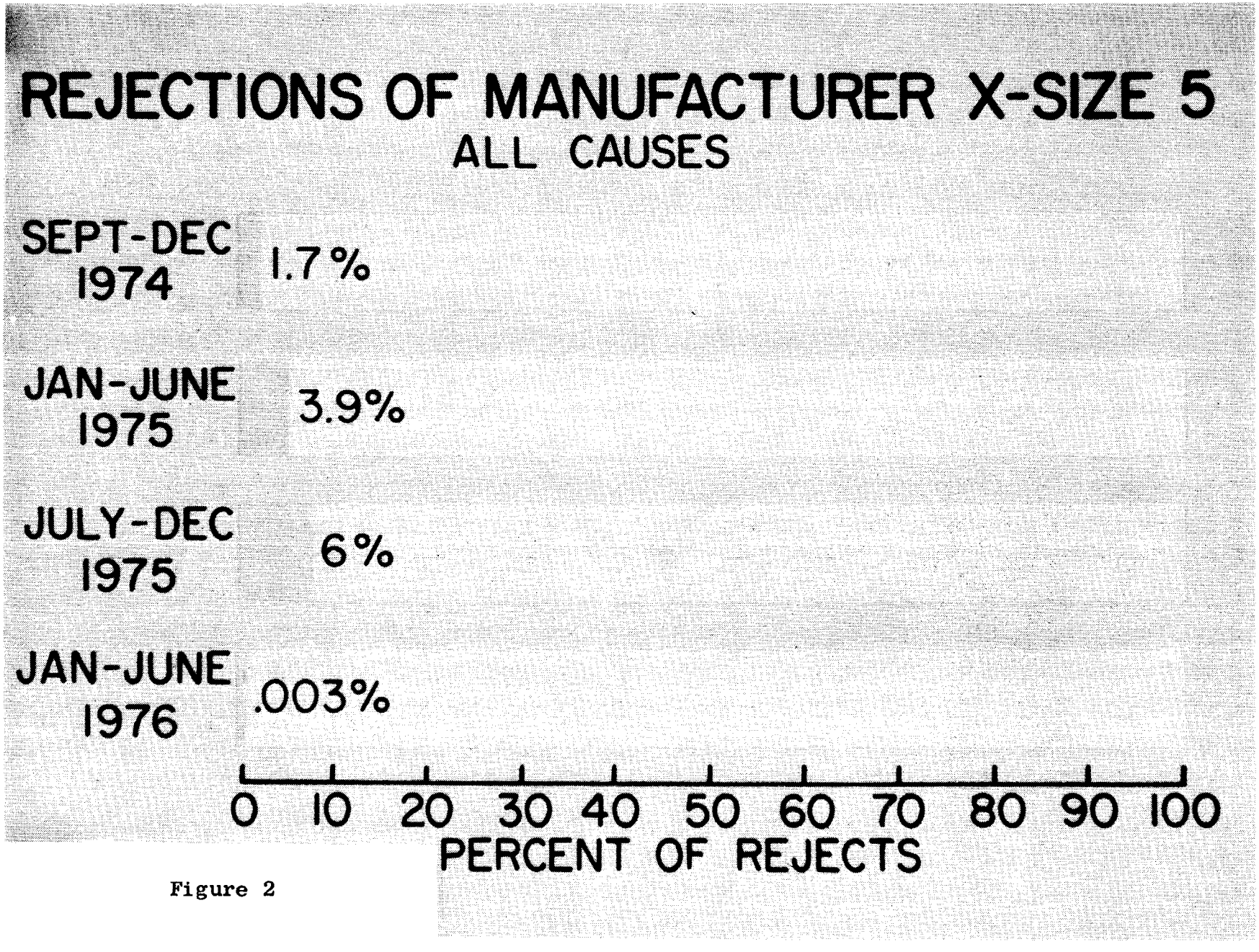
REJECTIONS OF MANUFACTURER X-SIZE 5
ALL CAUSES
SEPT-DEC 1974
1.7%
JAN-JUNE 1975
3.9%
JULY-DEC 1975
6%
JAN-JUNE 1976
.003%
0 10 20 30 40 50 60 70 80 90 100
PERCENT OF REJECTS

Figure 2

REJECTS BY CATEGORY - MANUFACTURER X

	HIGH PENETRATION	HOLE IN MEDIA	HANDLING DAMAGE	UNUSUAL DAMAGE	UNITS SHIPPED	PERCENT REJECTS
SEPT - DEC 1974	14	6		2	1292	1.7
JAN - JUNE 1975	29	4		9*	1060	3.9
JULY - DEC 1975	95	5	3	6*	1810	6
JAN - JUNE 1976	7				1838	.003

*SLITS IN MEDIA

Table I

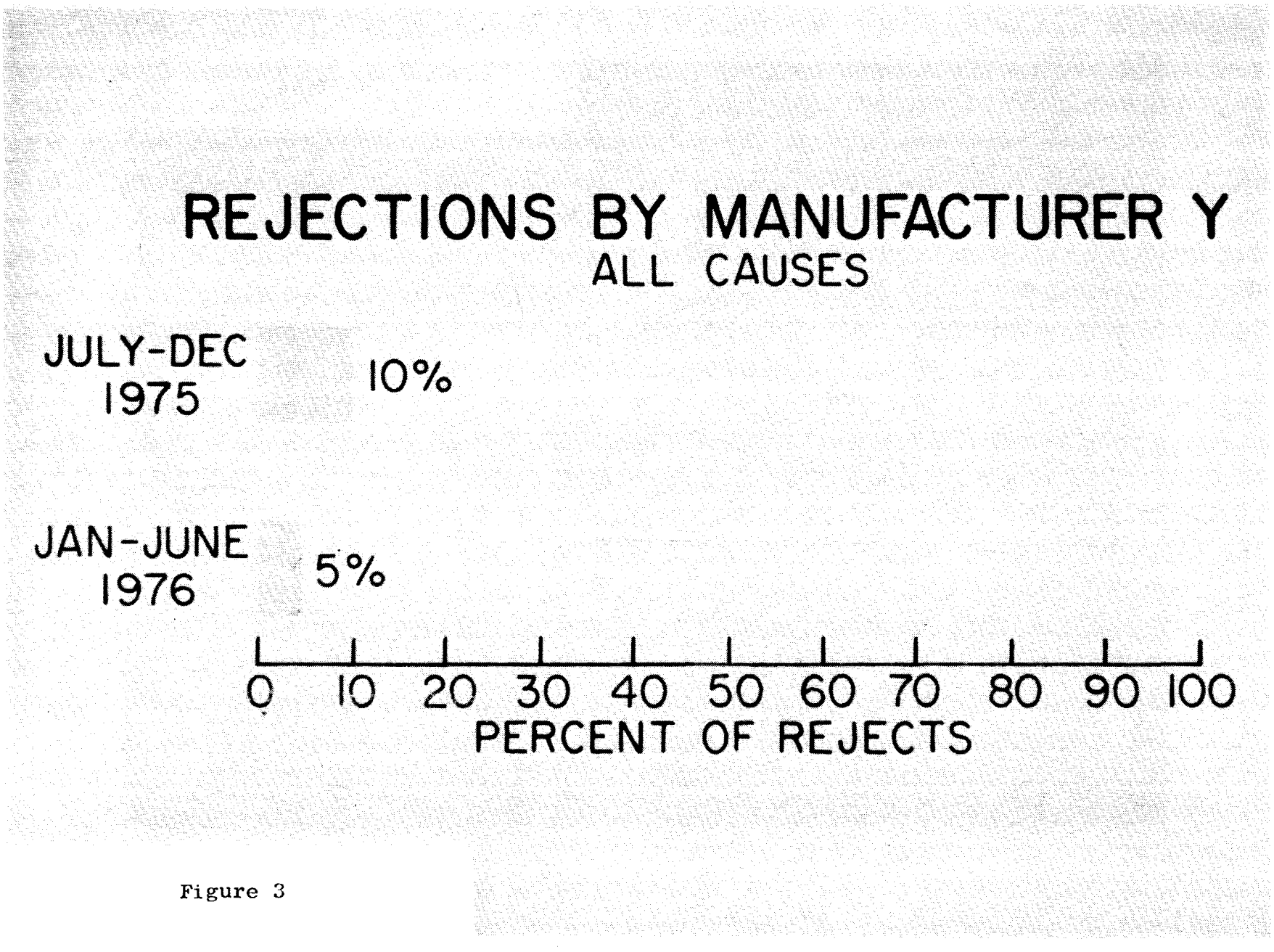
REJECTIONS BY MANUFACTURER Y
ALL CAUSES
JULY-DEC
1975
10%
JAN-JUNE
1976
5%
0 10 20 30 40 50 60 70 80 90 100
PERCENT OF REJECTS

Figure 3

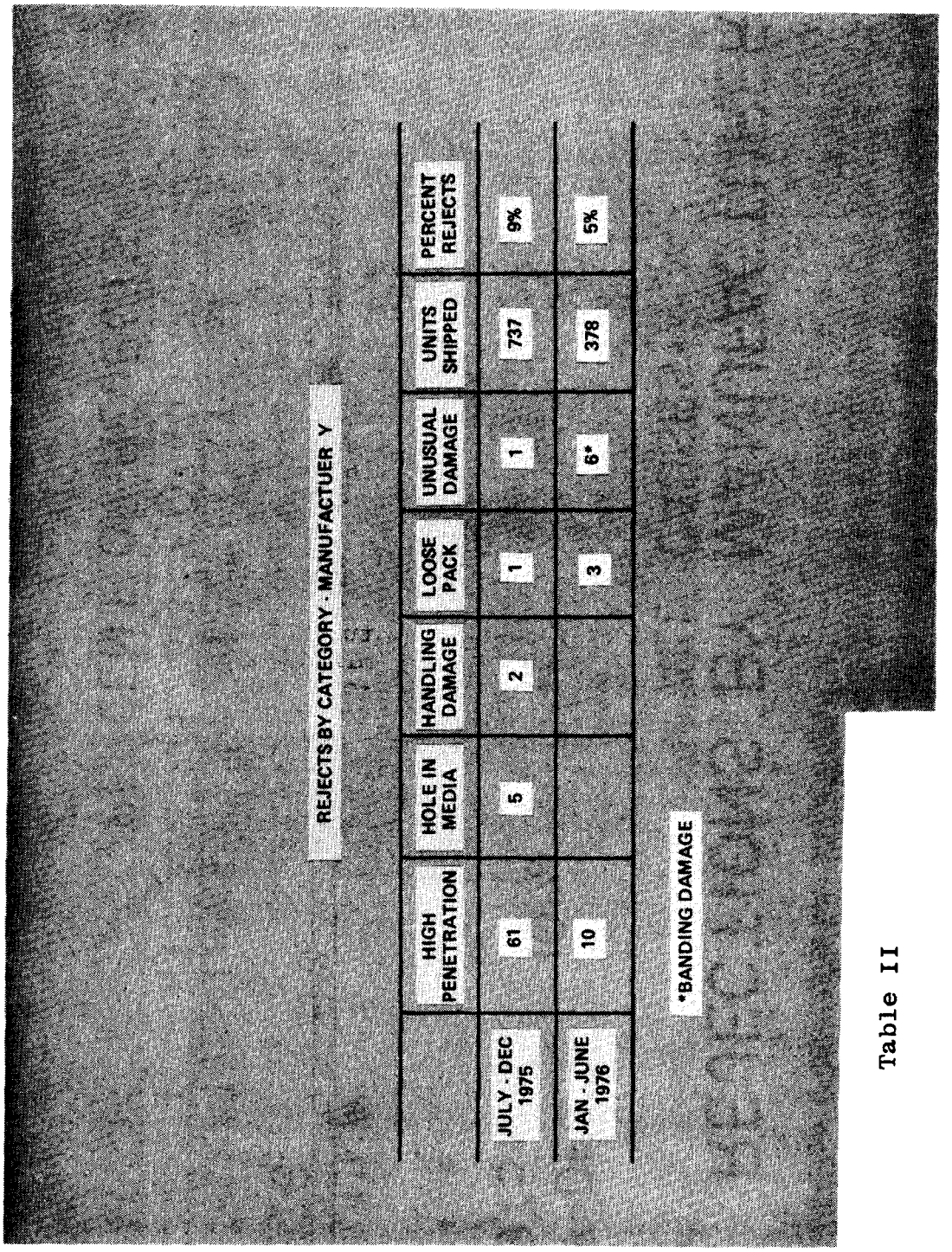

REJECTS BY CATEGORY - MANUFACTUER Y

	HIGH PENETRATION	HOLE IN MEDIA	HANDLING DAMAGE	LOOSE PACK	UNUSUAL DAMAGE	UNITS SHIPPED	PERCENT REJECTS
JULY - DEC 1975	61	5	2	1	1	737	9%
JAN - JUNE 1976	10			3	6*	378	5%

*BANDING DAMAGE

Table II

Figure 4 shows the percentage of rejects on a 6-month basis of filters supplied by Manufacturer Z. Table III gives the rejects by category.

TABLE III. Number of Manufacturer Z Rejects by Category.

Category	1975 January-June	1976 January-June
High Penetration	3	4
Hole in Media	4	2
Unusual Damage	1	0
Handling Damage	0	0
Loose Pack	8	2
Out-of-Square	9	2

Of the manufacturers, X, Y, and Z, one has given continuous authorization to destroy all filter units which were rejected for high penetration. The other manufacturers usually give permission after being notified of rejections.

Manufacturer X

The percentage of rejects from Manufacturer X from September 1974 to December 1974 was 1.7 percent. Examination of the reject usually pinpointed the problem, and little or no action was required.

It was not until the July-December 1975 reporting period that the reject rate increased by 20 percent over the September-December 1975 reject rate. Manufacturer X was notified of the finding. One rejected filter was then destroyed and the media tested to specification MIL-F-51079B. Findings were as follows:

1. High penetration
2. Cross machine tensile below specifications
3. Low pressure drop

Random samples of media were tested from other rejected filters. Manufacturer X was notified and corrective action was taken. Since that particular time period, Manufacturer X has had several shipments with zero rejects.

Manufacturer X later produced a special filter for use at Rocky Flats, but the reject rate was high. By cooperation between the manufacturer and user, the cause for the reject was isolated. The method of sealing the pack to the frame was such that any small deflection in the frame would cause the seal to crack. The manufacturer suggested a new sealant be used, since this was a special use filter. It was required that a complete test be made on the sealant. The sealant was approved, and the reject rate has since dropped to zero.

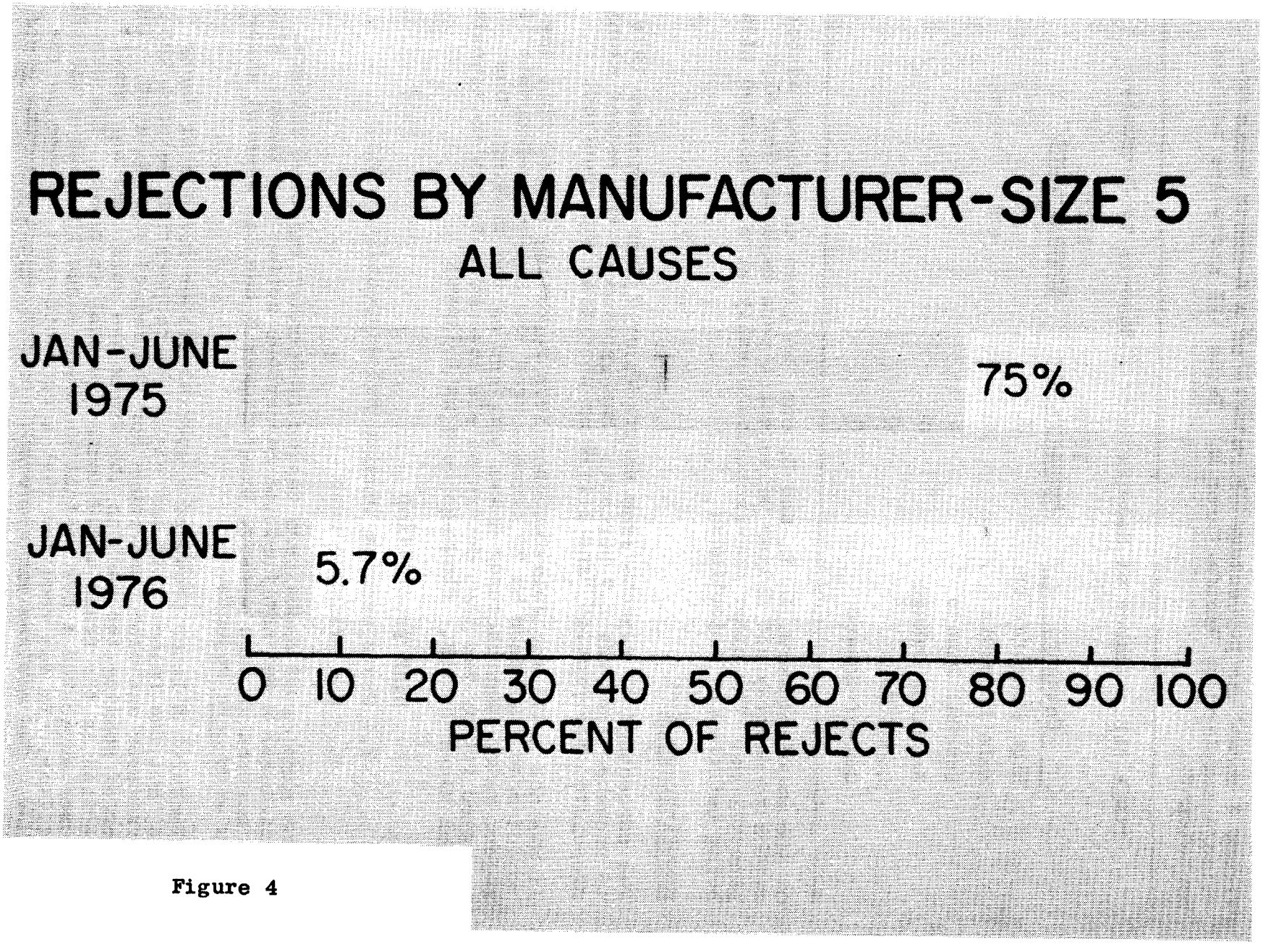
REJECTIONS BY MANUFACTURER-SIZE 5
ALL CAUSES
JAN-JUNE
1975
75%
JAN-JUNE
1976
5.7%
0 10 20 30 40 50 60 70 80 90 100
PERCENT OF REJECTS

Figure 4

REJECTS BY CATEGORY - MANUFACTURER Z

	HIGH PENETRATION	HOLE IN MEDIA	LOOSE PACK	OUT OF SQUARE	UNUSUAL DAMAGE	UNITS SHIPPED	PERCENT REJECTS
JAN - JUNE 1975	3	4	8	9	1	33	75%
JAN - JUNE 1976	4	2	2	2		176	6%

Table III

Manufacturer Y

Manufacturer-Y rejects were directly related to two causes, media and shipping damage. For the six-month period, July-December 1975, Manufacturer-Y rejects were directly traceable to defective media. Proceeding in the same manner as with those of Manufacturer X, tests were made on media samples. Although the media were marginal, they alone did not account for the high percentage of rejects. (See Figure 5.)

Not until the entire pack was removed from a filter, was a crease observed randomly which went along the length of the media. Samples were tested at the creased area and a high penetration was observed. Also at the crease was a thin detachment or delamination of the media. Samples of this media were sent to the Rocky Flats Service Laboratory. The samples were examined by 2000X magnification in the same general area. (See Figures 6 and 7.)

The detached film of Manufacturer Y had no binder present although the main section showed evidence of binder. Other rejected filters were disassembled and the same crease was found. The manufacturer's Quality Control Group was notified of the findings. They were unaware of the crease and could not determine how the defect could have occurred.

The question was: How many filters or rolls of media were affected? Through the use of lot numbers, the manufacturer was able to determine that all the media which could have the defects were used. The Plant was informed as to the serial numbers of the filters using that particular media lot, and was able to locate those filters and verify further that they had been tested and were rejects. These filters had been tested previously by the manufacturer and determined to be acceptable. Either through handling or shipping, a strain had been placed on the creased area causing the filter to fail.

Further discussions with the Quality Control Group of the Manufacturer revealed the following:

1. It was established that the media had been on hand for a long period of time.

2. The defective media had not been observed when the filters were manufactured.

This defect in the media was evaluated by two known filtration experts, and it was determined that the crease had occurred when the manufacturer produced the media.

For the six-month period, January-June 1976, Manufacturer Y shipped several loads. Each load of filters in individual cartons was banded and palletized. Rocky Flats normally receives loads in a nonbanded condition whether it be a full load or short load. In this instance, the banding of the load created the majority of the rejects consisting of broken frames, scraped media, out of square, and loose packs.

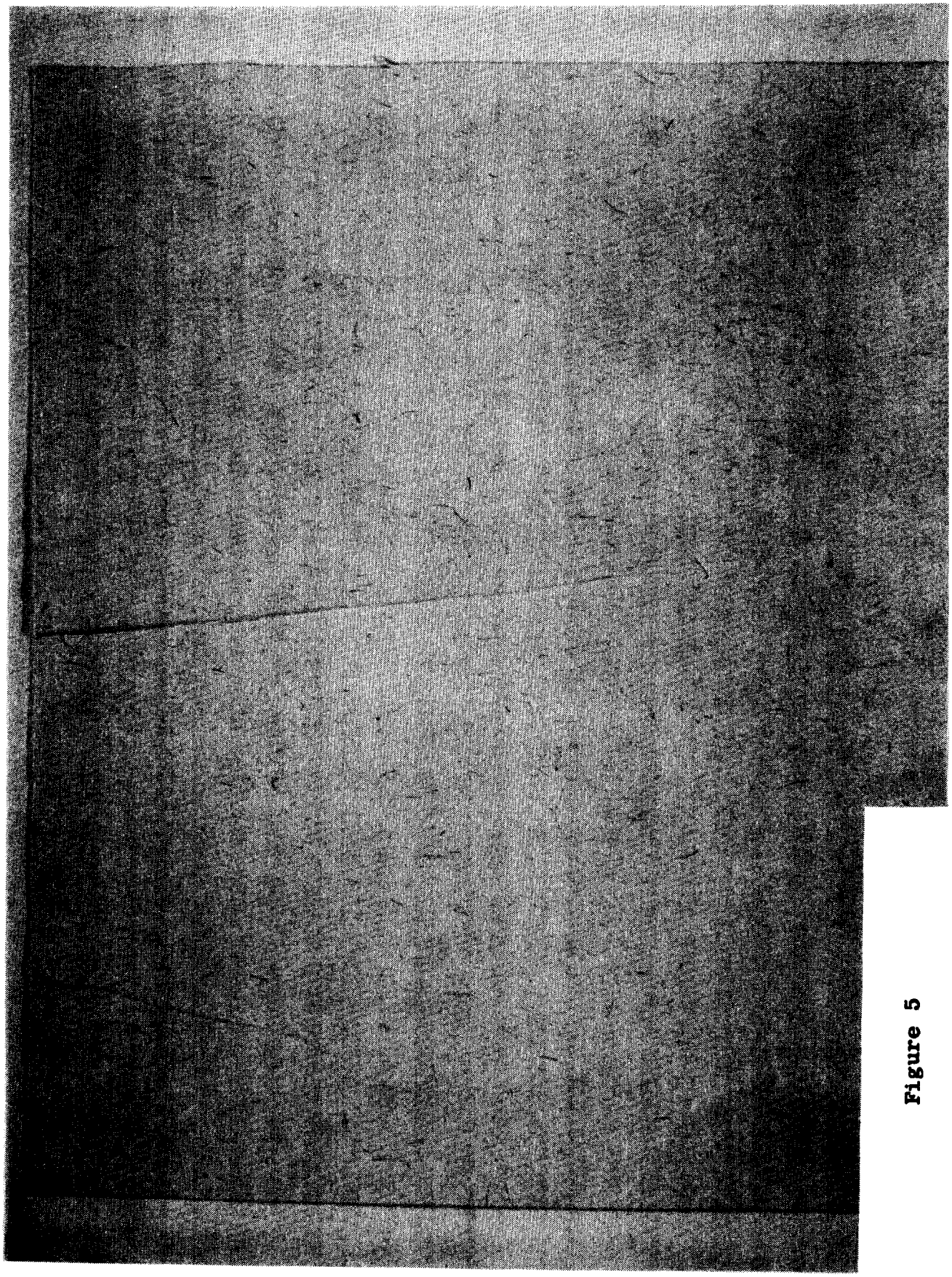

Figure 5

Figure 6

Figure 7

The Rocky Flats shipping procedure is as follows:

1. Full loads (320 to 340 filters) are shipped in an exclusive use trailer which is sealed by the manufacturer and routed directly to Rocky Flats. Once the trailer is on its way, it will arrive at Rocky Flats four to five days later.

2. Partial loads are loaded into a trailer and shored to prevent shifting or damage.

For over a year, the other Manufacturer, X, has shipped in this manner, with no shipping damage.

Manufacturer Z

Manufacturer Z has supplied Rocky Flats with only a token shipment of Size 4 and 5 filters during the reporting periods. From this amount, a trend was noted that could prevent future problems. Investigations into the cause for rejects by Manufacturer Z were conducted on the filter media. Differences arose between manufacturer and user on requirements for media to meet on test experiments. Basically, the disagreement was over tensile and penetration values. In addition, the media from Manufacturer Z was also found thinner than the 0.015-inch thickness in a predominance of cases.

Other than media quality, Manufacturer-Z rejects fell into three categories:

1. Filter being out of square

2. Loose packs

3. Gasket problems, either missing or not glued properly

The manufacturer and user have been cooperating to correct the deficiencies as soon as feasible.

Because of chemical contamination of some air streams, asbestos separators are required in filters for Rocky Flats plant. Better asbestos separators have been needed in the ERDA program for many years. The Plant derives much satisfaction in the report that two of the filter manufacturers are producing satisfactory asbestos separators for filters. There is also some optimism for further improvement in separators to resist chemical exposure. (See Figure 8.)

CONCLUSIONS

Referring to the paper by Humphrey Gilbert (see our Introduction Footnote), his data on percentage of rejects to the current percentages were compared by averaging his percentage from January 1960 to June 1961. The reject rate showed a decrease from 10.5 to 4 percent. The trend currently reflects on the continued cooperation being made to improve the HEPA filter.

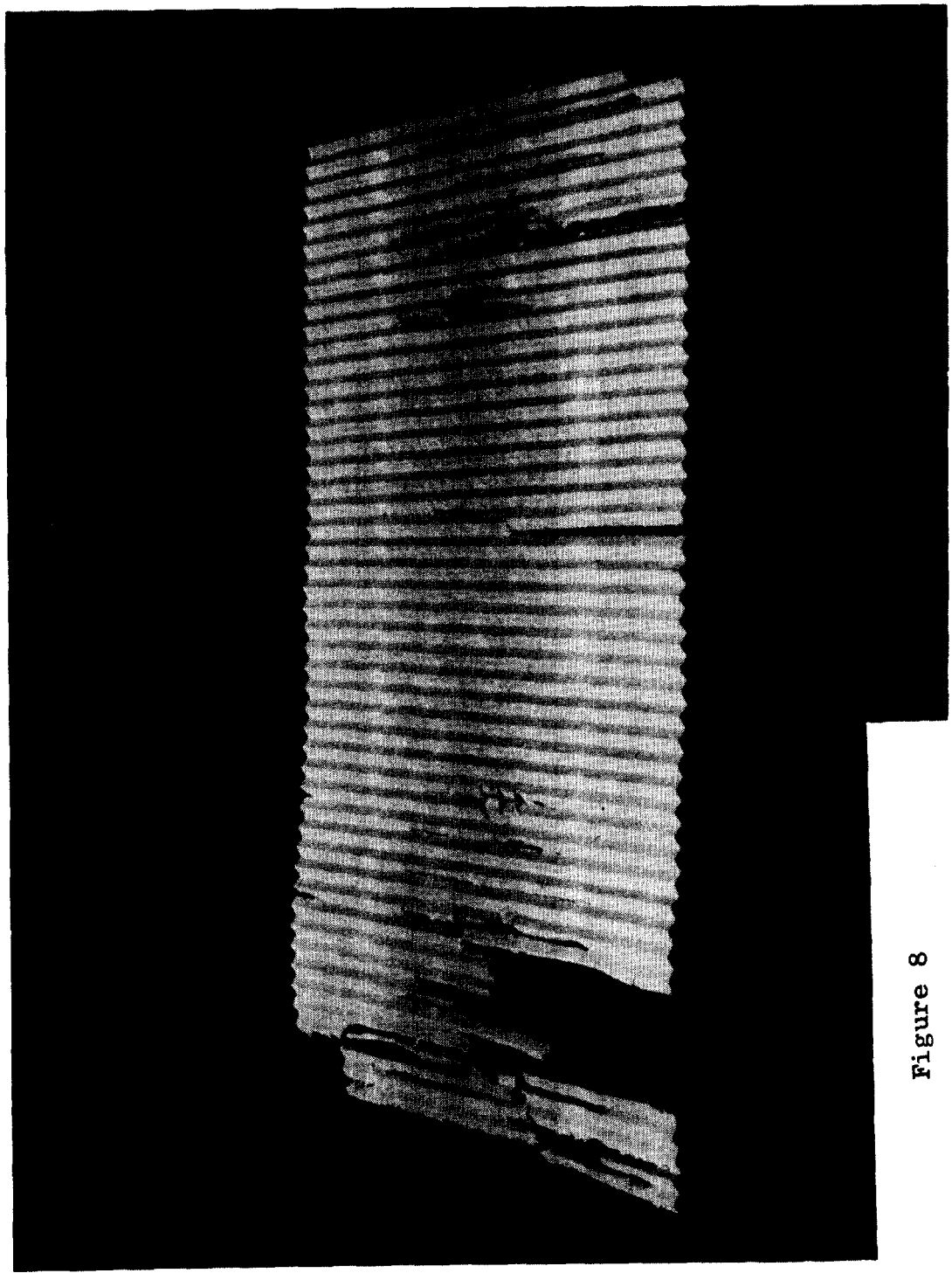

Figure 8

The decline in rejects for the period January-June 1976 (see TableI) indicated that manufacturers can produce an improved quality filter. Rocky Flats will continue to examine reject filters and data from those rejects will be relayed to respective manufacturers toward development of even better quality in filters.

Rocky Flats Plant does not wish to become a quality control unit for a manufacturer. However, since a reject at Rocky Flats can prove costly at the place of manufacture, the intent is to assist the manufacturer in resolving any problems as expeditiously as possible. This will assure a continued supply of inexpensive high quality filters for plant use.

Representatives from the three manufacturers (X, Y, and Z) have visited the test facility on several occasions to review defects or discuss problems that have occurred with their products. In most cases, the representatives have been appreciative of the test methods and the thoroughness of the filter testing program. With the ever-increasing cost of the filter, the enlarging demand for protection of the environment, and the pressing need to assure a quality product to provide protection, the certification group considers that continued investigations have merit for both supplier and user.

DISCUSSION

EDWARDS: First time I ever wanted to be Brand X. Do you have any information to indicate that the other test facilities are having the same kind of trends that you're having now, Mr. Skaats, at Rocky Flats?

SKAATS: I have seen some of the reports from some of the other test stations. They indicate reject rates similar to ours. We have found this out by talking with the Hanford or Oak Ridge test stations and from reports that Mr. Dempsey sends me.

DEMPSEY: I wonder if you have determined what percentage might be from shipment and what percentage from inherent defects?

SKAATS: In most of the shipments, we find the defect. Manufacturer X has had no problems with shipment. Manufacturer Y's problem was with banding. Their bands were too tight. I think this is very important as they crush the frames. With Z, we have not had enough experience. Their shipments have only been small filters which were packed very nicely. We've had no shipping damage. If handled properly and if the manufacturer bands them properly, the filters should come through in good shape.

DEMPSEY: I would like to thank you for the excellent paper you presented and I want the audience to know what Mr. Skaats was requested by the Program Committee to present this particular topic.